JOURNAL
OF
PHYSICS OF THE EARTH

Volume VI August 1958 Number 1

CONTENTS

Page

The Relation between the FOURIER Series Method and the $\frac{\sin x}{x}$ Method for Gravity Interpretations ..... C. TSUBOI and Y. TOMODA 1

Numerical Tables Facilitating Three Dimensional Gravity Interpretations ..... C. TSUBOI, C. H. G. OLDHAM and V. B. WAITHMAN 7

Fault Origin Model of Earthquakes, with Special Reference to the Tango Earthquake, 1927 ..... K. KASAHARA 15

Observation of Near-by Microearthquakes with Ultra Sensitive Seismometers at Matsushiro, Japan ..... T. ASADA, S. SUYEHIRO and K. AKAMATU 23

Earthquake Province—Domain of Sympathetic Seismic Activities ..... C. TSUBOI 35

PUBLISHED JOINTLY BY

THE SEISMOLOGICAL SOCIETY OF JAPAN
THE GEODETIC SOCIETY OF JAPAN
THE VOLCANOLOGICAL SOCIETY OF JAPAN

JOURNAL OF PHYSICS OF THE EARTH

The object of the publication of JOURNAL OF PHYSICS OF THE EARTH is to provide an international medium for the publication of original contributions in the field of geophysical science, more particularly concerning with physical properties and conditions of and phenomena occurring in the solid part of the earth.

The JOURNAL is open to any one who wishes to contribute his (or her) article. But the authors are, in principle, requested to pay page charges necessary for publishing their respective articles. The authors receive 100 copies of reprints free of charge.

In order to serve the purposes for which this JOURNAL is published, all contributions should be written in widely understandable languages, such as English, French and German, etc. Contributions should be sent to the Editor or to one of the Associate Editors.

For the time being, this JOURNAL will be issued at variable prices and at irregular intervals. The price of this issue is 200 yen inside Japan and $1.00 for foreign countries, the latter including postage.

Subscriptions may be made through Charles E. Tuttle Co., Booksellers and publishers; Rutland, Vermont, U.S.A. or 15, Edogawa-cho, Bunkyo-ku, Tokyo, Japan.

The Relation between the FOURIER Series Method and the $\frac{\sin x}{x}$ Method for Gravity Interpretations.

By

Chuji TSUBOI and Yoshibumi TOMODA

Geophysical Institute, Tokyo University, Tokyo.

Abstract

The relation between the FOURIER series method and the $\frac{\sin x}{x}$ method for gravity interpretations has been investigated and it is shown that the two methods are representing the same thing in the limiting case.

§ 1. In 1937, the senior author (TSUBOI: 1937) introduced a direct and objective method for deducing the underground mass distribution $M(x, y)$ that will produce a gravity anomaly distribution $\Delta g(x, y)$ given along the earth's surface. Of course, there can be no unique solution for the problem. In order that a definite answer may be obtained, a simplifying and yet plausible assumption had to be introduced in that method regarding the mass distribution. The assumption made was that the mass $M(x, y)$ is distributed on a single horizontal plane situated at a depth d below the earth's surface. This is a justifiable assumption, because in many actual cases, the underground mass anomaly is caused by an undulation of the interface between the lighter and the underlying denser materials and from the gravimetrical point of view, this arrangement can be replaced with a good approximation by a plane mass which is situated at the average depth of the interface and which is equal to the density difference of the two materials multiplied by the amplitude of undulation, so far as the undulation of interface is not very large compared with its average depth. With such an assumption as stated above, it was shown that if $\Delta g(x, y)$ is expressed by a double FOURIER series such as

$$\Delta g(x, y)=\sum_m\sum_n B_{mn}\begin{matrix}\cos\\ \sin\end{matrix} mx\begin{matrix}\cos\\ \sin\end{matrix} ny, \qquad (1)$$

the mass distribution that will produce this Δg is given by another double FOURIER series such as

$$M(x, y)=\frac{1}{2\pi k^2}\times\sum_m\sum_n B_{mn}\begin{matrix}\cos\\ \sin\end{matrix} mx\begin{matrix}\cos\\ \sin\end{matrix} ny\exp\sqrt{m^2+n^2}\,d, \qquad (2)$$

where k^2 is the NEWTONIAN constant of gravitation and d is the depth of the mass plane. In two dimensional case, (1) and (2) reduce themselves respectively into

$$\Delta g(x)=\sum_m B_m\begin{matrix}\cos\\ \sin\end{matrix} mx, \qquad (3)$$

$$M(x)=\frac{1}{2\pi k^2}\sum_m B_m\begin{matrix}\cos\\ \sin\end{matrix} mx\exp md. \qquad (4)$$

In order to deduce $M(x, y)$ from a given $\Delta g(x, y)$ according to this method, one proceeds as follows:

1) $\Delta g(x, y)$ [$\Delta g(x)$] is analysed into a double [single] FOURIER series,

2) Each of the FOURIER coefficients in this series is multiplied by appropriate $\exp\sqrt{m^2+n^2}d$ [$\exp md$],

3) The FOURIER series having these new coefficients is synthesized,

4) The value of the series at $x=x$, $y=y$, [$x=x$] is divided by $2\pi k^2$.

5) The final result is the required $M(x, y)$ [$M(x)$].

Although this FOURIER series method for gravity interpretation has proved itself to be very useful and competent in applications (TSUBOI, 1938, 1939, 1940, 1941, 1942, 1948, 1950), admittedly it has a kind of awkwardness

coming from the very nature of the FOURIER series. As in many other instances in which it is used, the FOURIER series expression of a quantity implies periodic repetition of the same pattern of distribution of that quantity even outside the domain in which we are interested. This circumstance has caused a kind of hindrance for unconditional usage of the method. In order to get over this difficulty, T. RIKITAKE (1952) suggested the usage of HERMITE function while Y. SATO (1954) proposed a modification of the FOURIER series method for this purpose.

§ 2. In 1955, the junior author (TOMODA) and and K. AKI (TOMODA and AKI, 1955) introduced the $\sin x/x$ method for gravity interpretations with the hope of getting rid of the said awkwardness of the FOURIER series method. This function $\sin x/x$ is characteristic in that it takes a unit value at $x=0$ and vanishes at all other grid points which are π apart. It is therefore fitted for representing the distribution of such a quantity as vanishes at all equally spaced grid points except at one of them where it takes a finite value. If applied to gravity problems,

$$\Delta g(x)=b\frac{\sin x}{x} \tag{5}$$

represents such a distribution of $\Delta g(x)$ as it is b at $x=0$ and is 0 at $x=n\pi$, where n can be any integer other than zero. Since

$$\frac{\sin x}{x}=\int_0^1 \cos mx\, dm, \tag{6}$$

it is readily seen that no harmonic components having higher frequecies than 1 are contained in this function. Making use of the formula (3) and (4), the mass distribution $M(x)$ that will give rise to the gravity anomaly distribution:

$$\Delta g(x)=b\frac{\sin x}{x}$$

is given by

$$M(x)=\frac{b}{2\pi k^2}\int_0^1 \cos mx \exp md\, dm. \tag{7}$$

This can be integrated into

$$M(x)=\frac{b}{2\pi k^2}\frac{1}{x^2+d^2}\times\{(d\cos x+x\sin x)\exp d-d\}. \tag{8}$$

Since $\sin x$ is zero and $\cos x$ is either $+1$ o -1 at $x=n\pi$ according as n is even or odd $M(x)$ at these points becomes simply

$$M(n\pi)=\frac{b}{2\pi k^2}\frac{d}{(n\pi)^2+d^2}(\pm\exp d-1). \tag{9}$$

In this formula, d is expressed in radian in case when the distance between two consecutive grid points is taken as π. If this spacing is a and the depth is δ in the actual scale, we may write

$$d=\frac{\delta\pi}{a}. \tag{10}$$

Inserting this in (9), we get

$$M(na)=\frac{b}{2\pi k^2}\frac{1}{\pi}\frac{\delta/a}{n^2+(\delta/a)^2}\left(\pm\exp\frac{\delta\pi}{a}-1\right). \tag{11}$$

The numerical values of

$$\Phi(n,\ \delta/a)=\frac{1}{\pi}\frac{\delta/a}{n^2+(\delta/a)^2}\left(\pm\exp\frac{\delta\pi}{a}-1\right) \tag{12}$$

for $\delta/a=0.5$ and 1 are given in Table I.

Table I.

Values of $\Phi(n,\ \delta/a)=\frac{1}{\pi}\frac{\delta/a}{n^2+(\delta/a)^2}\left(\pm\exp\frac{\delta\pi}{a}-1\right)$

$\pm n$	$\delta/a=0.5$	$\delta/a=1.0$
0	2.42583	7.04670
1	−0.73979	−3.84223
2	0.14270	1.40948
3	−0.10000	−0.76840
4	0.03730	0.41447
5	−0.03661	−0.29548
6	0.01673	0.19041
7	−0.01877	−0.15378
8	0.00945	0.10849
9	−0.01139	−0.09367
10	0.00605	0.06908
11	−0.00761	−0.06301
12	0.00419	0.04871
13	−0.00546	−0.04514
14	0.00309	0.03587
15	−0.00413	−0.03428
16	0.00236	0.02745
17	−0.00320	−0.02655
18	0.00187	0.02170
19	−0.00256	−0.02124
20	0.00149	0.01749

Any gravity anomaly distribution can be regarded as the linear superposition of

$$b_l \sin x/x,$$

with the origin of x shifted appropriately for each l. In a single mathematical expression, the whole distribution can be written as

$$\Delta g(x)=\sum_l b_l \frac{\sin(x-x_l)}{x-x_l}, \tag{13}$$

where b_l is the anomaly at $x=x_l$. Consequently the underground mass which is needed for producing this anomaly distribution will take the value

$$M(x_l)=\frac{1}{2\pi k^2}\times\sum_m \frac{1}{\pi} b_{l-m}\frac{\delta/a}{(l-m)^2+(\delta/a)^2}\left(\pm\exp\frac{\delta\pi}{a}-1\right)$$
$$=\frac{1}{2\pi k^2}\sum_m b_{l-m}\Phi(l-m,\ \delta/a) \tag{14}$$

beneath $x=x_l$.

§ 3. Thus there have been introduced two methods for the same purpose. The question naturally arises what the relationship between the two methods, the FOURIER series method and the $\sin x/x$ method, is. In what follows, it will be shown that the two methods are after all representing the same thing in the limiting case.

The finite FOURIER series expression of a function which takes a unit value at $x=0$ ($x=2\pi$) and which vanishes at all the $(2p-1)$ equally spaced intervenient points lying between $x=0$ and $x=2\pi$ is as follows:

$$f(x)=\frac{1}{p}\left\{\frac{1}{2}+\cos x+\cos 2x+\cdots\cdots+\cos(p-1)x+\frac{1}{2}\cos px\right\}. \tag{15}$$

If this function is regarded to be representing a gravity anomaly distribution, the mass distribution which will give rise to it is given by

$$M(x)=\frac{1}{2\pi k^2}\frac{1}{p}\left\{\frac{1}{2}+\cos x\exp d+\cos 2x\exp 2d+\cdots\cdots+\cos(p-1)x\exp(p-1)d+\frac{1}{2}\cos px\exp pd\right\}, \tag{16}$$

the mass being assumed to be condensed on a single horizontal plane at a depth d as before. The series (16) can be written as

$$M(x)=\frac{1}{2\pi k^2}\frac{1}{p}\mathscr{R}\left[1+\exp(d+ix)+\exp 2(d+ix)+\cdots\cdots+\exp\{(p-1)(d+ix)\}-\frac{1}{2}+\frac{1}{2}\exp p(d+ix)\right], \tag{17}$$

where $\mathscr{R}$ means the real part of the expression within the brackets which follow it. Since the terms in the brackets but the last two form a geometrical series with a common ratio $\exp(d+ix)$, (17) can be written as

$$M(x)=\frac{1}{2\pi k^2}\frac{1}{p}\mathscr{R}\left[\frac{1-\exp p(d+ix)}{1-\exp(d+ix)}-\frac{1}{2}+\frac{1}{2}\exp p(d+ix)\right]. \tag{18}$$

If d and x are both small as compared with 1, this expression is transformed as follows:

$$M(x)=\frac{1}{2\pi k^2}\frac{1}{p}\mathscr{R}\left[\frac{1-(\cos px+i\sin px)\exp pd}{1-(1+d+ix)}-\frac{1}{2}+\frac{1}{2}(\cos px+i\sin px)\exp pd\right]$$
$$=\frac{1}{2\pi k^2}\frac{1}{p}\left[\frac{-d+(d\cos px+x\sin px)\exp pd}{d^2+x^2}-\frac{1}{2}+\frac{1}{2}\cos px\exp pd\right]. \tag{19}$$

At the grid points where x is integral multiple of $2\pi/2p$, say

$$x=n\frac{2\pi}{2p}=\frac{n\pi}{p}, \tag{20}$$

$\sin px$ is zero and $\cos px$ is either 1 or -1 according as n is even or odd. Consequently, we get

$$M\left(\frac{n\pi}{p}\right)=\frac{1}{2\pi k^2}\frac{1}{p}\left[\frac{d\pm d\exp pd}{d^2+\left(\frac{n\pi}{p}\right)^2}-\frac{1}{2}\pm\frac{1}{2}\exp pd\right]. \tag{21}$$

In this expression, d is expressed in radian. If a is the actual distance between two consecutive grid points, 2π in radian corresponds to $2pa$ in the actual scale. So, if δ is the actual depth of the mass plane, there is a relation

$$d=\frac{\pi\delta}{pa}. \tag{22}$$

Putting (22) into (21) and making p very large, we get finally

$$M\left(\frac{n\pi}{p}\right)=\frac{1}{2\pi k^2}\Phi(n,\ \delta/a)$$

where

$$\Phi(n,\delta/a)=\frac{1}{\pi}\frac{\delta/a}{n^2+(\delta/a)^2}\left(\pm\exp\frac{\delta\pi}{a}-1\right). \quad (23)$$

This is exactly nothing but the formula (11), which was derived already. Thus it has been proved that the $\sin x/x$ method may be regarded to be the limiting case of the FOURIER series method in case the harmonic component in the series is taken up to a very high one.

§ 4. This conclussion is useful if we wish to extend the the $\sin x/x$ method so as to be applied to three dimensional gravity interpretations. In three dimensional cases, we have to evaluate the integral

$$\Phi=\int_0^1\int_0^1\cos mx\cos ny\exp\sqrt{m^2+n^2}\,d\,dm\,dn,$$

corresponding to (7) for two dimensional cases. This expression does not appear to be integrable analytically. From the conclusion obtained in the above, this integral can safely be replaced by a double FOURIER series such as

$$\begin{aligned}\Phi=\frac{1}{p^2}\Bigg[&\frac{1}{2}\left\{\frac{1}{2}+\cos\frac{\pi}{p}y\exp\frac{\pi}{p}\sqrt{0^2+1^2}\,d+\cos\frac{2\pi}{p}y\exp\frac{\pi}{p}\sqrt{0^2+2^2}\,d+\cdots\right.\\&\left.+\frac{1}{2}\cos p\frac{\pi}{p}y\exp\frac{\pi}{p}\sqrt{0^2+p^2}\,d\right\}\\&+\cos\frac{\pi}{p}x\left\{\frac{1}{2}\exp\frac{\pi}{p}\sqrt{1^2+0^2}\,d+\cos\frac{\pi}{p}y\exp\frac{\pi}{p}\sqrt{1^2+1^2}\,d+\cdots\right.\\&\left.+\frac{1}{2}\cos p\frac{\pi}{p}y\exp\frac{\pi}{p}\sqrt{1^2+p^2}\,d\right\}\\&+\cdots\cdots\\&+\cos(p-1)\frac{\pi}{p}x\left\{\frac{1}{2}\exp\frac{\pi}{p}\sqrt{(p-1)^2+0^2}\,d+\cos\frac{\pi}{p}y\exp\frac{\pi}{p}\sqrt{(p-1)^2+1^2}\,d+\cdots\right.\\&\left.+\frac{1}{2}\cos p\frac{\pi}{p}y\exp\frac{\pi}{p}\sqrt{(p-1)^2+p^2}\,d\right\}\\&+\frac{1}{2}\cos p\frac{\pi}{p}x\left\{\frac{1}{2}\exp\frac{\pi}{p}\sqrt{p^2+0^2}\,d+\cos\frac{\pi}{p}y\exp\frac{\pi}{p}\sqrt{p^2+1^2}\,d+\cdots\right.\\&\left.+\frac{1}{2}\cos p\frac{\pi}{p}y\exp\frac{\pi}{p}\sqrt{p^2+d^2}\,d\right\}\Bigg].\end{aligned} \quad (25)$$

This function, if divided by $2\pi k^2$, represents a mass distribution at a depth d which will produce a unit gravity at $x=0$, $y=0$ and zero gravity at all other two dimensional grid points. This double FOURIER series can be evaluated numerically (TSUBOI, OLDHAM, WAITHMAN: 1958).

References

RIKITAKE, T.:

1952 Analyses of Geomagnetic Field by Use of HERMITE Function. Bull. Earthq. Res. Inst., **30**, 293–304.

SATO, Y.:

1954 A Note on TSUBOI-NAGATA's Method. Bull. Earthq. Res. Inst., **32**, 259-269.

TSUBOI, C.:

1937 Relation between Gravity Anomalies and the Corresponding Mass Distribution. (I). Bull. Earthq. Res. Inst., **15**, 636–649.

1938 Relation between Gravity Anomalies and the Corresponding Mass Distribution. (II) Bull. Earthq. Res. Inst., **16**, 273–284.

1939 Relation between Gravity Anomalies and the Corresponding Mass Distribution. (III). Bull. Earthq. Res. Inst., **17**, 351–384.

〃 Relation between Gravity Anomalies and the Corresponding Mass Distribution. (IV). Bull. Earthq. Res. Inst., **17**, 385–410.

1940 Relation between Gravity Anomalies and the Corresponding Mass Distribution. (V). Bull. Earthq. Res. Inst., **18**, 384–400.

1941 Relation between Gravity Anomalies and

the Corresponding Mass Distribution. (VI). Bull. Earthq. Res. Inst., **19**, 26–38.

1942 Relation between Gravity Anomalies and the Corresponding Mass Distribution. (VII). Bull. Earthq. Res. Inst., **20**, 30–31.

〃 Relation between Gravity Anomalies and the Corresponding Mass Distribution. (VIII). Bull. Earthq. Res. Inst., **20**, 419–430.

1948 Undulation of the Isostatic Geoid in the East Indies as Calculated from Gravity Anomalies. Geophysical Notes, No. 40.

1950 Thickness of the Isostatic Earth's Crust in Various Parts of the United States of America. Geophysical Notes, **3**, No. 5.

〃 Dependence of the Isostatic Depth on the Horizontal Scale of the Topographies to be Compensated. Geophysical Notes, **3**, No. 6.

TSUBOI, C., OLDHAM, C. H. G., WAITHMAN, V. B.:

1958 Numerical Table Facilitating Three Dimensional Gravity Interpretations. Journ. Phys. Earth, **6**, 7–13.

Numerical Tables Facilitating Three Dimensional Gravity Interpretations.

By

Chuji TSUBOI

Geophysical Institute, Tokyo University, Tokyo

C. H. G. OLDHAM* and V. B. WAITHMAN

California Research Corporation, La Habra, California, U.S.A.

Abstract

This is an extension of the sin x/x method which was introduced by Y. TOMODA and K. AKI for two dimensional gravity interpretations. Numerical tables facilitating three dimensional gravity interpretations are presented.

Gravity values given at two dimensional grid points on the earth's surface are to be multiplied by corresponding tabular values and the products added up. The sum when divided by $2\pi G$ will represent the surface mass density at the assumed depth and immediately beneath the central grid point.

§1. The sin x/x method which was introduced by Y. TOMODA and K. AKI (1955) proved to be so useful a method for the purpose of two dimensional gravity interpretations (TSUBOI: 1956, 1957) that its extension to three dimensional cases appeared highly desirable. As was stated elsewhere (TSUBOI and TOMODA: 1958), the evaluation of the integral

$$\Phi(x, y, d)=\int_0^1\int_0^1 \cos mx \cos ny \cdot \exp \sqrt{m^2+n^2}\, d\, dm\, dn \qquad (1)$$

for various values of x, y and d is needed for this purpose. This function when divided by $2\pi G$ represents the surface mass density at square grid points over a horizontal underground plane which is situated at a depth d below the surface. This is the surface density which will produce unit gravity at $x=0$, $y=0$ and zero gravity at all other conformal grid points on the earth's surface.

Unlike the corresponding integral

$$\Phi(x, d)=\int_0^1 \cos mx \exp md\, dm \qquad (2)$$

in two dimensional cases, the expression (1) does not appear to be integrable analytically and numerical calculations have to be resorted to for its evaluation. The necessary numerical integration was carried out on a Datatron digital computor in Pasadena, California, U.S.A.

§2. The values of the function (1) which have been computed by means of this machine from 0th grid point up to 15th for both x and y are given in Table I and II for $d=0.5$ and $d=1.0$ respectively. Each of the tables represents only one quadrant of the complete rectangular table which has a symmetry as shown in Fig. 1.

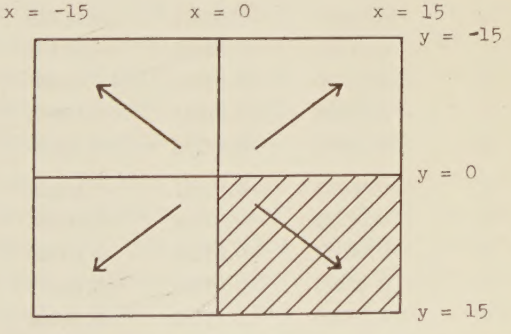

Fig. 1. Shaded portion is given in Table I and II.

Table I is for $d=0.5$, that is for the case in which the mass plane is assumed to be situated at a depth equal to half the horizon-

* Now with the California Exploration Company, San Francisco, California, U.S.A.

Table I. TSUBOI-OLDHAM

	0	1	2	3	4	5	6
0	+3.65742	−0.74169	+0.19159	−0.09485	+0.05113	−0.03430	+0.02309
1	−0.74169	+0.02208	−0.01953	+0.00340	−0.00441	+0.00153	−0.00182
2	+0.19159	−0.01953	+0.00040	−0.00335	+0.00009	−0.00112	+0.00012
3	−0.09485	+0.00340	−0.00335	−0.00025	−0.00106	−0.00012	−0.00045
4	+0.05113	−0.00441	+0.00009	−0.00106	−0.00019	−0.00046	−0.00010
5	−0.03430	+0.00153	−0.00112	−0.00012	−0.00046	−0.00012	−0.00024
6	+0.02309	−0.00182	+0.00012	−0.00045	−0.00010	−0.00024	−0.00008
7	−0.01750	+0.00086	−0.00052	−0.00004	−0.00023	−0.00007	−0.00014
8	+0.01309	−0.00098	+0.00010	−0.00024	−0.00005	−0.00013	−0.00005
9	−0.01059	+0.00055	−0.00029	−0.00001	−0.00013	−0.00004	−0.00008
10	+0.00843	−0.00061	+0.00008	−0.00014	−0.00002	−0.00008	−0.00003
11	−0.00712	+0.00038	−0.00019	0	−0.00008	−0.00002	−0.00005
12	+0.00593	−0.00042	+0.00006	−0.00009	−0.00001	−0.00005	−0.00002
13	−0.00519	+0.00028	−0.00013	+0.00001	−0.00006	−0.00001	−0.00004
14	+0.00450	−0.00032	+0.00005	−0.00007	−0.00001	−0.00004	−0.00001
15	−0.00412	+0.00023	−0.00010	+0.00001	−0.00004	−0.00001	−0.00003

Table II. TSUBOI-OLDHAM

	0	1	2	3	4	5	6
0	+15.78495	−5.84713	+2.18517	−1.08956	+0.63200	−0.41449	+0.28900
1	− 5.84713	+1.35318	−0.48663	+0.22434	−0.13492	+0.08545	−0.06161
2	+ 2.18517	−0.48663	+0.15329	−0.07843	+0.04144	−0.02851	+0.01833
3	− 1.08956	+0.22434	−0.07843	+0.03557	−0.02328	+0.01390	−0.01107
4	+ 0.63200	−0.13492	+0.04144	−0.02328	+0.01042	−0.00756	+0.00420
5	− 0.41449	+0.08545	−0.02851	+0.01390	−0.00756	+0.00543	−0.00465
6	+ 0.28900	−0.06161	+0.01833	−0.01107	+0.00420	−0.00465	+0.00165
7	− 0.21440	+0.04485	−0.01408	+0.00771	−0.00346	+0.00315	−0.00145
8	+ 0.16400	−0.03535	+0.00998	−0.00668	+0.00200	−0.00297	+0.00067
9	− 0.13029	+0.02781	−0.00809	+0.00512	−0.00174	+0.00222	−0.00066
10	+ 0.10541	−0.02315	+0.00606	−0.00464	+0.00098	−0.00217	+0.00022
11	− 0.08761	+0.01917	−0.00508	+0.00381	−0.00087	+0.00175	−0.00025
12	+ 0.07381	−0.01660	+0.00395	−0.00355	+0.00043	−0.00175	−0.00001
13	− 0.06367	+0.01432	−0.00340	+0.00306	−0.00038	+0.00149	−0.00002
14	+ 0.05575	−0.01287	+0.00273	−0.00294	+0.00012	−0.00150	−0.00015
15	− 0.05025	+0.01160	−0.00247	+0.00264	−0.00011	+0.00134	+0.00011

WAITHMAN Coefficients for $d=0.5$.

7	8	9	10	11	12	13	14	15
−0.01750	+0.01309	−0.01059	+0.00843	−0.00712	+0.00593	−0.00519	+0.00450	−0.00412
+0.00086	−0.00098	+0.00055	−0.00061	+0.00038	−0.00042	+0.00028	−0.00032	+0.00023
−0.00052	+0.00010	−0.00029	+0.00008	−0.00019	+0.00006	−0.00013	+0.00005	−0.00010
−0.00004	−0.00024	−0.00001	−0.00014	0	−0.00009	+0.00001	−0.00007	+0.00001
−0.00023	−0.00005	−0.00013	−0.00002	−0.00008	−0.00001	−0.00006	−0.00001	−0.00004
−0.00007	−0.00013	−0.00004	−0.00008	−0.00002	−0.00005	−0.00001	−0.00004	−0.00001
−0.00014	−0.00005	−0.00008	−0.00003	−0.00005	−0.00002	−0.00004	−0.00001	−0.00003
−0.00005	−0.00009	−0.00004	−0.00006	−0.00002	−0.00004	−0.00002	−0.00003	−0.00001
−0.00009	−0.00004	−0.00006	−0.00003	−0.00004	−0.00002	−0.00003	−0.00001	−0.00002
−0.00004	−0.00006	−0.00003	−0.00004	−0.00002	−0.00003	−0.00001	−0.00002	−0.00001
−0.00006	−0.00003	−0.00004	−0.00002	−0.00003	−0.00002	−0.00002	−0.00001	−0.00002
−0.00002	−0.00004	−0.00002	−0.00003	−0.00002	−0.00002	−0.00001	−0.00002	−0.00001
−0.00004	−0.00002	−0.00003	−0.00002	−0.00002	−0.00001	−0.00002	−0.00001	−0.00001
−0.00002	−0.00003	−0.00001	−0.00002	−0.00001	−0.00002	−0.00001	−0.00001	−0.00001
−0.00003	−0.00001	−0.00002	−0.00001	−0.00002	−0.00001	−0.00001	−0.00001	−0.00001
−0.00001	−0.00002	−0.00001	−0.00002	−0.00001	−0.00001	−0.00001	−0.00001	−0.00001

WAITHMAN Coefficients for $d=1.0$.

7	8	9	10	11	12	13	14	15
−0.21440	+0.16400	−0.13029	+0.10541	−0.08761	+0.07381	−0.06367	+0.05575	−0.05025
+0.04485	−0.03535	+0.02781	−0.02315	+0.01917	−0.01660	+0.01432	−0.01287	+0.01160
−0.01408	+0.00998	−0.00809	-0.00606	−0.00508	+0.00395	−0.00340	+0.00273	−0.00247
+0.00771	−0.00668	+0.00512	-0.00464	+0.00381	−0.00355	+0.00306	−0.00294	+0.00264
−0.00346	+0.00200	−0.00174	+0.00098	−0.00087	+0.00043	−0.00038	+0.00012	−0.00011
+0.00315	−0.00297	+0.00222	−0.00217	+0.00175	−0.00175	+0.00149	−0.00150	+0.00134
−0.00145	+0.00067	−0.00066	+0.00022	−0.00025	−0.00001	−0.00002	−0.00015	+0.00011
+0.00160	−0.00158	+0.00113	−0.00116	+0.00089	−0.00093	+0.00076	−0.00080	+0.00069
−0.00158	+0.00049	−0.00052	+0.00024	−0.00029	+0.00011	−0.00015	+0.00003	−0.00008
+0.00113	−0.00052	+0.00043	−0.00047	+0.00029	−0.00033	+0.00021	−0.00025	+0.00017
−0.00116	+0.00024	−0.00047	+0.00048	−0.00053	+0.00040	−0.00044	+0.00035	−0.00039
+0.00089	−0.00029	+0.00029	−0.00053	−0.00021	+0.00017	−0.00027	+0.00023	−0.00029
−0.00093	+0.00011	−0.00033	+0.00040	+0.00017	+0.00072	−0.00076	+0.00069	−0.00072
+0.00076	−0.00015	+0.00021	−0.00044	−0.00027	−0.00076	−0.00066	+0.00063	−0.00068
−0.00080	+0.00003	−0.00025	+0.00035	+0.00023	+0.00069	+0.00063	+0.00098	−0.00100
+0.00069	−0.00008	+0.00017	−0.00039	−0.00029	−0.00072	−0.00068	−0.00100	−0.00096

Table IV. Sum of

y up to	Column						
	$x=0$	$x=1$	$x=2$	$x=3$	$x=4$	$x=5$	$x=6$
$y=0$	3.65742	−0.74169	0.19159	−0.09485	0.05113	−0.03430	0.02309
$y=1$	2.17404	− 69753	15253	− 8805	4231	− 3124	1945
$y=2$	2.55722	− 73659	15333	− 9485	4249	− 3348	1969
$y=3$	2.36752	− 72979	14663	− 9525	4037	− 3372	1879
$y=4$	2.46978	− 73861	14681	− 9737	3999	− 3464	1859
$y=5$	2.40118	− 73555	14457	− 9761	3907	− 3488	1811
$y=6$	2.44736	− 73919	14481	− 9851	3887	− 3536	1795
$y=7$	2.41236	− 73747	14377	− 9859	3841	− 3550	1767
$y=8$	2.43854	− 73943	14397	− 9907	3831	− 3576	1757
$y=9$	2.41736	− 73833	14339	− 9909	3805	− 3584	1741
$y=10$	2.43422	− 73955	14355	− 9937	3801	− 3600	1735
$y=11$	2.41998	− 73879	14317	− 9937	3785	− 3604	1725
$y=12$	2.43184	− 73963	14329	− 9955	3783	− 3614	1721
$y=13$	2.42146	− 73907	14303	− 9953	3771	− 3616	1713
$y=14$	2.43046	− 73971	14313	− 9967	3769	− 3624	1711
$y=15$	2.42222	− 73925	14293	− 9965	3761	− 3626	1705
Corresponding Coefficients	2.42583	− 73979	14270	− 10000	3730	− 3661	1673

Table V. Sum of

y up to	Column						
	$x=0$	$x=1$	$x=2$	$x=3$	$x=4$	$x=5$	$x=6$
$y=0$	15.78495	−5.84713	2.18517	−1.08956	0.63200	−0.41449	0.28900
$y=1$	4.09069	−3.14077	1.21191	−0.64088	63784	− 24359	16578
$y=2$	8.16403	−4.11403	1.51849	− 79774	44504	− 30061	20244
$y=3$	6.28191	−3.66535	1.36163	− 72660	39848	− 27281	18030
$y=4$	7.54591	−3.93519	1.44451	− 77316	41932	− 28793	18870
$y=5$	6.71693	−3.76429	1.38749	− 74536	40420	− 27707	17940
$y=6$	7.29493	−3.88751	1.42415	− 76750	41260	− 28637	18270
$y=7$	6.86613	−3.79781	1.39599	− 75208	40568	− 28007	17980
$y=8$	7.19413	−3.86851	1.41595	− 76544	40968	− 28601	18114
$y=9$	6.93355	−3.81289	1.39977	− 75520	40620	− 28157	17982
$y=10$	7.14437	−3.85919	1.41189	− 76448	44816	− 28591	18026
$y=11$	6.96915	−3.82085	1.40173	− 75686	40642	− 28241	17976
$y=12$	7.11677	−3.85405	1.40963	− 76396	40728	− 28591	17974
$y=13$	6.98943	−3.82541	1.40283	− 75784	40652	− 28293	17970
$y=14$	7.10093	−3.85115	1.40829	− 76372	40676	− 28593	17940
$y=15$	7.00043	−3.82795	1.40335	− 75844	40654	− 28325	17962
Corresponding Coefficients	7.04670	−3.84223	1.40948	− 76840	41447	− 29548	19041

Values in Table I.

Column								
$x=7$	$x=8$	$x=9$	$x=10$	$x=11$	$x=12$	$x=13$	$x=14$	$x=15$
−0.01750	0.01309	−0.01059	0.00843	−0.00712	0.00593	−0.00519	0.00450	−0.00412
− 1578	1113	− 949	721	− 636	509	− 463	386	− 366
− 1682	1113	− 1007	737	− 674	521	− 489	396	− 386
− 1690	1085	− 1009	709	− 674	503	− 487	382	− 384
− 1736	1075	− 1035	705	− 690	501	− 499	380	− 392
− 1750	1049	− 1043	689	− 694	491	− 501	372	− 394
− 1778	1039	− 1059	683	− 704	487	− 509	370	− 400
− 1788	1021	− 1067	671	− 708	479	− 513	364	− 402
− 1806	1031	− 1079	665	− 716	475	− 519	362	− 406
− 1814	1001	− 1085	657	− 720	469	− 521	358	− 408
− 1826	995	− 1093	653	− 726	465	− 525	356	− 412
− 1830	987	− 1097	647	− 730	461	− 527	352	− 414
− 1838	983	− 1103	643	− 734	459	− 531	350	− 416
− 1842	977	− 1105	639	− 736	455	− 533	348	− 418
− 1848	975	− 1109	637	− 740	453	− 535	346	− 420
− 1850	971	− 1111	633	− 742	451	− 537	344	− 422
− 1877	945	− 1139	605	− 761	419	− 546	309	− 413

Values in Table II.

Column								
$x=7$	$x=8$	$x=9$	$x=10$	$x=11$	$x=12$	$x=13$	$x=14$	$x=15$
−0.21440	0.16400	−0.13029	0.10541	−0.08761	0.07381	−0.06367	0.05575	−0.05025
− 12470	9330	− 7467	5911	− 4927	4061	− 3503	3001	− 2705
− 15286	11326	− 9085	7123	− 5943	4851	− 4183	3547	− 3199
− 13744	9990	− 8061	6195	− 5181	4141	− 3571	2959	− 2671
− 14436	10390	− 8409	6391	− 5355	4227	− 3647	2983	− 2693
− 13806	9796	− 7965	5957	− 5005	3877	− 3349	2683	− 2425
− 14096	9930	− 8097	6001	− 5055	3875	− 3353	2653	− 2403
− 13776	9614	− 7871	5769	− 4877	3689	− 3201	2493	− 2265
− 14092	9712	− 7975	5817	− 4935	3711	− 3231	2499	− 2281
− 13866	9608	− 7889	5723	− 4877	3645	− 3189	2449	− 2247
− 14098	9656	− 7983	5819	− 4983	3725	− 3277	2519	− 2325
− 13920	9598	− 7925	5713	− 5025	3759	− 3331	2565	− 2383
− 14106	9620	− 7991	5793	− 4991	3903	− 3483	2703	− 2527
− 13954	9590	− 7949	5705	− 5045	3751	− 3615	2829	− 2663
− 14114	9596	− 7999	5775	− 4999	3889	− 3489	3025	− 2863
− 13976	9580	− 7965	5697	− 5057	3745	− 3625	2825	− 3055
− 15378	10849	− 9367	6908	− 6301	4871	− 4514	3587	− 3428

tal spacing between grid points. Likewise, Table II is for $d=1.0$, that is for the case in which the plane is assumed to be situated at a depth equal to the grid spacing.

The usage of the table is simple in principle. Prepare transparent stencils, say A, on which values given in Table I and II respectively are written down in a complete rectangular mesh form. Write down the observed gravity values (in mgals) to be investigated on a sheet of paper, say B, with the same spacing as A. Take whichever appropriate one of A's as the case may be and place it on B so that the mesh on both will coincide. Calculate all the products of values which appear at the same grid points and add them up. The sum, when divided by $2\pi\times 6.67\times 10^{-11}$ will represent the surface mass density in gr/cm^2 at the assumed depth and immediately beneath the central point of A ($x=0$, $y=0$). Shift A by one step relative to B and make the same calculation. Repeat this until the area of interest will completely be covered.

§ 3. This method of projecting the gravity field downwards, or alternatively of computing a surface mass distribution, is ideally suited for solution on an electronic computor. If a computor is not available, then the arithmetic labor involved is prohibitive, and some simplifying modification of the above process is needed. Such a modification must involve a compromise between accuracy and the practicability of computing the results. One way to shorten the calculations is to use only a portion of the tables. For example, we have found that by using the portion of the tables from $x=0$, $y=0$ to $x=9$, $y=9$, we achieve a reasonable compromise. If still less accuracy can be tolerated in the final results, the tables can be shortened even further.

§ 4. From the potential theory, it is evident that $\Phi(x, y, d)$ must add up to 1 if the summation is extended to infinity both for x and y. Actual sums of the values of Φ given in Table I and II when added up to various x and y are listed in Table III.

From the values given in Table III, it is noted that while a good result can be obtained by including only a small number of terms in the summation for $d=0.5$, many more terms need be included in order that a similarly good result may be obtained for $d=1.0$.

Table III.

	Number of terms included in the summation (in both x and y directions)	Sum of coefficients
$d=0.5$	3	1.0107
	4	1.1714
	5	1.0324
	6	1.1045
	7	1.0332
	8	1.0739
	9	1.0306
	10	1.0568
	11	1.0277
	12	1.0461
	13	1.0248
	14	1.0387
	15	1.0220
$d=1.0$	3	0.2213
	4	1.8569
	5	0.7269
	6	1.4511
	7	0.8936
	8	1.2802
	9	0.9629
	10	1.1937
	11	0.9936
	12	1.1468
	13	1.0048
	14	1.1219
	15	1.0036

Also, in Table IV and V, the sums of values in each column of the Table I and II are compared with the corresponding coefficients appearing in the two-dimensional $\sin x/x$ method, to which they should converge if the summation is extended to infinity. The asymptotic approach of the sums to their respective final values is generally good, but it cannot be said to be very satisfactory numerically, especially for $d=1.0$. This divergence may be due to some approximations used in the process of computing tabular values.

§ 5. In conclusion, the writers wish to thank Professor C. H. DIX of the California Institute of Technology for suggesting the coopera-

ion of our two groups in this work. We lso wish to thank the California Research Corporation for making it possible for us to se a digital computor to compute the tables, nd also for permission to publish them.

References

TOMODA, Y., and AKI, K.:
1955 Use of the Function $\sin x/x$ in Gravity Problems. Proc. Japan Acad., **31**, 443–448.

TSUBOI, C.:
1956 Crustal Structure in Northern and Middle California from Gravity Pendulum Data. Bull. Geol. Soc. Amer., **67**, 1641–1646.
1957 Crustal Structure along a Certain Profile across the East Indies as Deduced by a New Calculation Method. Gedenkboek F. A. Vening MEINESZ, 287–294.

TSUBOI, C., and TOMODA, Y.:
1958 The Relation between the FOURIER Series Method and $\sin x/x$ Method for Gravity Interpretations. Journ. Earth, **6**, 1–5.

Fault Origin Model of Earthquakes, with Special Reference to the Tango Earthquake, 1927.

By

Keichi KASAHARA

Earthquake Research Institute, Tokyo University.

Abstract

Geodetic and seismological characteristics due to a fault movement have been studied on the basis of a simple model. It is intended to examine whether or not such a model is acceptable as a possible representation of earthquake origins. The model is proposed from the standpoint similar to that of REID's hypothesis and the sudden occurrence of a fracture fault in the upper part of the earth's crust is taken as the immediate cause of earthquake shocks as well as of crustal deformations.

First, we deal with statical deformation of the earth's crust caused by stress change (shear) on the fault plane, which is assumed to be developed from the surface vertically down to a certain depth. It has been found that by this model, the general decrease of horizontal displacement of triangulation points with distance from the fault is explained reasonably well. From the comparison of the theory with the observed geodetic data, probable conditions at the actual earthquake fault can be surmised. In the case of the Gômura fault (Tango earthquake), for instance, the depth (H) is estimated at 15 km, while the stress change on the fault plane $(Y_x)_0$ and the total amount of strain energy (E_{fault}), at 3×10^7 c.g.s. and 4×10^{22} ergs, respectively (length of the fault being assumed to be 30 km).

Discussion is also made about the characteristics of seismic waves which are generated by the supposed fault movement. The analysis based on a two-dimensional model has shown that the push-pull distribution of the initial P-wave is of the quadrant type, one of the nodal lines coinciding with the fault. The maximum of the spectral intensity (P-wave) falls on the component, whose wave-length (referred to S-wave) is approximately 1.2 times as large as the fault's length.

These results also agree satisfactorily well with the observed seismological data. The deduced conditions at the fault are also acceptable judging from the mechanical strength of the crust which is already known. The model adopted here affording satisfactory explanations of various aspects of the Tango earthquake, we might say that the physical conditions at the seismic origin do not differ much from those of the model. Possibility of applying the similar model to other cases is also discussed.

1. Introduction

It is an almost established fact that earthquakes are caused by a sudden release of the strain energy which has been accumulated within some limited portion of the earth.[1] Although the mechanism of such energy release has not been known in detail yet, a majority of seismologists believe that some fracture-like event that occurs in the extremely strained portion would probably be the immediate cause of it.

The above theory is supported most positively by those seismologists who pay attention to the systematic distribution of the push-pull sense of initial earthquake motion recorded at many stations. P. BYERLY (1955), J. H. HODGSON (1957) and others have given the "fault-plane solutions" for a number of earthquakes, in which they obtained the

1) The present paper deals only with such earthquakes of large magnitude as sometimes called tectonic earthquakes.

directions of faulting assumed as the immediate cause of them.

In fact, the solutions obtained by them for some destructive earthquakes are in good harmony with observed features of the respective seismic faults especially in regard to their direction of motion. The theory has, however, almost nothing to do with the other source of observational data, such as the period and the form of seismic waves, distribution of crustal deformation around the fault, and so on, from which much can be learned about the processes at earthquake origins. It is indisputable that these deta provide valuable informations about what occurs at the seismic origin (*f.i.* H. HONDA, 1957). If we could examine the proposed model taking such additional aspects of earthquakes into consideration, we would be more confident in our conclusion.

It is desirable, therefore, to improve the model if necessary so as to make it agree with all the geodetic and seismological evidences of earthquakes. While it would be very difficult to find appropriate models for all the earthquakes, it is worth conducting an analysis for some special cases. In that case, more concrete knowledge about the physical conditions at seismic origin will be obtained.

§ 2. Crustal deformation associated with a lateral fault

Statistics shows that shallow earthquakes in the Japan area whose magnitude exceeds a certain limit are usually accompanied by crustal deformations (K. KASAHARA, 1957). Although the deformation is complicated in general, in several cases, such as the Tango earthquake of 1927, it is of a fairly simple feature (Fig. 1).

It is characterized by a long fault running across the epicentral area as well as by the systematic distribution of the earth's deformation. Triangulation points on both sides of the fault were displaced parallel to the fault in opposite directions. The amplitude of the displacement diminishes monotonously with distance from the fault. If we disregard its detailed feature, such a tendency is likely to be interpreted by taking a simple model of fault production. We therefore assume the conditions as follows (Fig. 2).

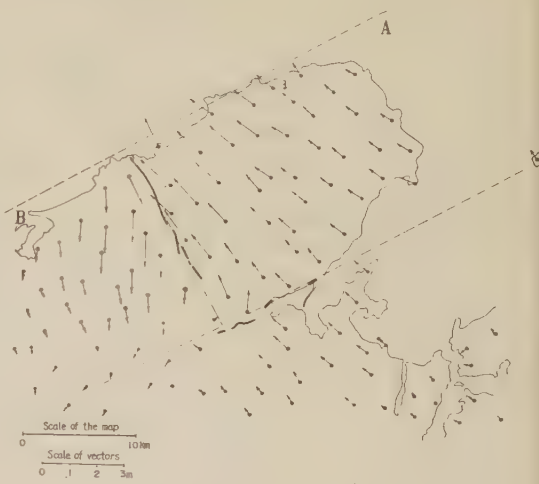

Fig. 1. Horizontal displacements of triangulation points in the Tango district (after C. TSUBOI); (thick lines: seismic faults).

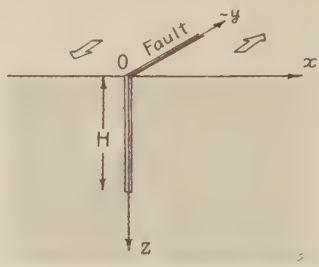

Fig. 2. Model of a lateral fault.

A large part of the crust (half-space) is initially subject to uniform shear stress, which exceeds, at a certain moment, the limit of strength of the medium. Accordingly, a single fracture plane takes place, which is assumed to be in the direction bisecting the angle between the two principal stress axes. We also assume that the fracture plane is infinitely long but is finite in depth. This plane being liberated from the stress (shear), deformation of the medium takes place around it due to the stress change. We are able to investigate such a deformation analytically from the viewpoint of theory of elasticity (K. KASAHARA, 1957).

The solution, which satisfies the fundamental

equation of equilibrium as well as the boundary conditions at the free surface, is given as follows,

$$\left.\begin{aligned} u &= 0\ , \\ v &= \sum_n \left(\frac{F_n}{\mu n}\right)(\sinh nx - \cosh nx)\cos nz\ , \\ w &= 0\ , \end{aligned}\right\} \qquad (1)$$

where, u, v, and w denote the displacements in x, y, and z directions, while $F_n (n=1,2,3,\cdots)$ are the constants which are to be determined from the following relation,

$$(Y_x)_{x=0} = \sum_n F_n \cos nz\ . \qquad (2)$$

Accordingly, if we know the stress distribution along the fault plane, F_n and v are calculated. Fig. 3 illustrates the distribution

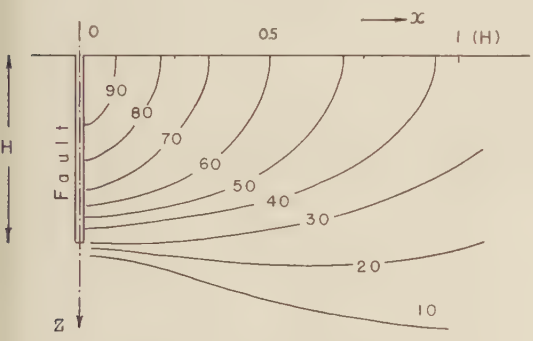

Fig. 3. Distribution of v in the vertical cross-section.

of v in the vertical cross-section perpendicular to the fault plane, which is needed to make the plane free from the initial stress. We see that v is the largest at $x=z=0$ and decreases with x as well as with z. K. Sagisaka (1954), who investigated the crustal deformation accompanying the North-Izu earthquake (1930), assumed the constant amplitude of horizontal displacement with depth, whereas S. Homma (1952) arrived at the conclusion that v increases with z. The writer's result is different from both of them. Since we have no data about the features of deformation below the earth's surface, we can not conclude which one of the three is the most reasonable.

In order to compare the theory with the observational results, we illustrate the relation

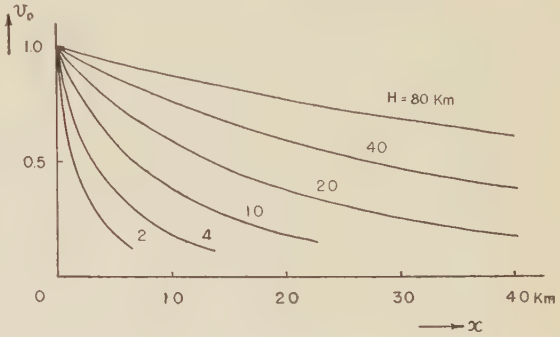

Fig. 4. Diminution of v_0 with distance (x).

between v_0 and x in Fig. 4, wherein the depth of the fault, H, is taken as a parameter. The curves are in the tendency quite similar to the distribution of v_0 as actually observed (see Fig. 5). The fact that the displacement of triangulation points shows a characteristic tendency has already been pointed out by H. F. Reid (1911), who investigated the crustal deformation accompanying the California earthquake of 1906. However, no quantitative discussion of such a tendency has not been given yet. The present model provides a reasonable interpretation for the above-mentioned tendency and makes it possible to estimate the probable value of H, by applying the curves in Fig. 4 to the observed data. Fig. 5 shows that the diminution of v_0 can be well explained provided we take $H=15$ km.

In the foregoing discussion we dealt with the

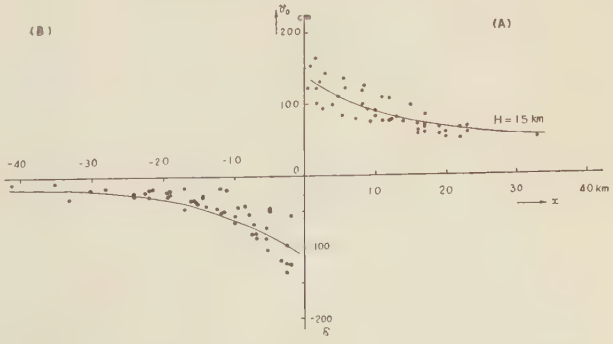

Fig. 5. Diminution of horizontal displacement (v_0) with distance (the Tango district).

relative value of v_0 taking v at $x=z=0$ as a unit. The absolute value of $v(x=z=0)$ is given, in the present theory, as the function of the rigidity of the crust, μ, and of the magnitude of stress change on the fracture plane, $(Y_x)_{x=0}$. Taking μ as 5×10^{11} c.g.s., for instance, we get, $(Y_x)_{x=0}=3\times10^{7}$ c.g.s.. This is of the order of strength of ordinary rocks, so that the agreement of both the quantities may be regarded as another proof for the present model. Since the displacement is known from point to point, strain energy associated with the deformation can be estimated, too. Taking the above-mentioned values into consideration, we estimate the energy at 4×10^{22} ergs, where the integration of energy is carried out for the volume which is 30 km long along the fault. This is an approximate value of the fault's length, which is presumed on the basis of some aspects of the earthquake. Seismometrical studies of the Tango earthquake have concluded that the energy of seismic waves was as much as 10^{23} ergs, approximately. Such amount of wave energy can be supplied from the fault movement of the above-mentioned condition, provided it takes place in a very short time (see Section 4).

§ 3. Seismic waves caused by fault movement

The wave-form and direction of the initial motion are regarded as another kind of information about what occurs at the seismic origin. It is necessary to examine how well the proposed model can explain the observed facts in regard to those points. Although it is difficult to deal with the dynamical characteristics of faulting strictly, an approximate examination for a two-dimensional case will be effected in the following.

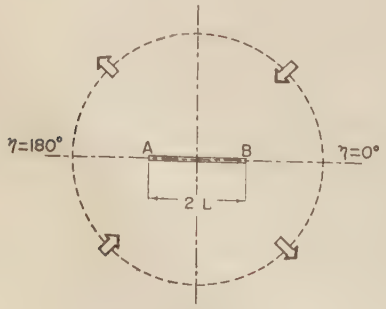

Fig. 6. Type of the initial stress and the fracture (AB).

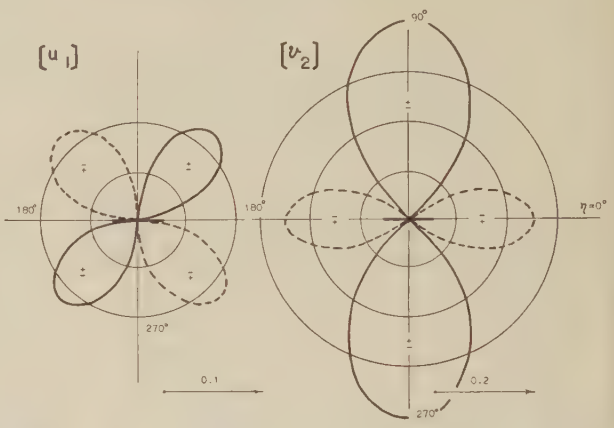

Fig. 7. Azimuthal distribution of displacements u_1 and v_2 at a distant point caused by periodic origin force ($\lambda_S/2L=1.12$).

Let us consider that the medium is initially subject to uniform shear stress and that the fracture $\overline{AB}$ (length: $2L$) takes place in it abruptly (Fig. 6). Such a case can be treated by studying the wave equation in elliptic coordinates (ξ, η). K. SEZAWA (1928) had given the general solution for the equation, on the basis of which the writer worked out a study of wave generation from a fault (K. KASAHARA, 1958). The condition that a fault appears abruptly may be represented by the apparent stress change working so as to cancel the initial stress on the fault plane. Since it is convenient to deal with the stress change in time with respect to its spectrum, we take the following equation as the boundary condition at the origin ($\xi=0$),

$$\widehat{\xi\xi}=0\,, \qquad \widehat{\xi\eta}=Se^{ipt}. \tag{3}$$

In practice, we take several different values of p and carry out numerical calculation for the purpose of obtaining displacement due to P- and S-waves. Fig. 7 illustrates an example of azimuthal distribution of the real part of

u_1 and v_2 at a great distance, where u_1 and v_2 denote displacements due to P-(ξ-component) and S-wave (η-component), respectively. As to P-wave, it is evident that the distribution is of the quadrant type whose nodal lines appear along and perpendicular to the fault. Such a tendency being noticed for all the cases, we may conclude that the model is consistent with the observed pattern of push-pull distribution as shown in Fig. 8.

Fig. 8. Azimuthal effect of the push-pull distribution (initial P-wave) observed in the case of the Tango earthquake (after S. KUNITOMI).

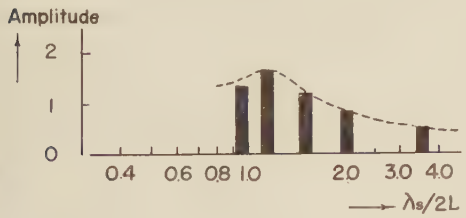

Fig. 9. Amplitude of u_1 plotted against $\lambda_s/2L$.

The result of numerical calculation for various values of p enables us to deduce the spectrum of the wave which is to be generated from the fault. In Fig. 9 are shown the amplitudes of u_1 (relative values) for different periods of the origin force, wherein the abscissa is given with respect to the ratio of λ_s (wave-length referred to the velocity of S-wave) to $2L$. Taking the spectrum of an impulse into consideration, it is readily seen that Fig. 9 also indicates the spectrum of the wave caused by an impulsive excitation at the origin. Accordingly we know that the maximum intensity of the spectrum of P-wave falls on the component whose wave-length, λ_s, is about 1.2 times as large as $2L$. That is to say, the period of the maximum intensity (we called it as the characteristic period, T_0) becomes as long as 11 sec, provided we take $2L$ and v_s as 30 km and 3.2 km/sec, respectively. It is more natural to consider that the stress change associated with faulting is step-like rather than impulsive. If we take this supposition, the characteristic period will be estimated at a larger value, 20 sec or more, say. Seismograms of the Tango earthquake recorded at Hongo, Tokyo, indicates 23 sec as the characteristic period, so that the present model does not contradict with this fact.

§ 4. Synthetical examination of the model and discussion of the related problems

The foregoing two sections have dealt with geodetic and seismological characteristics of the fault model, separately. In the present section, therefore, we shall make synthetical examination taking all the sorts of evidence of the Tango earthquake into consideration. Discussion that has been made previously indicates that the probable condition of the faulting is as shown in the central part of Fig. 10 (model A), where, $2L$, H, θ, and φ denote, respectively, length, depth, strike, and dip of the fault plane, whereas $(Y_x)_0$ is the stress change (shear) to which the plane was subject. Although it is desirable to make all the discussion referring to model A, we shall take more simplified models, B and C, to avoid difficulties in mathematical treatment of the original one. Model B is derived from A by taking L as infinity while all the other conditions are kept unchanged. Model C is given in the similar way by taking H as infinity.

Items which are arranged on the left of the proposed models in Fig. 10 are geodetic aspects of the earthquake. The previous discussion (see Section 2) has proved that the diminution of v_0 can be well interpreted from the standpoint of model B. Geodetic observations revealed, also, more complicated features of deformation distribution at the tails of the faults. Characteristics of these

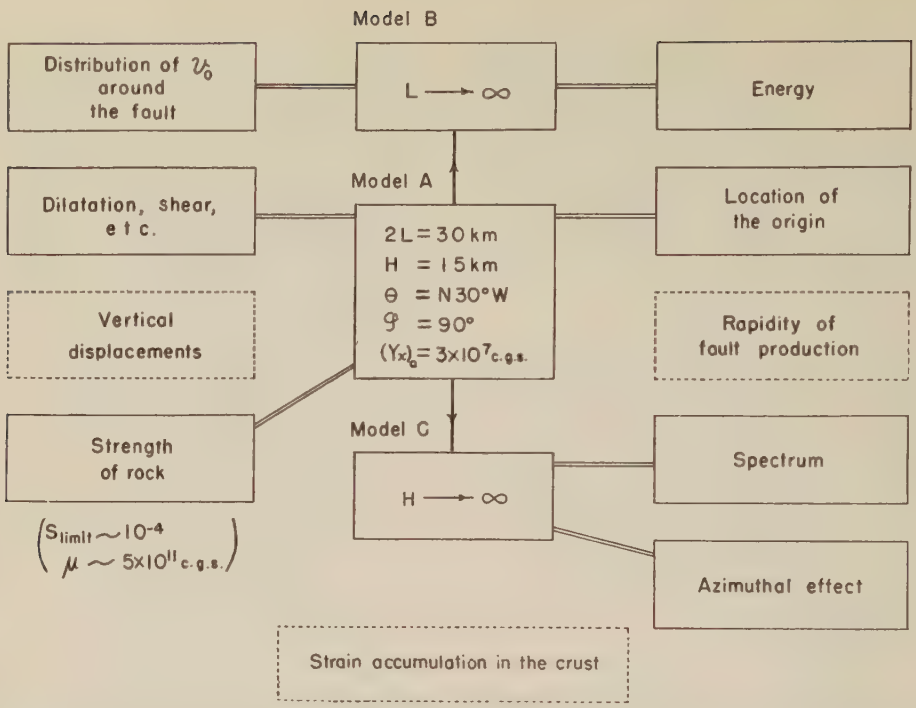

Fig. 10. Relation between the proposed model and various sorts of aspects of the Tango earthquake. Items surrounded by broken lines are the assumptions taken in the discussion.

secondary effects can be seen more clearly with respect to distribution of various sorts of strain components, such as dilatation, shear, and so on (C. TSUBOI, 1933). As it was hardly possible to deal with such effects mathematically, we carried out model experiments previously, by which it was shown that some part of the above-mentioned features could be explained from the viewpoint of model A (K. KASAHARA, 1957).

It is a well-known fact that the mechanical strength of the crust is not infinitely large but there is a certain limit of strain energy to be accumulated there. This information has been got from the distribution of the maximum shear around seismic faults as well as from the upper limit of the magnitude of great earthquakes (C. TSUBOI, 1956). It is notable that the value of $(Y_x)_0$ as given in model A does not contradict with this fact.

We shall now turn the point of discussion to seismological aspects of the earthquake, which are arranged in the right half of Fig. 10. The energy of seismic waves of the Tango earthquake has been estimated at about 10^{23} ergs. We know, after rough estimation based on model B, that the strain energy associated with the crustal deformation amounts to 4×10^{22} ergs. That is to say, the energy which is as much as 4×10^{22} ergs is to be radiated as elastic wave, provided such a deformation arises instantly. The energy associated with the vertical component of deformation and with other strain components is excluded from the present estimation, so that we shall find better agreement of both kinds of energy if they are taken into account.

Seismometrical studies of the Tango earthquake have found out that the epicentre was located on the fault. However, lack of knowledge about the depth of the fault plane has left uncertainty in our discussion of spatial relation of the seismic origin with the faults. The present study provides a concrete answer for the question that the hypocentre (focal depth: 14 km) located at the lower part

of the fault plane. We can not explain what this fact means, but we may suppose, as one of the possible explanations, that the first breaking of the fault arose at that point.

Spectrum and azimuthal effect of the initial P-wave have been investigated in the former section. Seismograms recorded at Tokyo (Hongo) indicates the characteristic period, T_0, to be 23 sec. Mathematical study of model C proved that T_0 is about 11 sec in the case of impulsive excitation at the origin while 20 sec or more, for the step-like one. We have no concrete basis of presuming the mode of stress change, but we might imagine, approximately, that the faulting causes step-like stress change. The azimuthal effect which is derived from the model is also consistent with the observed result (see Fig. 8). Thus we may conclude that the proposed model is acceptable with respect to spectrum and azimuthal effect, provided it is permitted to apply the two-dimensional model to the actual case.

Results of the foregoing discussion appear, therefore, to justify the proposed conditions for the Tango earthquake. We have to remark, however, that no discussions have been made about some other factors notwithstanding their importance. These are shown in Fig. 10 being surrounded with broken lines. First, we did not discuss the physical meaning of the vertical component of deformation. It is needless to say that the factor brings, also, valuable information about the nature of the origin, so that further improvement of the fault model should be made so as to take the mentioned factor into consideration. Second, we assumed that the faulting took place in a very short time. Rapidity of fault production has much influence on the efficiency of energy radiation as well as on the feature of spectrum. Although we have no observational data accurate enough for discussing the rapidity, some macroseismic studies of other earthquakes are likely to suggest that main part of the crustal deformation is completed within a short time, some ten seconds, say. If it is so, the above-mentioned conclusions would not suffer any drastic alteration. The third assumption was taken on the possibility of strain accumulation. Geophysicists have discussed the problem in relation to the tectonophysical conditions of the earth (*f.i.* H. Jeffreys, 1952; T. Matuzawa, 1953), who found out several possible causes of strain accumulation. Although the problem has not been solved completely yet, we may say that we have good reason to justify the above-mentioned assumption. The writer worked out a study of Matuzawa's model for the purpose of examining whether or not the strain accumulation is much influenced by viscous flow of rocks (K. Kasahara, 1956). According to the study, energy dissipation due to the viscous flow is not so large as to deny the possibility of strain accumulation.

Thus it has been shown that the proposed conditions of faulting is acceptable as a possible model of the origin of the Tango earthquake. The question that is to be raised on the next step is if the similar model is applicable to the other cases. Unfortunately, we are far away from getting a definite answer for the question. However, we know some special cases, such as the North-Izu earthquake (1930), whose aspects (geodetic and seismological) were similar to those of the Tango earthquake. It is very likely that the present model is also applicable to them without great alteration of its fundamental conditions.

On the contrary, it would be hardly possible to find out concrete conditions at origins for the other earthquakes which are not accompanied by crustal deformation of simple features. The writer would like here only to mention the result of his previous analysis, which treated the density of energy accumulation around seismic origins and proved that there was no significant difference, from such a standpoint, between earthquakes occurring at different depth in the earth (K. Kasahara, 1957). This fact might be the evidence for their mechanism of occurrence being similar with each other.

§ 5. Conclusions and acknowledgement

The writer worked out a study of geodetic and seismological characteristics of a model

of faulting with the intention of finding out the probable physical conditions at seismic origins. It is assumed that a vertical fracture plane of finite dimension takes place in the extremely strained crust (half-space), which results in radiation of seismic waves as well as in crustal deformation around the fault.

We applied the results of the writer's previous studies to the case of the Tango earthquake, and determined, numerically, various conditions at the seismic origin as shown in Fig. 10. Synthetical examination of the proposed conditions with the observational data has proved that the model adopted here is consistent not only with the geodetic aspects but also with seismological ones. Taking this result into consideration, we might conclude that the physical conditions at the actual origin do not differ much from those of the model.

We can not say much about further application of the model to other cases. Some of the earthquakes, such as the North-Izu earthquake, are likely to be of the similar features with those of the Tango earthquake. In such cases, there is a possibility of interpreting the mechanism at their origins from the present standpoint.

The writer expresses his sincere thanks to Prof. Chuji TSUBOI and Prof. Takahiro HAGIWARA of Tokyo University for their encouragement and support throughout the preparation of this paper. Also the writer owes many thanks to Dr. Tsuneji RIKITAKE who gave him valuable advice.

Notes added in proof. Crustal deformation around a fault has also been investigated by L. KNOPOFF (1958, Geophys. Journ., R.A.S., **1**, 44–52) and P. BYERLY and J. DENOYER (1958, Contributions in Geophysics in Honor of Beno GUTENBERG, 17–35), recently. They dealt with the diminution of v_0 with distance and arrived at a conclusion which does not differ much from the writer's.

References

BYERLY, P.:
1955 Nature of faulting as deduced from seismograms. Geol. Soc. Amer., Special Paper **62**, 75–85.

HODGSON, J. H.
1957 Nature of faulting in large earthquakes. Bull. Geol. Soc. Amer., **68**, 611–644.

HOMMA, S.:
1952 Energy of the crustal deformation. Quart. Journ. Seismology, C.M.O., **16**, 57–66 (in Japanese).

HONDA, H.:
1957 The mechanism of the earthquakes. Sci. Rep. Tohoku Univ., Ser. 5, **9**, Supplement.

JEFFREYS, H.:
1952 "The Earth" 3rd ed. (Cambridge).

KASAHARA, K.:
1956 Strain energy in the visco-elastic crust. Bull. Earthq. Res. Inst., **34**, 157–165.
1957 The nature of seismic origins as inferred from seismological and geodetic observations (1). Bull. Earthq. Res. Inst., **35**, 473–532.
1958 The nature of seismic origins as inferred from seismological and geodetic observations (2). Bull. Earthq. Res. Inst., **36**, 21–53.

KUNITOMI, S.:
1930 Note on the Tango earthquake of March 7, 1927. Geophys. Mag., **2**, 65–89.

MATUZAWA, T.:
1953 Feldtheorie der Erdbeben. Bull. Earthq. Res. Inst., **31**, 179–201.

REID, H. F.:
1911 The elastic-rebound theory of earthquakes. Bull. Dept. Geol. Sci., Univ. California, **6**, 413–444.

SAGISAKA, K.:
1954 On the energy of earthquakes. Geophys. Mag., **26**, 53–82.

SEZAWA, K.:
1928 Propagation of elastic waves from an elliptic or a spheroidal origin. Bull. Earthq. Res. Inst., **2**, 29–48.

TSUBOI, C.:
1933 Investigation on the deformation of the earth's crust found by precise geodetic means. Jap. Journ. Astro. Geophys., **10**, 93–248.
1956 Earthquake energy, earthquake volume, aftershock area, and strength of the earth's crust. Journ. Phys. Earth, **4**, 63–66.

Observation of Near-by Microearthquakes with Ultra Sensitive Seismometers at Matsushiro, Japan.

By

Toshi ASADA

Geophysical Institute, Tokyo University

Shigeji SUYEHIRO

Japan Meteorological Agency

Kei AKAMATU

Geophysical Institute, Tokyo University

Abstract

A temporary observation of near-by microearthquakes was made with Ultra Sensitive Seismometers at Matsushiro. The purpose of this experiment was to see the relation between the frequency of near-by microearthquakes and the annual number of near-by shocks felt at Matsushiro.

The results and conclusions are as follows. An average of one microearthquake occurs every hour. The average annual number of earthquakes felt at Matsushiro is about 1.2. As M of the microearthquakes are from less than -1 to 0, and M of near-by felt earthquakes are about 4∼5, we have an equation,

$$\log N = 3.6 - 0.77M,$$

where N is the annual number of earthquakes whose M are between M–0.5 and M+0.5. This equation holds good in the relation between N and M of earthquakes with M from -1 to 5 occurring in the vicinity of Matsushiro (area $\approx 60 \times 60$ km^2).

As the equation is valid in such a wide range of M, it will be possible to determine the seismicity of a certain region within a rather short period of time through observing microearthquakes.

The E of the minimal recorded earthquake was about 10^9 ergs in this experiment. Its M was approximately -2.

§ 1. Introduction

One of the present writers made a temporary observation of near-by microearthquakes at Mt. Tsukuba with Ultra Sensitive Seismometers in 1955 (ASADA, 1957a). The principal purpose of this experiment was to estimate the energy of the smallest detectable shock and to see if the equation between the number and magnitude, $\log N = a - bM$, holds good in a wider range of M than has ever been investigated.

The conclusions of the experiment at Mt. Tsukuba are as follows.

1) The energy of the minimal recorded shock was of the order of 10^{10} ergs. This value was calculated according to the formula of the kinetic energy of spherical waves, assuming a proper constant of absorption. Also the M of this shock was determined to be -1.1.

2) In the vicinity of Mt. Tsukuba an average of 200 shocks of energy (10^{10}∼10^{13} ergs) occur every 24 hours. Shocks of M 4∼5 occur 40 to 50 times every year in the same area. Accordingly, we can conclude safely that the equation, $\log N = a - bM$, ($b \fallingdotseq 0.8$), is valid in the range of M from less than 0 up to 5.

3) The space distribution of the shocks of $M \lesssim 0$ agrees with that of the shocks of M 4∼5.

4) The predominant frequencies in the motions due to near-by microearthquakes are about several tens of a cycle per second. Ac-

cordingly, these shocks can be recorded only by a seismometer sensitive enough in the frequency band from 10 cps to 100 cps.

In order to check the above conclusions the present writers installed the Ultra Sensitive Seismometers at the Matsushiro Observatory of Japan Meteorological Agency and made a temporary observation in August 1956. The location of Matsushiro is shown in the map in Fig. 1.

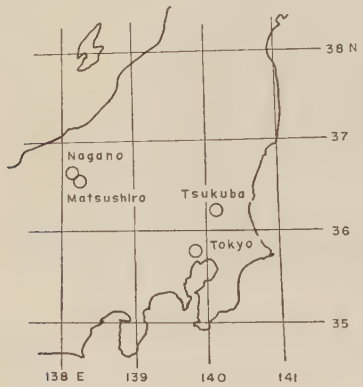

Fig. 1.

Two ten-cps velocity seismometers, vertical and horizontal, and one one-second horizontal velocity seismometers were set up in a vault-(a), and a one-second horizontal velocity seismometer was set up at a position-(b) about 200 meters apart from the position-(a) in order to discriminate small earthquakes from disturbing noises (ASADA, 1957a).

Their electrical outputs were amplified and recorded side by side on a photograhic paper with an oscillograph. The out put of a ten-cps vertical seismometer was amplified and differenciated in another channel simultaneously and recorded on the same photographic paper. A visible recorder was also used. Its galvanometer was fed by a power amplifier connected to the preamplifier of one-second seismometer (No. 3, in Table 1). The visible recorder was operated continuously for 13 days. The oscillograph was operated only when the ground was very quiet.

Frequency responses of the ten-cps and one-second velocity seismometers are given in Fig. 2 and Fig. 3. The sensitivity of the ten-cps

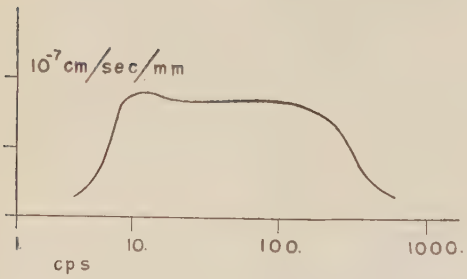

Fig. 2. Frequency response of ten-cps velocity seismometer.

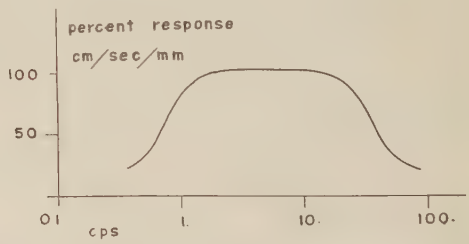

Fig. 3. Frequency response of one-second velocity seismometer.

Table 1. Natural periods, components and positions of seismometers.

No.	T_0	Component	Position	Trace in photographic paper
No. 1	10 cps	Vertical	a	A B*
No. 2	10 cps	Horizontal	a	C
No. 3	1 sec	Horizontal	a (Power amplifier—Smoked paper recorder)	D
No. 4	1 sec	Horizontal	b	E

* The output of the No. 1 ten-cps seismometer was amplified and differentiated in another channel and recorded in Trace B on the same paper.

seismometer is 8.6×10^{-7} cm/sec/mm or 1.2×10^{6} mm/cm/sec in the frequency band from 10 cps to 200 cps. The sensitivity of the one-second seismometer is about the same order as that of the ten-cps seismometer in the frequency band from 2 cps to 20 cps. However, the former is not appropriate for recording the shocks of M less than 0. The frequency responses of Galitzin and other seismometers for routine observation compared with those of Ultra Sensitive Seismometers are given in Fig. 4.

Table 2. Frequency distribution of trace amplitude of seismograms recorded with one-second velocity seismometer with visible recorder.

Trace Amplitude	Frequency	
1.1– 2.0 mm	24	
2·1– 3.0	16	
3.1– 4·0	22	86
4.1– 5·0	8	
5.1– 6·0	16	
6.1– 7.0	6	
7.1– 8.0	11	
8.1– 9.0	4	29
9.1–10.0	6	
10.1–11.0	2	
11.1–12.0	4	
12.1–13.0	0	
13.1–14.0	5	11
14.1–15.9	1	
15.1–16.0	1	
16.1–17.0	1	
17.1–18.0	4	
18.1–19.0	0	6
19.1–20.0	1	
20.1–21.0	0	

§ 2. Minimal recorded earthquake and its energy

One hundred and twenty one shocks of hypocentral distances smaller than 70~80 km were recorded by the visible recorder during the course of 13 days. Forty-three shocks occurring within the distance of 70~80 km from the observatory were recorded on the oscillograph during 45 hours in total, or an average of about 24 shocks occurred every 24 hours. The frequency distribution of the maximum trace amplitude of the seismograms on the visible recorder of the one-second velocity seismometer is shown in Table 2 and Fig. 5. This distribution can satisfy the equation (Suzuki, 1953),

$$N(A)\cdot dA=kA^{-m}dA, \qquad (2.1)$$

where the value of m is approxima-

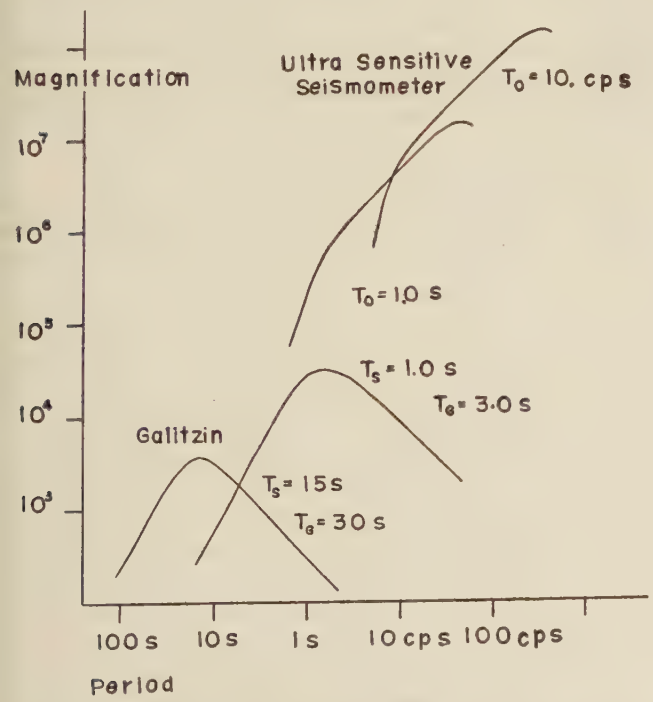

Fig. 4. Frequency responses of Ultra Sensitive seismometers, Suyehiro vertical seismometer (T_s=1.0s, T_g=3.0s), and Galitzin seismometer.

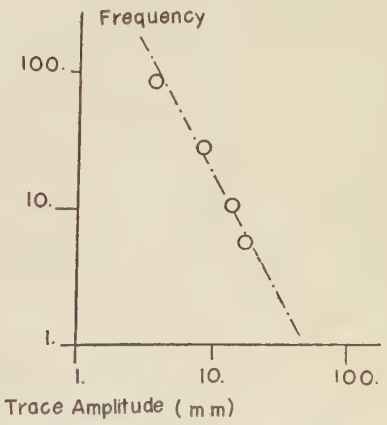

Fig. 5. Frequency distribution diagram of trace amplitudes of seismograms recorded by one-second velocity seismometer with visible recorder.

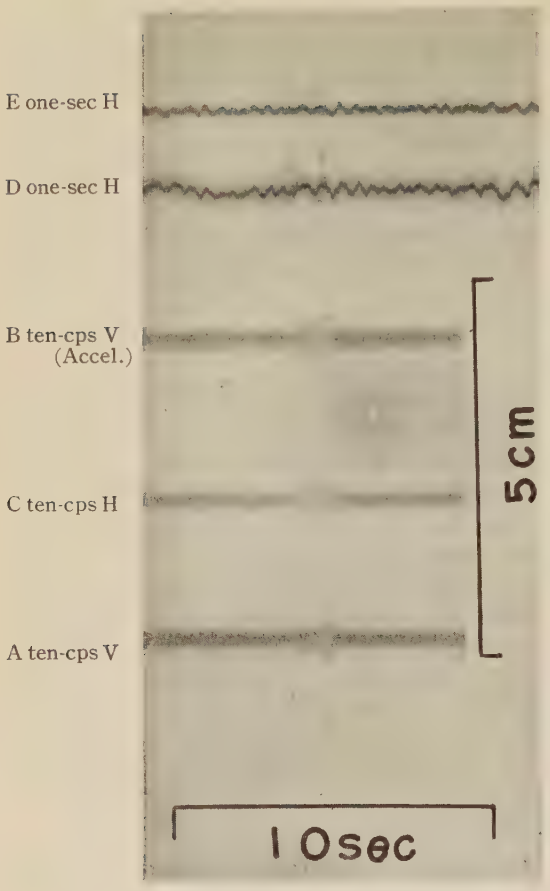

Fig. 6. Seismograms of minimal recorded earthquake recorded at Matsushiro.

tely 1.8. The E of these shocks are from 10^{10} ergs to 10^{12} ergs as will be described below.

In Fig. 6 the seismograms of one of the minimal recorded earthquakes are given. These seismograms give us the information on the predominant periods because the seismometers of different responses are used. Comparing the seismograms A, C, and B with D and E, one can easily see that their predominant frequency is higher than several tens of a cycle per second.

The P-S interval of this shocks is 0.96 sec, and the maximum velocity amplitude is about $5\times8.6\times10^{-7}$ cm/sec, or 4×10^{-6} cm/sec. The minimal detectable earthquake recorded at Mt. Tsukuba in 1955 had a P-S interval of 4.0 sec and a maximum velocity amplitude of 3.5×10^{-6} cm/sec. Its E was estimated at about 10^{10} ergs (ASADA, 1957a). Accordingly, we may determine the E of the shock shown in Fig. 6 if the wave attenuation in the crust is assumed. Now assuming that the attenuation is proportional to 2nd or 1.5th power of the distance (DEN, 1953) and E is proportional to the square of the amplitude, E of this minimal recorded shock is

$10^{10}\times(4/3.5)^2\times(0.96/4)^2=6.2\times10^8$ ergs, or
$10^{10}\times(4/3.5)^2\times(0.96/4)^{1.5}=1.1\times10^9$ ergs.

In determining E of a shock, the accuracy being very low, we may say that E of this shock is about of the order of 10^9 ergs. The approximate value of its M can be obtained also, if we assume the decay of waves is proportional to 1.5th power of the hypocentral distance. The maximum trace amplitude of this shock should be about 0.012 microns if it were recorded by a " standard " seismometer at the hypocentral distance of 100 km as its maximum displacement at the hypocentral distance of about 7 km is 2.3×10^{-8} cm at 30 cps or 4×10^{-6} cm/sec. Accordingly, the values of its M is about -2.

As the sensitivity of the seismometer with power amplifier and visible recorder decreases in the frequency range higher than about 20 cps, E of the shocks (P-S $<$ 10 sec) recorded on the smoked paper are from 10^{10} ergs to 10^{12} ergs.

§ 3. Space distribution of microearthquakes and small shallow shocks felt at Matsushiro

The frequency distribution of P-S intervals of microearthquakes occurring in the vicinity of Matsushiro is given in Table 3 and Fig. 7. The frequency distribution of P-S intervals of the microearthquakes recorded at Mt. Tsukuba is given in Fig. 8. The diagram in Fig. 8 shows that most of the shocks have P-S intervals larger than 5 sec, although the greater part of the shocks recorded at Matsushiro have P-S intervals smaller than 5 sec. From this we interprete that the earthquakes occur not in the crust but in the upper part of the mantle in the vicinity of Mt. Tsukuba, while in the vicinity of Matsushiro the shocks occur in the crust only (ASADA and DEN, 1954).

The list of the shocks felt at Matsushiro is given in Table 4. Comparing the frequency diagram in Fig. 7 with the data in Table 4, it may be seen that the microearthquakes occur almost in the same part of the crust as the shocks of M 4~5 listed in the table.

The list in Table 4 shows that the number of near-by earthquakes felt at Matsushiro is an average of 1.2 every one year. As the magnitudes of microearthquakes occurring in the vicinity of Matsushiro (area$\approx 60\times 60\,km^2$) are approximately from -1 to 0 and the annual frequency is about 8700 (24 eqks/day), we can calculate the values of a and b in the equation, $\log N = a - bM$ (GUTENBERG and RICHTER, 1942, 1956), for the range of M from -1 to 5. Putting into the equation the number of shocks of M 4~5, we get,

$$a = 3.6, \text{ and } b = 0.77.$$

Of course the second digits of these values are of little significance.
The equation

$$\log N = 3.6 - 0.77M \qquad (3.1)$$

holds good in the range of M from -0.5 to 4.5 where N is the annual number of earthquakes whose M is between M–0.5 and M+0.5. As the equation is valid in such a wide

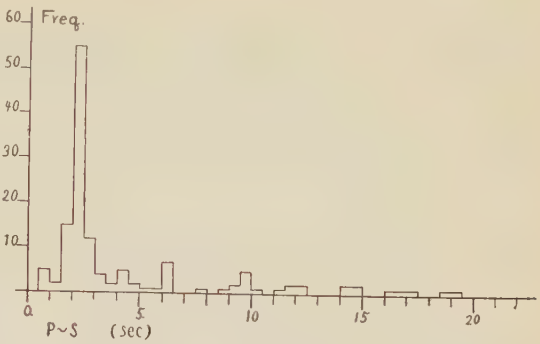

Fig. 7. Frequency distribution of P-S intervals of near-by microearthquakes recorded at Matsushiro.

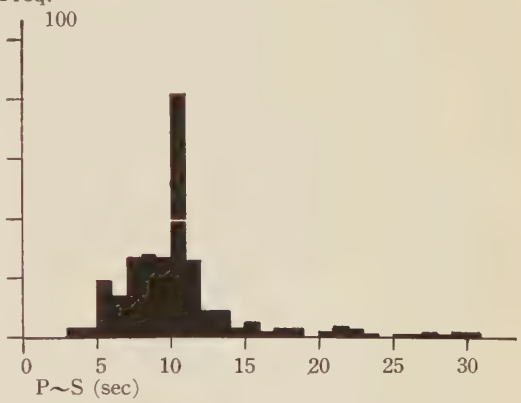

Fig. 8. Frequency distribution of P-S intervals of near-by microearthquakes recorded at Tsukuba.

Table 3. Frequency distribution of P-S intervals of shocks recorded at Matsushiro

P-S (sec)	Frequency	P-S (sec)	Frequency	P-S (sec)	Frequency
0.5 ≤<0.6	0	2.8 — 2.9	4	5.1 — 5.2	0
0.6 — 0.7	0	2.9 — 3.0	0	5.2 — 5.3	1
0.7 — 0.8	4	3.0 — 3.1	1	5.3 — 5.4	0
0.8 — 0.9	0	3.1 — 3.2	1	5.4 — 5.5	0
0.9 — 1.0	1	3.2 — 3.3	1	5.5 — 5.6	1
1.0 — 1.1	0	3.3 — 3.4	0	5.6 — 5.7	0
1.1 — 1.2	0	3.4 — 3.5	1	5.7 — 5.8	0
1.2 — 1.3	0	3.5 — 3.6	0	5.8 — 5.9	0
1.3 — 1.4	1	3.6 — 3.7	2	5.9 — 6.0	0
1.4 — 1.5	1	3.7 — 3.8	0	6.0 — 6.1	1
1.5 — 1.6	1	3.8 — 3.9	0	6.1 — 6.2	1
1.6 — 1.7	2	3.9 — 4.0	0	6.2 — 6.3	4
1.7 — 1.8	3	4.0 — 4.1	0	6.3 — 6.4	0
1.8 — 1.9	6	4.1 — 4.2	1	5.4 — 6.5	1
1.9 — 2.0	3	4.2 — 4.3	1	6.5 — 6.6	1
2.0 — 2.1	9	4.3 — 4.4	1	6.6 — 6.7	0
2.1 — 2.2	6	4.4 — 4.5	2	6.7 — 6.8	0
2.2 — 2.3	36	4.5 — 4.6	1	6.8 — 6.9	0
2.3 — 2.4	2	4.6 — 4.7	0	6.9 — 7.0	0
2.4 — 2.5	2	4.7 — 4.8	0	7.0 — 7.1	0
2.5 — 2.6	0	4.8 — 4.9	1	7.1 —10.1	9
2.6 — 2.7	3	4.9 — 4.0	0	10.1 —20·1	14
2.7 — 2.8	5	5.0 — 4.1	0	20.1 ≤	13

Table 4. Minor shocks felt at Matsushiro and its visinity

		d.	h.	m. (J.S.T.)	C.M.O. Intensity	P-S sec	
1952	July	17	07	32	0		
1953	Dec.	27	14	59	III	1.4	[36.5N, 138.2D]
	Feb.	1	15	47	0	2.3	felt at Yashiro
	May	7	01	52	0	3.0	felt at Nagano
	July	6	03	35	0	1.1	
	July	6	03	38	1	1.2	
1954	Feb.	15	14	44	1	4.1	[36.7N, 137.8E]
	Sept.	10	04	56	0		felt ot Nagano
1955	Aug.	7	12	50	0		felt at Nagano.
	Oct.	6	07	21	0	2.1	felt at Nagano
	Oct.	24	03	40	0	1.3	
1956	Jan.	27	15	04	1	?	
	May	23	13	27	0	4.6	

range of M, it is possible to determine the seismicity of a certain region within a rather short period of time through observing micro-earthquakes.

This was the case in the "shallow" earthquakes occurring in the vicinity of Mt. Tsukuba in the depth from 30 to 70 km, although the value of coefficient b is slightly different from the present one.

The frequencies of bigger earthquakes occurring in this area calculated according to this equation (3.1), are shown in Table 5. The major earthquakes which have actually occurred in this region are listed in Table 6. The calculated values seem to agree with the actual ones. The difference is of course statistically insignificant. The size of the data is, however, too small to conclude decisively that the equation (3.1) holds good in the magnitude range from −0.5 to 7.5.

Table 5. Number of shocks calculated according to the equation, (3.1).

M	Frequency
4~5	1.2/1 year
5~6	2/10 year
6~7	3.4/100 years
7~8	5.7/1000 year

§ 4. Seismograms

The seismograms in Fig. 6 show very clearly that their predominant frequencies are more than several tens of a cps. It can be seen that the one-second velocity seismometer cannot register the minimal recorded earthquake well. Most of electro-magnetic seismometers coupled directly with galvanometers have their maxi-

Table 6. Earthquakes ($M \gtrsim 6.0$) occurred in the vicinity of Nagano and Matsushiro.

1953	October 13	Nojiriko	138.2°E	36.8°N	M=6.0
1941	January 15	Nagano	138.2°E	36.7°N	M=6.4
1897	January 17	Chikuma-gawa			M=6.3
1858	April 23	Shinano-Matsushiro			M=5.9
1853	January 26	Shinano-Hanishinagun			M=5.9
1847	May 8	Zenkoji			M=7.4

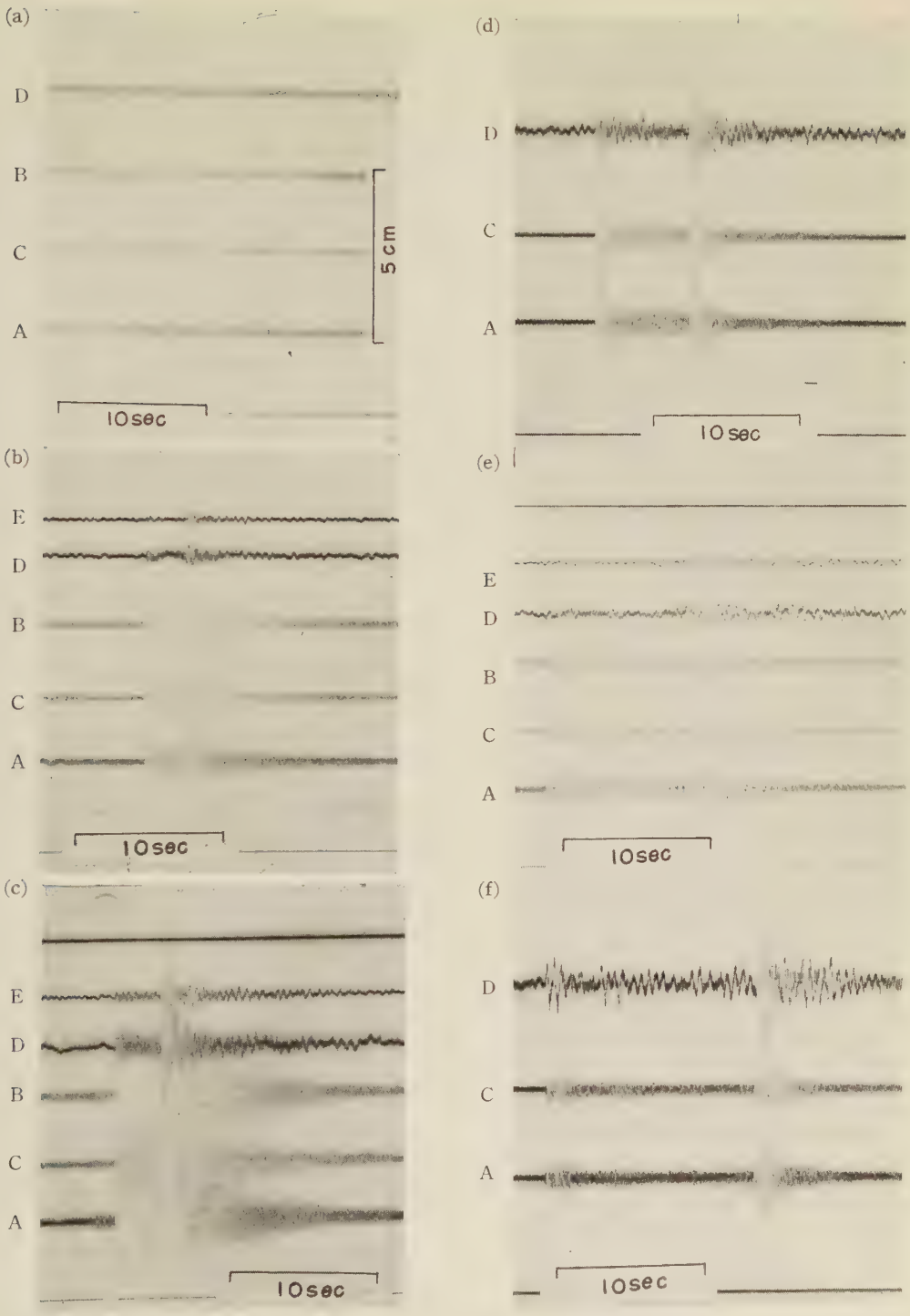

Fig. 9. Seismograms of shocks whose hypocentral distances are smaller than 180 km.

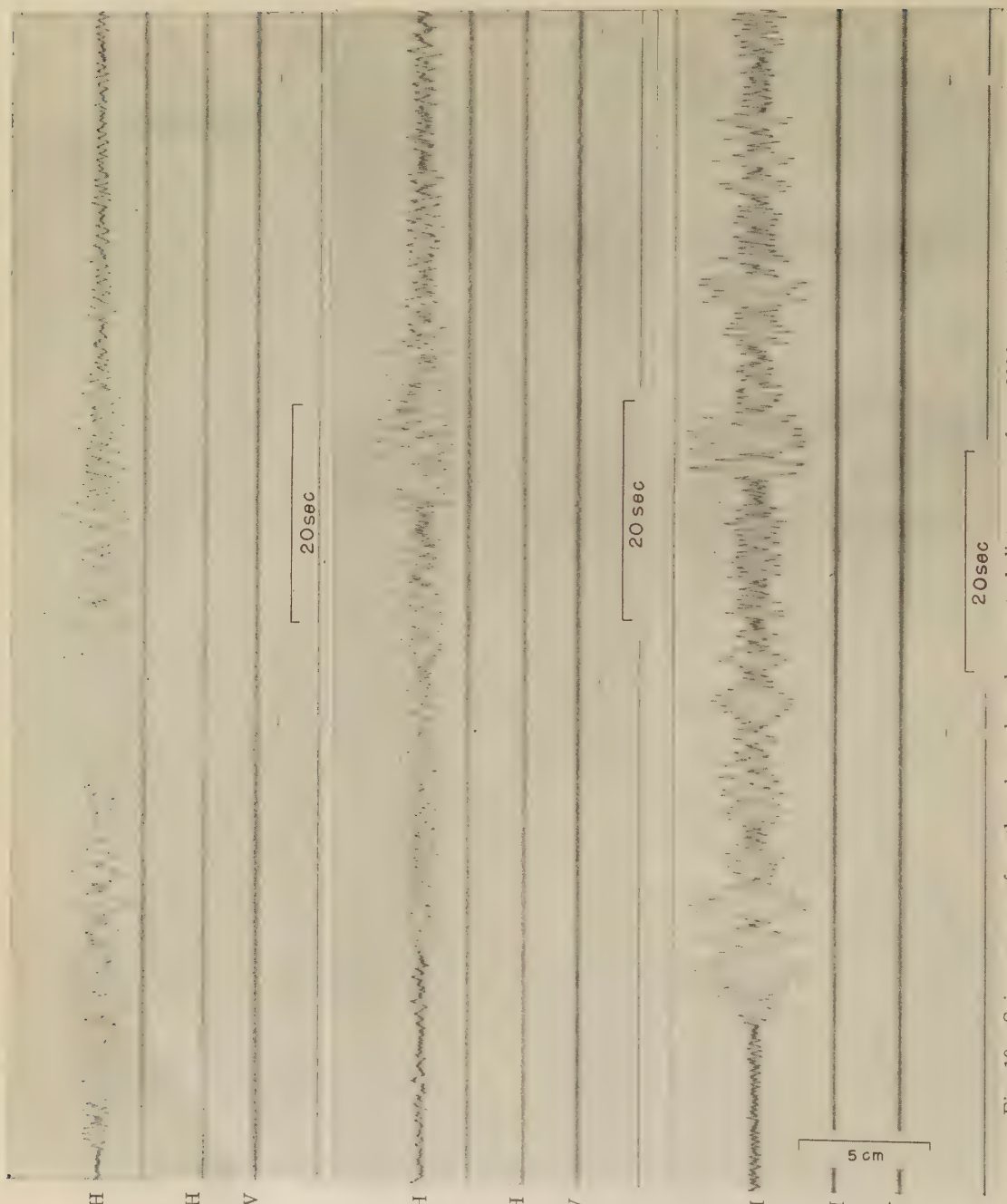

Fig. 10. Seismograms of earthquakes whose hypocentral distance are from 200 km to 400 km.

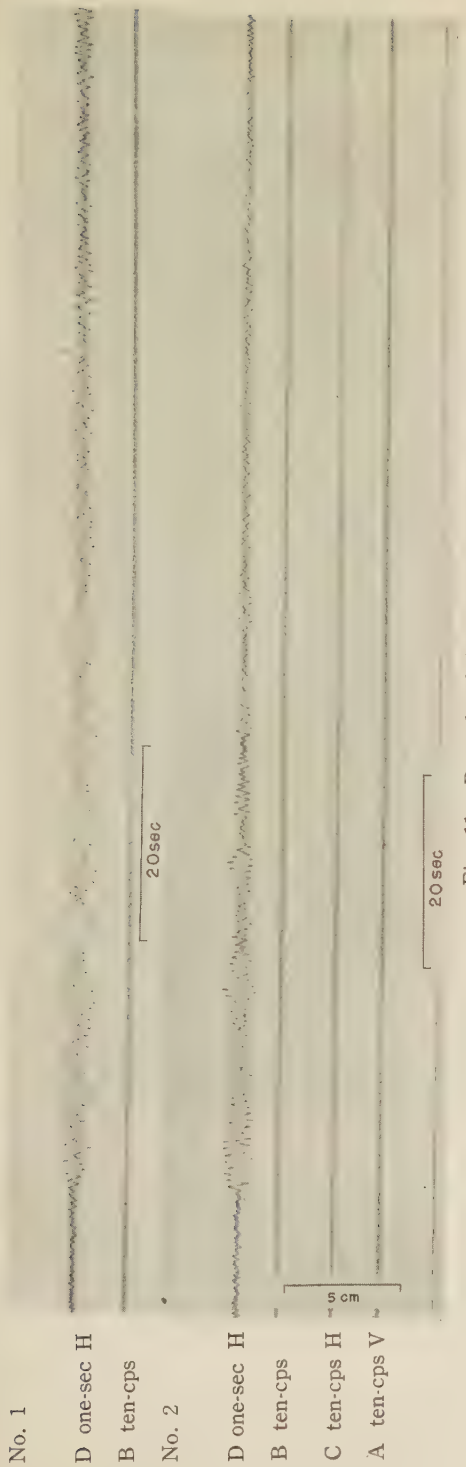

Fig. 11. Records of distant earthquakes.

mum magnification at 0.2 sec or longer periods and their magnification mostly 10^5 or smaller. Accordingly, the earthqukes with E (10^{12} ergs or smaller) cannot be registered well by these seismometers even if the hypocentral distances are 10 to 20 km.

The present writers have obtained many seismograms of near-by microearthquakes in this experiment. These have enabled us to see qualitatively the relation between the predominant frequency and the magnitude of microearthquakes (Asada, 1953) (Aki 1955). Several examples of near-by earthquakes are given in Fig. 9. In comparing these seismograms recorded by the seismometers with different responses, one can see that the waves of several tens of a cps are predominant. Only the earthquakes of E (10^{12} ergs or bigger) (e.g., (d), (e), and (f) in Fig. 9) have the wave trains with periods of about 0.5 sec.

The seismograms in Fig. 10 are those of shocks with hypocentral distances from about 200 km to 400 km. The waves of these shocks are not recorded by ten-cps velocity seismometers.

In Fig. 11 the examples of seismograms of distant earthquakes are given. Fig. 12 shows the seismograms of the same earthquakes recorded by a seismometer of $T_0=1$ sec and $T_g=3$ sec whose response is shown in Fig. 4.

The seismogram A in Fig. 12 is due to the same earthquake as No. 3 in Fig. 10. In Fig. 12, B is the same as No. 2 in Fig. 10, and C in Fig. 12 is the same as No. 1 in Fig. 11. The epicenter of the earthquake, No. 1 in Fig. 10, is in Bolivia, 15°S 68°W, $h=100$ km $M=6\frac{1}{2}\sim 6\frac{3}{4}$). The earthquakes shown in Fig. 10 occurred in Molucca Passage ($M\approx 5$).

The earthquakes shown in Fig. 9 were not recorded by the seismometer of $T_0=1$ sec and $T_g=3$ sec because of its low sensitivity.

It should be stated also that the seismograms of the earthquakes with hypocentral distances from several hundred to one thousand km recorded at Mt. Tsukuba contain the waves with frequencies shorter than 10 to 20 cps. This stands in a striking contrast with the case of Matsushiro and may be

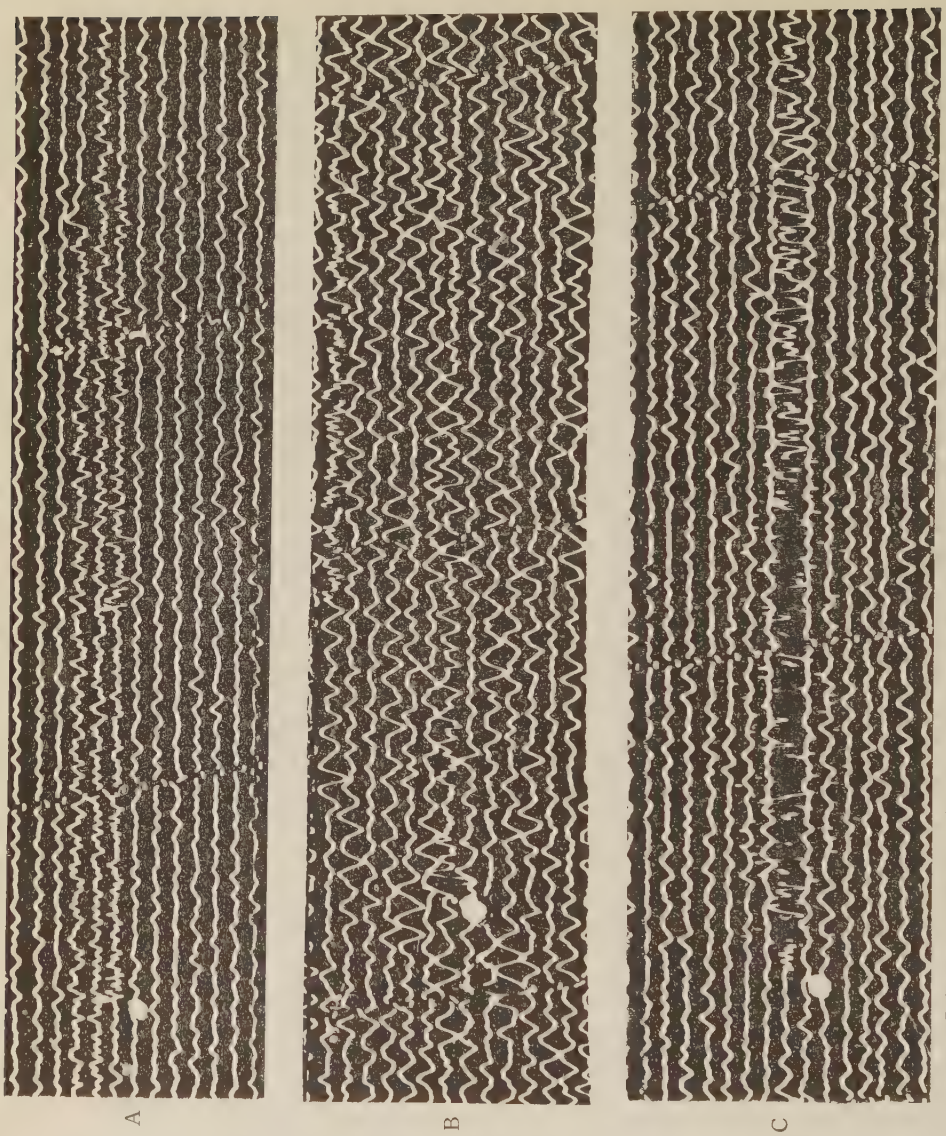

Fig. 12. Seismograms recorded by a SUYEHIRO vertical seismometer. A—Fig. 10, No. 3, B—Fig. 11, No. 2, C—Fig. 11, No. 1.

because the attenuation of wave in the crust or in the upper part of the mantle under Mt. Tsukuba is smaller than that under Matsushiro.

§ 5. Conclusion

The results of the present experiment made at Matsushiro lead to the following conclusions.

(1) Microearthquakes of E from 10^{10} to 10^{12} ergs and bigger shocks of magnitudes up to 4 or 5 occur in the shallow part of the crust in the vicinity of Matsushiro. No earthquake occurs under the Mohorovičić discontinuity here. This is the case in the greater part of other areas in the world although almost all earthquakes occur in the upper part of the mantle in the vicinity of Mt. Tsukuba.

(2) The energy of the minimal detectable earthquakes recorded at Matsushiro is about 10^9 ergs.

(3) In the vicinity of Matsushiro an average of 24 microearthquakes occur every 24 hours. Six earthquakes of M 4~5 occurred during

these 5 years in the same area (area is approximately 60×60 km^2).
Accordingly, the equation,

$$\log N = 3.6 - 0.77M,$$

holds good in the range of M from -0.5 to 4.5, where N is the annual number of earthquakes whose magnitude is between $M-0.5$ and $M+0.5$ occurring in this area.

The seismicity of this area is about 1/5～1/10 of that in the vicinity of Mt. Tsukuba.
(4) The problem still is to see whether or not that the extrapolated values of N in the equation written above for larger values of M coincide with the actual values of frequency of earthquakes of M from 4.5 to 7.5. No statistically significant difference between the calculated and actual values is found but the size of the present data is small and insufficient to conclude that the range of M in which the equation holds good can cover from -0.5 up to 7.5.

Aknowledgment

The authors wish to express their thanks to Drs. Wadati and Sagisaka who permitted them to carry their experiment at The Matsushiro Observatory of Japan Meteorological Agency. The authors also thank the members of the Observatory for their kind help and Messrs. Kurimoto and Terashima for their generous assistance.

Bibliography

Aki, K.,
1955 Correlogram Analysis of Seismograms. Zisin II (Journal of Seism. Soc. Japan), **8**, pp 99–107.

Asada, T.,
1953 On the Relation between the Predominant Period and the Maximum Amplitude of Earthquake Motions. Zisin II (Journal of Seism. Soc. Japan), **6**, pp 69–73.
1957 a. Observation of Near-by Earthquakes with Ultra Sensitive Seismometers. Journal of Physics of the Earth, **5**, pp 83–113.
b. Frequency Distribution of Earthquake Magnitude, Seismicity and Related Problems. Zisin II (Journal of Seism. Soc. Japan), **10**, pp 24–34.

Asada, T. and Den, N.,
1954 On the Frequency Distribution of the P-S Intervals of Earthquakes Recorded at a Certain Station. Zisin II (Journal of Seism. Soc. Japan), **7**, pp 37–44.

Den, N.,
1953 On Very Low Frequency Amplifiers to Observe the Explosion Seismic Waves. Zisin II (Journal of Seism. Soc. Japan), **6**, pp 101–108.

Gutenberg, B. and Richter, C. F.,
1951 Earthquake Magnitude, Intensity, Energy and Acceleration B.S.S.A., **32**, pp 163–191.
1956 Earthquake Magnitude, Intensity, Energy and Acceleration B.S.S.A., **46**, pp 105–146.

Suzuki, Z.,
1953 A Statistical Study on the Occurrence of Small Earthquakes, I, Sci. Rep. Tohoku Univ., Ser. 5, Geophys., **6**, pp 177–182.

Earthquake Province—Domain of Sympathetic Seismic Activities

By

Chuji TSUBOI

Geophysical Institute, Tokyo University, Tokyo.

Abstract

The notion of earthquake province has been introduced. It is a domain within which various portions show sympathetic seismic activities. It may be interpreted to be representing a stationary site over which one seismic field continues to exist, although its intensity may vary according to time. By means of correlation studies of earthquake numbers in various compartments, six such earthquake provinces have been established in Japan.

§ 1. The term "earthquake zone" or "earthquake belt" has long been used in seismological literatures for describing the characteristic pattern of distribution of earthquake epicentres on the earth's surface. As is well-known, epicentres are not evenly distributed all over the earth's surface, but are significantly crowded in several well-defined long strips of area which really deserve the name of zone or belt. Either of the terms is undoubtedly appropriate and useful for representing the global picture of epicentre distribution. The Circum-Pacific Zone is one of the well-known examples. But going into a little further detail, one will easily find that the belt or zone is not one continuous figure at all, but is actually an array of clusters of epicentres arranged at irregular longitudinal intervals.

As an illustration, the epicentres of 3,147 important earthquakes (felt beyond 200 km) which took place from 1900 through 1950 in and near Japan are plotted in Fig. 1. Even in this Japanese area, which is noted for its extremely high seismic activity and which, as a whole, is regarded to be a representative portion of the Circum-Pacific Earthquake Zone, the number of earthquake epicentres is seen to vary considerably along the island arc. At several places, the epicentres are clustered to form more or less definite groups, while there are several other places from which earthquakes occur rarely. In a case like this, the favorite term earthquake zone or belt will easily cease to have its original significance.

§ 2. In order to make this uneveness in the distribution of epicentres in and near Japan appear more clearly, the following simple method of representation has been attempted.

Japanese islands as a whole are of a form of approximately circular arc, the centre being located near Vladivostok. From the approximate centre of this circle, equally spaced 128 radiating lines were drawn by means of which the whole plane was divided into as many sectors. The sectors are called (1), (2), ···, (128), the numbering starting from the one that lies to the due east of the centre and proceeding in clockwise direction (Fig. 2). These sectors into which Japanese islands are divided will be called "compartments" in this paper. The compartments are all approximately 40 km long as measured longitudinally along the island arc. The compartments that cover the area under study are 44 in number, namely, (122), (123), ···, (128), (1), (2), ···, (37).

In Table I are given the number of earthquake epicentres in each of the compartments. The earthquakes taken in this statistics are those which took place from 1912 through 1955 and which were reported as felt beyond 200 km from the respective epicentres. Hereafter, these earthquakes will simply be referred to as earthquakes. In column A of the table are given the total numbers of earthquakes for the whole length of the said period of time, while in column B and C, the numbers for its first half (1912–1933) and for

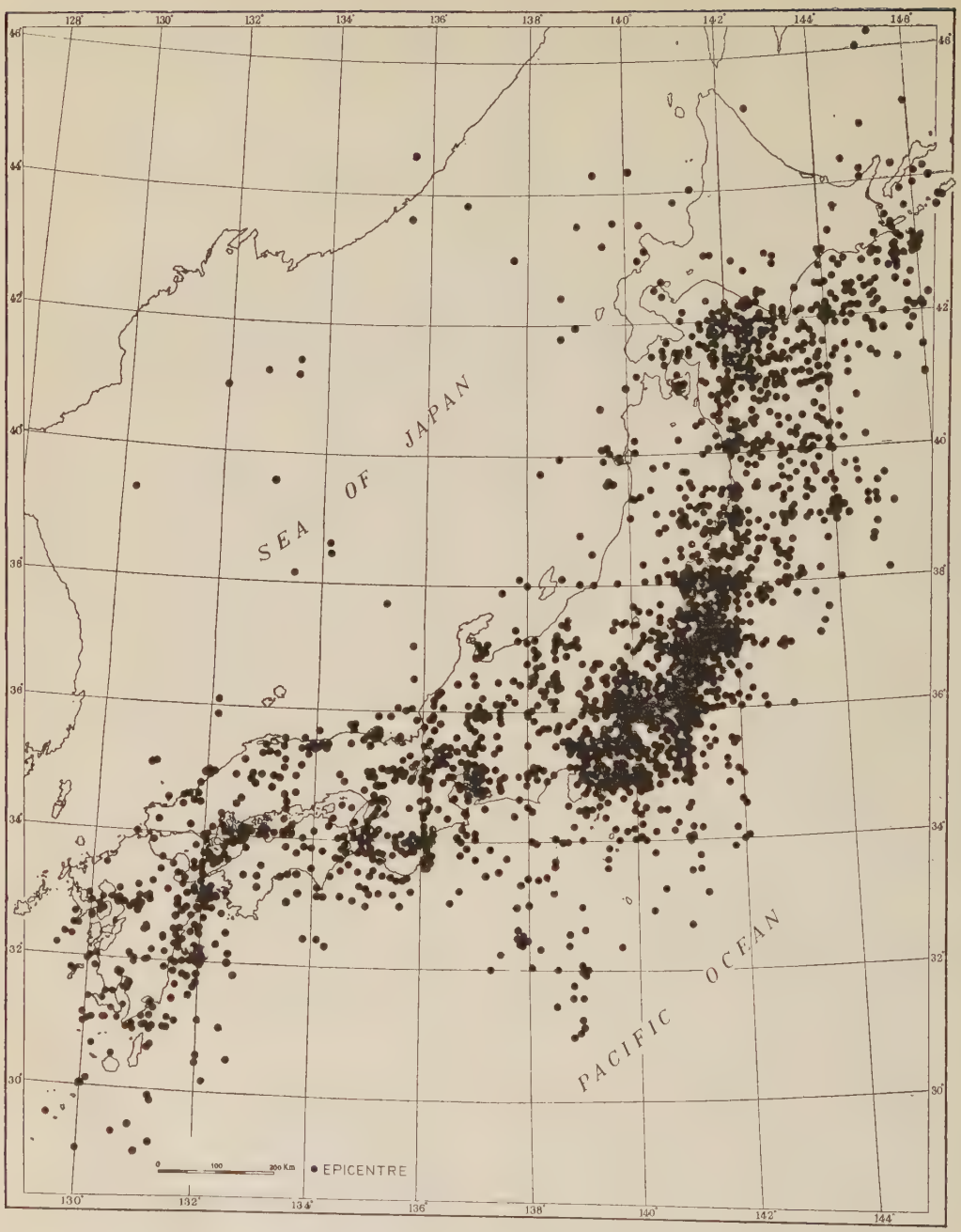

Fig. 1. Epicentres of 3,147 earthquakes in and near Japan. (Felt beyond 200 km. 1900–1950).

its latter half (1934–1955) separately. The values given in Table I are shown graphically by the curves in Fig. 3.

Two things of importance are noticed in Fig. 3. First, the curve A is not a flat and smooth one at all and its several maxima correspond to epicentre groups. Secondly, the curve B and C which represent the numbers of earthquakes during two different time intervals are similar in shape to each other in-

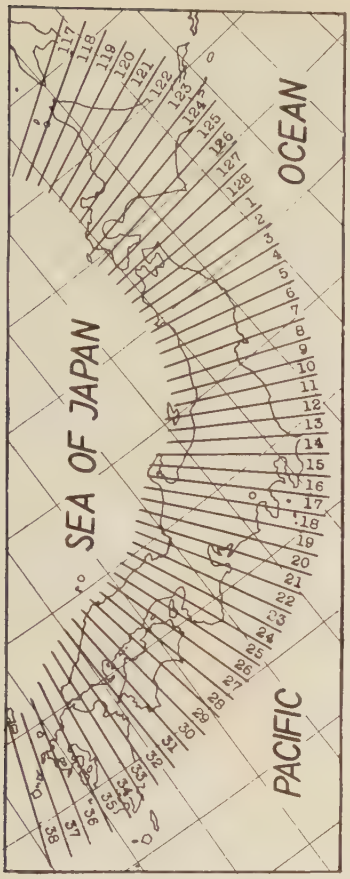

Fig. 2. Division of Japanese islands into compartments.

dicating that the biased spatial distribution of epicentres along the island arc is a time-persistent feature. So, if we investigate this distribution, it is unlikely that we are dealing with phenomena of accidental or sporadic nature. On the contrary, from this very distribution, something significant about the nature of earthquake occurrence is likely to be learned

§ 3. In the foregoing sections, the word " epicentre group " has vaguely been used. Many authors have also used this term. But the question in what way a great many of epicentres can significantly divided into such groups will not be easy to answer. No clear criterion for this purpose appears to have been given.

It may be possible to establish groups of epicentres merely by seeing where their areal densities are high and simply state there is a group here and there is another there. As will be illustrated later, there are several instances, however, that although two adjoining areas show equally high seismic activities, earthquake frequencies in them vary in no

Table I. Number of earthquake epicentres (perceptible beyond 200 km from epicentres)

A 1912–1955
B 1912–1933
C 1934–1955.

Compartments	A	B	C
122	12	4	8
3	31	8	23
4	40	15	25
5	91	48	43
6	124	60	64
7	125	69	56
128	100	69	31
1	62	28	34
2	56	37	19
3	74	44	30
4	94	54	40
5	61	49	12
6	58	38	20
7	53	26	27
8	61	27	34
9	64	28	36
10	158	82	76
1	91	61	30
2	149	94	55
3	96	69	27
4	167	123	44
5	102	67	35
6	112	85	27
7	67	54	13
8	29	10	19
9	22	11	11
20	41	13	28
1	41	12	29
2	52	34	18
3	28	7	21
4	22	11	11
5	19	4	15
6	24	7	17
7	18	0	18
8	6	2	4
9	3	3	0
30	9	5	4
1	15	9	6
2	63	47	16
3	23	15	8
4	20	13	7
5	17	17	0
6	10	10	0
7	6	2	4
Total	2516	1471	1045

sympathetic way with time indicating that any direct causative relationship is not likely to be existing between the seismic activities. In a case like this, if earthquake epicentres are plotted on a map on the basis of data of ten odd years, two such areas with numerous epicentres will appear to form one apparently single group of epicentres. But this process of grouping cannot be meaningful if we are interested in causative relationship which might be existing among the occurrences of earthquakes.

What will be described below is the result of an attempt to establish groups of earthquake epicentres in and near Japan on a physical basis. By " on a physical basis " is meant here that particular effort is going to be made to find groups of epicentres which are not only located in a more or less confined area but also there are reasons to believe are causatively related. Each of such areas, if established, will be called an " Earthquake Province ".

§ 4. As was stated before, Japanese islands

Table II. Yearly number of

Comp. / Year.	122	123	124	125	126	127	128	1	2	3	4	5	6	7	8	9	10	11	12	13	14	15
1912			1	2	4	4					2	3	2	2	1	5	3	4	2	3	15	6
3			2		8	1	2			5				1		2		4	2	9	5	6
4			1		2	3	2	2	2		3	2	2	5	1		5	5	6	2	5	4
5	1				1	2	5	4	3	3		10	6	5	6	8	6	2	6	7	9	3
6		1			2	3	6	2	5		1	6	4		2		7	6	5	4	3	3
7				1		6	3			5	6	2					9	1	6		10	6
8		1	1	1		4	5	2	4					1		3	2	1	7	2	5	3
9							9	4		4	3			2	2		6	1	2	3	7	4
20		1	2	5	4	5	5	2				1	2			2	5	6	8	2		2
1				3	6	3	4		2								3	1	3		2	1
2			1		5	4		2	2	2				2			8	3	5	4	9	5
3			1	6	2		1			2			2				7	4	7	13	10	6
4		1	2	2	1	7	2	2			1	2			1	1		7	15	6	17	3
5					2	4	5	2			1			2	5	1	3	3	3	3	8	5
6					2	9	10				1		1		2	2	1	2	2	2	4	3
7	1		1	5	2	2	1						3	1	1	1	6	3	5	1	2	2
8					2	1			2	8			2			2			2	1	7	2
9			3		5	1	1			1			3	1			3	2	2	2		
30		4		4	6	4	1					2		2	1		4	1		2	4	
1	2			10	1	3			6	2		2			1	1	3	5	4		1	3
2				5	2	3	5	1	2	2	1	2			3					3		
3				4	3		2	5	9	10	35	17	11	2	1		1		2			
4		2			1	1				2	2	1	2		3	1	2			1		
5				4	3	2	1		9	3	1			1			7		2			
6	2		1			2	3	1						2	2	1	1	1	1	1		
7	2	5			1	1				3		1	2	2						1	5	
8		4	2		1			1		2			2	1		6	35	7	6		4	2
9			2	3	3						4		2	5		3	1	8				
40	2					1	1			3			2	2		1		1	1		5	
1					1	2			1		5		1		2			1	3	2	1	1
2		1		1	4	1	2									1	2	1	4	3		
3			1	1	2		2	6		1								1	9	1	1	1
4				1	2	2	2	4	1			1		4	1	2					1	1
5				2	2	2	5	6	1			1			3	4	5	1	1	2	3	
6		1	1		2	4	2	1				2	1	2	2	2	2	1	2	1	1	2
7			1	1	5	1	2	2		1			1			3	1	1	2		2	
8	1			2			2	2			1				10		1		4	1	3	
9				5	4	1	1		1	1		1		3		2	3	2	2	5	1	
50	1		1	1	3	3	3			1	1			1	2	2	3		2	1	1	1
1			2	1	1	3	2	1		1	1			1	3	2	6			2	1	3
2		1	5	5	14	20		3	3	4	17	3				1	1		4	3	1	4
3		1		6	5	6		2			3		4		3		2	2	6	3	5	17
1954		6	5	8	6	4	2	4			4	2	2	2	2	3	2		3		6	2
Sum	12	29	36	89	120	125	99	61	53	66	93	61	57	52	60	62	156	88	146	96	164	101

have been divided into a number of compartments as shown in Fig. 2. The yearly numbers of earthquake epicentres in each of the compartments are listed in Table II. This will be the datum for the subsequent studies. First of all, the year-to-year variations in earthquake frequencies in various compartments will be compared.

Let the number of earthquakes in the l-th compartment in the t-th year be denoted by $N(l, t)$. Generally speaking, $N(l, t)$ and $N(l+s, t)$ vary with t similarly if s is small (that is if the two compartments are close to each other) and do less so if s becomes larger (that is if the two compartments are farther apart). This phenomenon is well illustrated by an example shown in Fig. 4 in which the yearly earthquake numbers in the compartments (4), (5), (6), (7), (8) and (9) are comparatively shown. While the graph for $N(5, t)$ is very similar in shape to that for $N(4, t)$, that for $N(6, t)$ is a little less similar to it, and that for $N(7, t)$ is still less similar and so on until that for $N(9, t)$ shows no similarity

epicentres in various compartments.

16	17	18	19	20	21	22	23	24	25	26	27	28	29	30	31	32	33	34	35	36	37	Sum
6	5			2		2		1	3				1			4	1	1	1			86
4	5		2				2	1							2	5	4	2	3			77
8	2							1									2		2			67
13	1		2							1						2						106
6													1				3	3	1			74
1	1		2			2	2							1								64
3	1		1		1		1								3	2		1				55
1	1	1		2	1					2				3		2	1		1			62
1	6				1			2					1	1		2		1	1			68
3						3										3			2			39
						2	1			1						1	1			2		60
22	11	1	1	2	3		1					2			2	6	1			1		114
6	3		1		3			3		2					1	2				2		93
2		1				3										2						55
2			2	1		2		2								3						53
1	1	1		1	1	1			1								1			4		49
				1		2				1						1		1	1		1	37
3	2				2			1								2		2		1		37
1	6	2														3		1	2			50
2	8	2				1										5			3		1	66
		2				8										2	1	1				43
	1			4		8									1							116
1	1					2										2		1				25
2		2	1				1											1				40
	3	3				4															2	30
1	1				1										2	1	2	1				32
									1	2												76
																		2				33
						1	2	2			1											25
1			1	1	2	2				1					1	1	1					31
1		1	1	1	3					1					1	3					1	33
1	1			1	2		1		1	6	5					1						45
	1	1			1		4	2								1						32
			3	8	10	1	1															61
	1	2	1		1			2	4	2	1	1				1						45
	1	1	1	1	1		2		6	2	5	1				1	2	1			1	49
				9	4		2	1	2							3	1					50
1															1		1					45
2	1	2		1		1	2		1		1						1					37
	1				2	1		1		1	1			1	1							
																		1				41
2		1		3	1		2					1										102
1	1		1	2		1	4	2			1											86
8		3	2	1		2		1		1				2		1						75
6		1				2					1			1		1						
112	66	27	22	41	40	51	28	22	19	23	16	5	3	9	15	63	23	20	17	10	6	2464

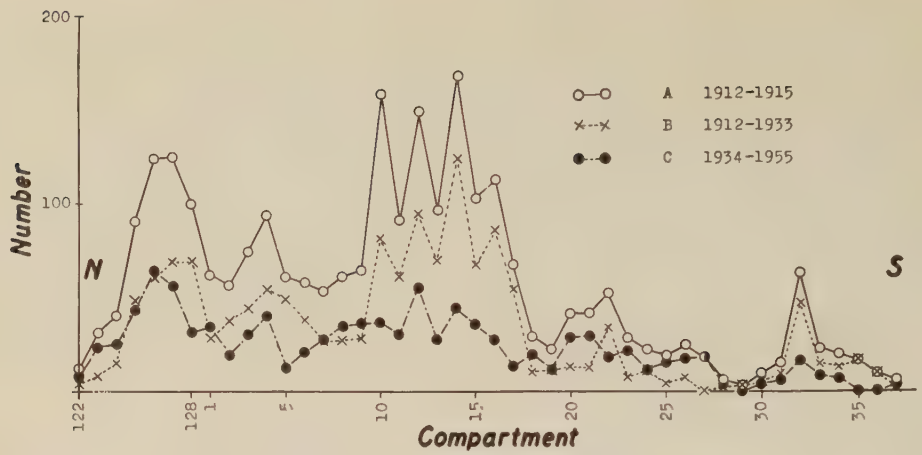

Fig. 3. Number of epicentres in various compartments.

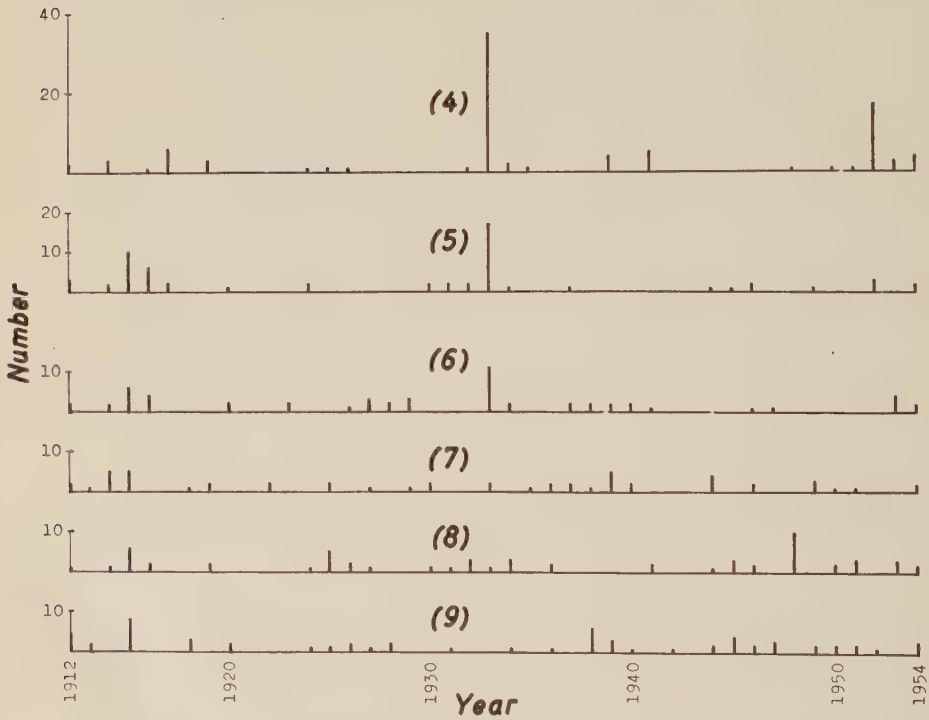

Fig. 4. Yearly earthquake numbers in compartments (4), (5), (6), (7), (8) and (9).

at all.

A useful numerical measure for expressing the degree of similarity of two variable quantities x and y is the correlation coefficient $r(x, y)$ which is defined as follows:

$$r=\frac{\sum(x-\bar{x})(y-\bar{y})}{\sqrt{\sum(x-\bar{x})^2\sum(y-\bar{y})^2}},$$

where $\bar{x}$ and $\bar{y}$ represent respectively the average values of x and y taken over the whole range of variables. If $x(t)$ in the above expression is representing the number of earthquakes in the l-th compartment in the t-th year which is $N(l, t)$, and $y(t)$ that in the m-th compartment which is $N(m, t)$, the cor-

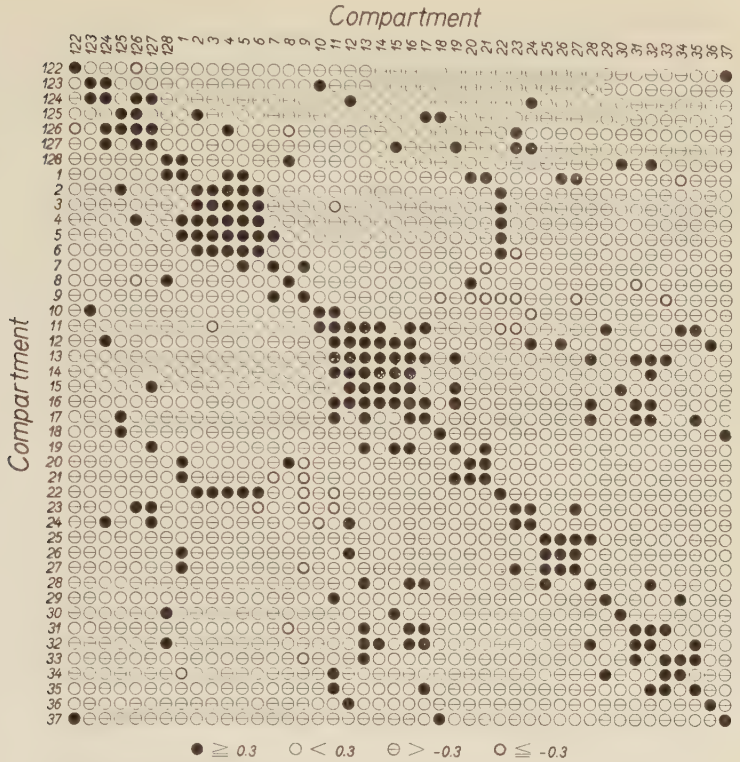

Fig. 5. Symbolic representation of correlation coefficients.

relation coefficient between $N(l, t)$ and $N(m, t)$, which will be denoted by $r(l, m)$,

$$r(l, m)=\frac{\sum_n\{N(l,t)-\bar{N}(l)\}\{N(m,t)-\bar{N}(m)\}}{\sqrt{\sum_n\{N(l,t)-\bar{N}(l)\}^2\sum_n\{N(m,t)-\bar{N}(m)\}^2}}$$

will represent the similarity of year-to-year variation in earthquake numbers in the two compartments l and m. In calculating the correlation coefficients $r(4, 5)$, $r(4, 6)$, $r(4, 7)$, $r(4, 8)$ and $r(4, 9)$, n in the above formula is 44 in our case, since we are dealing with yearly numbers of earthquakes during 44 years from 1912 through 1955. The correlation coefficients which have thus been deduced are given in Table III.

Table III. Correlation coefficients $r(4, m)$.

$r(4, 4)$	1.00
$r(4, 5)$	0.74
$r(4, 6)$	0.62
$r(4, 7)$	0.04
$r(4, 8)$	−0.05
$r(4, 9)$	−0.17

The correlation coefficient is seen to decrease monotonously with the distance between the two compared compartments.

In order to investigate the problem from a more general standpoint, that is to find out the rule of decrease of the correlation coefficient with distance, $r(l, m)$ for all possible combinations of l and m should be known. For this purpose, Table IV has been prepared. The value of $r(l, m)$ is to be found at the intersection of the l-th column and the m-th row of the table. The values given in the table are naturally symmetrical with respect to the diagonal from upper left to lower right. Fig. 5 shows the same thing symbolically by means of different marks as indicated in it.

First, of all, we wish to investigate how the correlation coefficient depends on the distance between the two compared compartments. For instance, corresponding to the unit distance (40 km),

Table IV. Correlation coefficients between earthquake numbers in various compartments.

Comp. \ Comp.	122	123	124	125	126	127	128	1	2	3	4	5	6	7	8	9	10	11	12	13	14	15
122	**1.00**	0.05	−0.19	0.05	−0.34	−0.16	−0.14	−0.20	0.00	0.03	−0.15	−0.01	0.02	0.12	0.16	−0.01	−0.13	−0.09	−0.15	−0.19	−0.08	−0.20
3	0.05	**1.00**	**0.33**	16	14	6	−20	1	−17	−10	− 4	− 0	5	2	9	11	27	− 2	− 5	−16	6	− 8
4	−19	**0.33**	**1.00**	23	**57**	**44**	−22	13	−18	− 8	15	− 8	− 5	2	−23	19	9	17	**30**	6	1	5
5	5	16	0.23	**1.00**	**32**	21	−23	1	27	− 4	19	11	6	−17	− 8	−12	− 8	8	17	3	−12	16
6	−34	14	**57**	**0.32**	**1.00**	**56**	−24	2	4	7	26	3	4	− 9	−30	− 4	−14	− 5	− 7	−15	−13	17
7	−16	6	**44**	21	**0.56**	**1.00**	9	5	4	− 6	24	3	−18	−21	− 7	− 4	−12	− 3	21	4	13	**33**
128	−14	−20	−22	−23	−24	0.09	**1.00**	31	− 0	−12	− 8	9	− 7	− 6	27	7	− 5	− 4	4	9	4	− 2
1	−20	1	13	1	2	5	0.31	**1.00**	17	8	**33**	**41**	23	13	25	17	− 4	14	23	− 4	2	3
2	0	−17	−18	27	4	4	− 0	0.17	**1.00**	**44**	**50**	**58**	**39**	2	− 9	−11	0	− 8	0	−13	−20	−11
3	3	−10	− 8	− 4	7	− 6	−12	8	**0.44**	**1.00**	**59**	**49**	**43**	− 4	−20	− 8	2	−25	−13	3	6	− 0
4	−15	− 4	15	19	26	24	− 8	**33**	**50**	**0.59**	**1.00**	**74**	**62**	4	− 5	−17	−10	−18	− 5	−14	−13	5
5	− 1	− 0	− 8	11	3	3	9	**41**	**58**	**49**	**0.74**	**1.00**	**80**	25	14	15	− 4	− 3	5	4	4	− 6
6	2	5	− 5	6	4	−18	− 7	23	**39**	**43**	**62**	**0.80**	**1.00**	23	5	13	5	8	2	0	− 2	8
7	12	2	2	−17	− 9	−21	− 6	13	2	− 4	4	25	0.23	**1.00**	4	**33**	1	16	−23	− 2	7	−10
8	16	9	−23	− 8	−30	− 7	27	25	− 9	−20	− 5	14	5	0.04	**1.00**	12	−10	−20	− 7	4	4	5
9	− 1	11	19	−12	− 4	− 4	7	17	−11	− 8	−17	15	13	**33**	0.12	**1.00**	21	14	−15	− 9	5	−14
10	−13	27	9	− 8	−14	−12	− 5	− 4	0	2	−10	− 4	5	1	−10	0.21	**1.00**	**35**	13	−11	4	− 0
1	− 9	− 2	17	8	− 5	− 3	− 4	14	− 8	−25	−18	− 3	8	16	−20	14	**0.35**	**1.00**	**48**	29	**30**	23
2	−15	− 5	**30**	17	− 7	21	4	23	0	−13	− 5	5	2	−23	− 7	−15	13	**0.48**	**1.00**	**34**	**48**	**35**
3	−19	−16	6	3	−15	4	9	− 4	−13	3	−14	4	0	− 2	4	− 9	−11	29	**0.34**	**1.00**	**45**	**38**
4	− 8	6	1	−12	−13	13	4	2	−20	6	−13	4	− 2	7	4	5	4	**30**	**48**	**0.45**	**1.00**	**47**
15	−20	− 8	5	16	17	**33**	− 2	3	−11	− 0	5	− 6	8	−10	5	−14	− 0	23	**35**	**38**	**0.47**	**1.00**
6	− 9	− 1	8	22	1	− 1	2	1	0	− 8	−10	15	25	10	9	3	1	28	**41**	**75**	**48**	**0.47**
7	13	− 1	9	**41**	9	− 2	−15	−21	− 4	− 1	−10	1	− 4	− 8	−22	−12	− 3	**36**	22	**51**	24	17
8	15	3	−16	**43**	− 0	− 3	− 8	−13	4	−21	−16	−15	−18	2	7	−46	−21	−18	−22	− 1	−24	18
9	−20	−16	− 8	− 7	10	28	25	15	− 1	3	− 2	3	− 6	−22	8	− 5	−16	− 5	18	**33**	21	**37**
20	− 3	−20	−11	6	− 8	− 9	8	**39**	2	6	24	12	5	−23	**53**	−30	−23	−25	− 9	1	− 4	− 9
1	− 5	−12	− 7	− 5	−16	−15	12	**35**	−19	−24	−15	−16	−20	−29	23	−35	−23	− 9	12	13	0	−20
2	− 0	14	−18	19	− 0	4	10	8	**30**	**36**	**53**	**43**	**32**	−11	11	−31	−23	−29	−25	−16	−12	− 3
3	− 6	−22	19	0	**31**	**30**	−16	18	− 1	13	9	−12	−31	0	− 7	−39	−24	−29	−10	5	− 9	− 1
4	− 1	−10	27	− 7	18	**49**	7	1	−22	−16	1	− 6	−11	− 1	1	−19	−30	17	27	6	18	15
25	− 7	− 7	2	−10	5	−11	−13	0	−20	−17	−11	− 6	− 4	− 5	6	− 6	− 7	− 3	− 6	−16	1	9
6	−15	− 2	1	−24	−11	−15	− 1	**39**	−19	− 1	−12	−10	−10	−15	−10	−10	− 6	2	**42**	− 4	7	2
7	− 5	− 4	15	− 4	16	− 6	− 7	**32**	−15	− 5	− 5	−10	−12	−14	−18	−27	−23	− 2	11	−17	−17	−17
8	−14	−10	1	9	− 5	−12	− 9	−11	−17	− 5	−10	−10	− 2	−13	− 6	−25	−20	− 1	2	**42**	7	11
9	−12	− 0	4	3	6	9	16	− 1	5	−19	− 5	17	18	−10	− 6	14	7	**41**	15	8	15	12
30	−10	8	2	13	− 3	5	**33**	21	−19	7	4	−10	0	− 5	7	−25	− 0	− 8	9	− 3	13	**47**
1	4	11	− 2	− 4	− 5	−13	− 5	−16	7	13	5	1	0	− 7	−25	−12	−19	− 1	18	**45**	14	3
2	− 1	− 5	−10	22	8	− 8	**78**	−25	−12	− 7	−25	−12	−18	−24	8	−11	−19	16	12	**53**	**30**	20
3	2	− 5	− 5	−20	13	−19	3	−14	− 4	5	12	− 2	− 1	2	− 4	−28	−11	20	− 6	**39**	9	10
4	−18	6	11	−16	14	−16	− 1	−27	11	2	−14	− 0	10	− 3	−18	−11	−12	26	−24	8	−15	−11
35	6	− 3	− 8	18	22	− 4	1	−20	15	9	−12	− 0	−12	1	−17	−11	− 4	**30**	− 3	11	5	13
6	6	−11	14	12	− 1	2	−18	−11	−12	−12	−11	−11	6	− 7	−13	−15	8	25	**37**	20	25	7
7	**40**	−12	− 9	1	−10	−13	− 9	−15	2	5	−13	−12	−14	−13	−10	− 9	−15	− 8	−12	−16	−18	−17

Comp. \ Comp.	16	17	18	19	20	21	22	23	24	25	26	27	28	29	30	31	32	33	34	35	36	37
122	−0.09	0.13	0.15	−0.20	−0.03	−0.05	−0.00	−0.06	−0.01	−0.07	−0.15	−0.05	−0.14	−0.12	−0.10	0.04	−0.01	0.02	−0.18	0.06	0.06	**0.40**
3	− 1	− 1	3	−16	−20	−12	14	−22	−10	− 7	− 2	− 4	−10	− 0	8	11	− 5	− 5	6	− 3	−11	−12
4	8	9	−16	− 8	−11	− 7	−18	19	27	2	1	15	1	4	2	− 2	−10	− 5	11	− 8	14	− 9
5	22	**41**	**43**	− 7	6	− 5	19	0	− 7	−10	−24	− 4	9	3	13	− 4	22	−20	−16	18	12	1
6	1	9	− 0	10	− 8	−16	− 0	**31**	18	5	−11	16	− 5	6	− 3	− 5	8	13	14	22	− 1	−10
7	− 1	− 2	− 3	28	− 9	−15	4	**30**	**49**	−11	−15	− 6	−12	9	5	−13	− 8	−19	−16	− 4	2	−13
128	2	−15	− 8	25	8	12	10	−16	7	−13	− 1	− 7	− 9	16	**33**	− 5	**78**	3	− 1	1	−18	− 9
1	1	−21	−13	15	**39**	**35**	8	18	1	0	**39**	**32**	−11	− 1	21	−16	−25	−14	−27	−20	−11	−15
2	0	− 4	4	− 1	2	−19	**30**	− 1	−22	−20	−19	−15	−17	5	−19	7	−12	− 4	11	15	−12	2
3	− 8	− 1	−21	3	6	−24	**36**	13	−16	−17	− 1	− 5	− 5	−19	7	13	− 7	5	2	9	−12	5
4	−10	−10	−16	− 2	24	−15	**53**	9	1	−11	−12	− 5	−10	− 5	4	5	−25	12	−14	−12	−11	−13
5	15	1	−15	3	12	−16	**43**	−12	− 6	− 6	−10	−10	−10	17	−10	1	−12	− 2	− 0	− 0	−11	−12
6	25	− 4	−18	− 6	5	−20	**32**	−31	−11	− 4	−10	−12	− 2	18	0	0	−18	− 1	10	−12	6	−14
7	10	− 8	2	−22	−23	−29	−11	0	− 1	− 5	−15	−14	−13	−10	− 5	− 7	−24	2	− 3	1	− 7	−13
8	9	−22	7	8	**53**	23	11	− 7	1	6	−10	−18	− 6	− 6	7	−25	8	− 4	−18	−17	−13	−10
9	3	−12	−46	− 5	−30	−35	−31	−39	−19	− 6	−10	−27	−25	14	−25	−12	−11	−28	−11	−11	−15	− 9
10	1	− 3	−21	−16	−23	−23	−23	−24	−30	− 7	− 6	−23	−20	7	− 0	−19	−19	−11	−12	− 4	8	−15
1	28	**36**	−18	− 5	−25	− 9	−29	−29	17	− 3	2	− 2	− 1	**41**	− 8	− 1	16	20	26	**30**	25	− 8
2	**41**	22	−22	18	− 9	12	−25	−10	27	− 6	**42**	11	2	15	9	18	12	− 6	−24	− 3	**37**	−12
3	**75**	**51**	− 1	**33**	1	13	−16	5	6	−16	− 4	−17	**42**	8	− 3	**45**	**53**	**39**	8	11	20	−16
4	**48**	24	−24	21	− 4	0	−12	− 9	18	1	7	−17	7	15	13	14	**30**	9	−15	5	25	−18
15	**47**	17	18	**37**	− 9	−20	− 3	− 1	15	9	2	−17	11	12	**47**	3	20	10	−11	13	7	−17
6	**1.00**	**51**	2	25	− 5	2	−19	−11	− 1	−12	− 9	−15	**49**	12	3	27	**46**	17	− 2	8	12	−18
7	**0.51**	**1.00**	16	− 2	−10	1	−17	− 6	10	− 1	−14	−10	**41**	24	− 5	27	**68**	14	6	**49**	10	14
8	2	0.16	**1.00**	− 3	−15	−18	17	− 6	−15	11	− 6	− 0	19	−19	19	−16	2	−16	−16	1	− 5	**40**
9	25	− 2	−0.03	**1.00**	22	**40**	−13	16	14	1	1	− 3	11	−18	7	18	11	1	−13	−10	− 8	8
20	− 5	−10	−15	0.22	**1.00**	**69**	5	24	− 4	15	− 7	− 3	10	− 4	− 1	− 6	2	− 3	−20	−17	− 6	− 8
1	2	1	−18	**40**	**0.69**	**1.00**	−22	8	4	4	12	4	15	− 9	− 5	13	4	− 7	−18	−23	−10	− 5
2	−19	−17	17	−13	5	−0.22	**1.00**	−22	−20	−16	−21	−15	−19	− 8	− 4	−10	− 9	−15	−20	−11	− 7	12
3	−11	− 6	− 6	16	24	8	−0.22	**1.00**	26	12	− 8	26	16	−17	−14	4	−13	7	− 9	−14	−10	−10
4	− 1	10	−15	14	− 4	4	−20	0.26	**1.00**	8	1	− 3	− 4	16	2	− 7	5	− 9	−13	− 2	7	−21
25	−12	− 1	11	1	15	4	−16	12	0.08	**1.00**	**32**	**60**	**40**	13	−13	−16	1	19	0	−11	− 1	16
6	− 9	−14	− 6	1	− 7	12	−21	− 8	1	**0.32**	**1.00**	**68**	7	−14	15	− 9	−11	− 8	−23	−16	2	4
7	−15	−10	− 0	− 3	− 3	4	−15	26	− 3	**60**	**0.68**	**1.00**	23	− 9	− 5	−11	−16	8	− 7	−17	−11	15
8	**49**	**41**	19	11	10	15	−19	16	− 4	**40**	7	0.23	**1.00**	− 8	−11	19	26	9	− 3	−15	7	4
9	12	24	−19	−18	− 4	− 9	− 8	−17	16	13	−14	− 9	−0.08	**1.00**	1	−13	10	24	**45**	20	− 9	− 9
30	3	− 5	19	7	− 1	− 5	− 4	−14	2	−13	15	− 5	−11	0.01	**1.00**	−12	− 6	− 4	−17	2	−11	−12
1	27	27	−16	18	− 6	13	−10	4	− 7	−16	− 9	−11	19	−13	−0.12	**1.00**	**30**	**33**	9	0	2	− 9
2	**46**	**68**	2	11	2	4	− 9	−13	5	1	−11	−16	26	10	− 6	**0.30**	**1.00**	16	6	**49**	− 1	5
3	17	14	−16	1	− 3	− 7	−15	7	− 9	19	− 8	8	9	24	− 4	**33**	0.16	**1.00**	**44**	**38**	6	− 8
4	− 2	6	−16	−13	−20	−18	−20	− 9	−13	0	−23	− 7	− 3	**45**	−17	9	6	**0.44**	**1.00**	24	− 1	− 6
35	8	**49**	1	−10	−17	−23	−11	−14	− 2	−11	−16	−17	−15	20	2	0	**49**	**38**	0.24	**1.00**	−15	11
6	12	10	− 5	− 8	− 6	−10	− 7	−10	7	− 1	2	−11	7	− 9	−11	2	− 1	6	− 1	−0.15	**1.00**	−11
7	−18	14	**40**	8	− 8	− 5	12	−10	−21	16	4	15	4	− 9	−12	− 9	5	− 8	6	11	−0.11	**1.00**

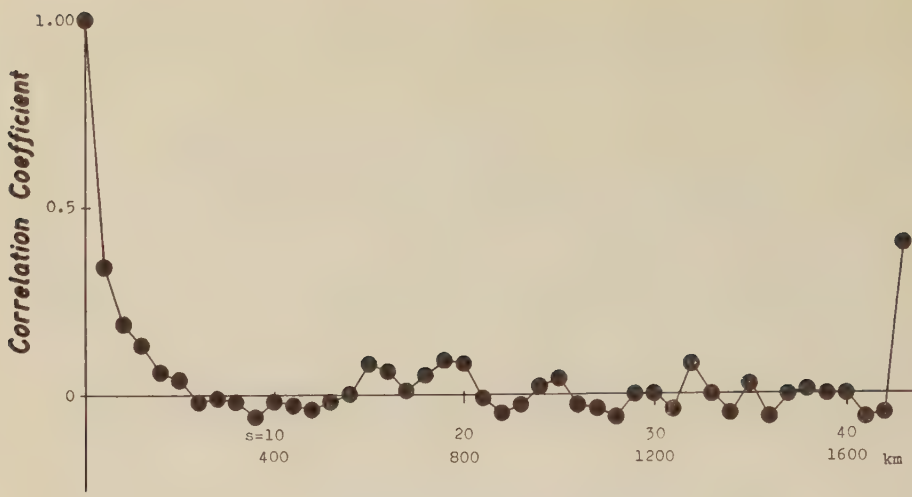

Fig. 6. Average correlation coefficient r as a function of distance s.

$r(122, 122+1)=r(122, 123)$
$r(123, 123+1)=r(123, 124)$
. . . . . .
$r(36, 36+1)=r(36, 37)$

should be averaged. Generally the value of $r(l, l+s)$ averaged over l will give the correlation coefficient corresponding to the distance s and this should be calculated for all of $s=1, 2, \cdots, 43$. The results of calculations are given in Table V. The values given in Table V are the weighted means of $r(l, l+s)$ averaged over l, the weight being given proportional to the sum of earthquake numbers in the compartments l and $(l+s)$. Fig. 6 in which these average values are plotted clearly shows that the correlation becomes lower and lower with distance (TSUBOI: 1949). The coefficient is naturally 1.0 for $s=0$ and decreases smoothly with distance until it is almost 0 at $s=4$ or 5. Since the compartment is each 40 km long, the conclusion is that earthquakes taking place within the range of $40\times4=160$ km or $40\times5=200$ km are positively correlated in their occurrence and that they may be regarded to be common offspring of some specific seismic condition prevailing within and not beyond this extent. The site of this "some specific seismic condition" may appropriately be called a seismic field. It may be added that the curve shown in Fig. 6 appears to have a small maximum around $s=20$. This point will be discussed later.

Table V. Average correlation coefficients for various s.

s	r	s	r
0	1.00	22	−0.05
1	0.34	3	−0.03
2	0.19	4	0.02
3	0.13	5	0.04
4	0.06	6	−0.03
5	0.04	7	−0.04
6	−0.02	8	−0.06
7	−0.01	9	0.00
8	−0.02	30	0.00
9	−0.06	1	−0.04
10	−0.02	2	0.08
1	−0.03	3	0.00
2	−0.04	4	−0.05
3	−0.02	5	0.03
4	0.00	6	−0.06
5	0.08	7	0.00
6	0.06	8	0.01
7	0.01	9	0.00
8	0.05	40	0.00
9	0.09	1	−0.06
20	0.08	2	−0.05
1	−0.01	3	0.40

§ 5. What has been stated above is just an apparent conclusion which could be drawn at once from the materials given in Table IV. But going into a little further detail, Table IV involves several other facts of interest.

First of all, the correlation coefficients between earthquake numbers in two adjoining compartments ($s=1$) are extracted in Table VI and shown in Fig. 7, together with earthquake numbers involved. The average of the coefficients is 0.34 but each individual value varies considerably along the island arc. The largest coefficient is 0.80, while the lowest is 0.01.

Table VI. Correlation coefficient r between earthquake numbers in two adjoining compartments.

Comp.	r	Total earthquake number
122		
3	0.05	12
4	0.33	29
5	0.23	36
6	0.32	89
7	0.56	120
128	0.09	125
1	0.31	99
2	0.17	61
3	0.44	53
4	0.59	66
5	0.74	93
6	0.80	61
7	0.23	57
8	0.04	52
9	0.12	60
10	0.21	62
1	0.35	156
2	0.48	88
3	0.34	146
4	0.45	96
5	0.47	164
6	0.47	101
7	0.51	112
8	0.16	66
9	−0.03	27
20	0.22	22
1	0.69	41
2	−0.22	40
3	−0.22	51
4	0.26	28
5	0.08	22
6	0.32	19
7	0.68	23
8	0.23	16
9	−0.08	5
30	0.01	3
1	−0.12	9
2	0.30	15
3	0.16	63
4	0.44	23
5	0.24	20
6	−0.15	17
7	−0.11	10
		6
average	0.34	

It is noteworthy that the coefficient does vary in no parallel way with earthquake numbers. There are instances that although two adjoining compartments both show high seismic activities, the correlation coefficient between them is low, like $r(127, 128)=0.09$ with 224 earthquakes, while there are other instances that although two adjoining compartments both show low activities, the correlation coefficient is high, like $r(26, 27)=0.68$ with 39 earthquakes. This fact indicates above all that the correlation coefficient is not a function of the distance between the two compared compartments alone.

The above argument is just regarding two adjoining compartments. In order to investigate this problem from a more general standpoint, let us look into Table IV again. In Table IV, the correlation coefficients that are larger than 0.3 in absolute values are printed in Gothic type. The mode in which these relatively high correlation coefficients are arranged in the table and in Fig. 5 is remarkable in that they are clustered to form several squares along the diagonal (Fig. 8a), instead of dispersing generally away from the diagonal with statis-tical irregularities (Fig. 8b).

If the correlation coefficient is a function of the distance between the two compared compartment alone, the latter distribution (Fig. 8b) is likely to occur but actually this is not the case. This peculiar distribution of relatively higher correlation coefficients would indicate that the several compartments belonging to each one of the square groups are closely related in seismic activities showing sympathetic variations. In this sense, these compartments may be said to form an "earthquake province".

Referring to Table IV from this standpoint, six earthquake provinces may be established, one of which, however, is doubtful. These provinces are listed in Table VII.

§ 6. The overall average of the correlation coefficients is 0.48, if the compartments are

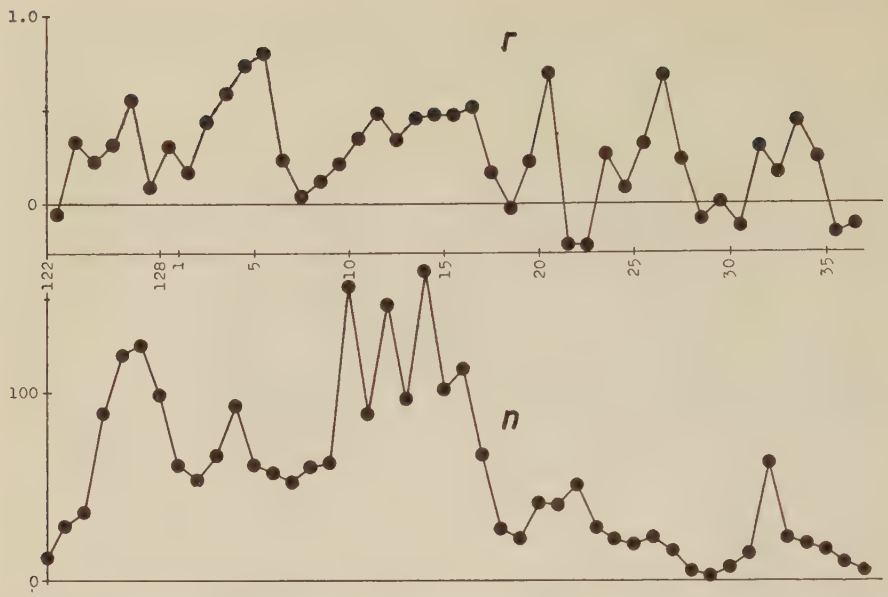

Fig. 7. r: Correlation coefficient between earthquake numbers in adjoining compartments.
n: Earthquake numbers.

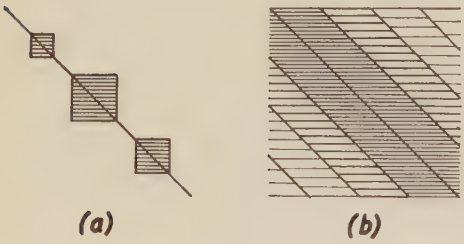

Fig. 8.

Table VII. Earthquake provinces

Province	Compartments					
A	125	126	127			
B	2	3	4	5	6	
C	11	12	13	14	15	16
D (doubtful)	19	20	21			
E	25	26	27			
F	31	32	33	34		

both inside an earthquake province, while it is 0.13 if they are both outside it.

The overall decrease of the correlation coefficient with distance was shown in Fig. 6. In that calculation, no distinction was made as to whether or not the two compartments compared are within one earthquake province. Now that six earthquake provinces have been established, the decreases of the correlation coefficient with distance inward and outward them can be calculated separately. They are compared in Table VIII and in Fig. 9. The decrease is notably different in the two cases. Inward the earthquake province, the correlation coefficient does not decrease greatly with distance while outward it falls sharply down to a very small value.

All these findings equally point to the physical significance of the earthquake province.

Table VIII. Correlation coefficients inside and outside earthquake province

	Inside earthquake province						Outside earthquake province				
Distance (unit 1=40 km)	5	4	3	2	1	0	1	2	3	4	5
Correlation coefficient	0.28	0.34	0.42	0.42	0.46	1.00	0.10	0.03	0.04	0.04	0.03

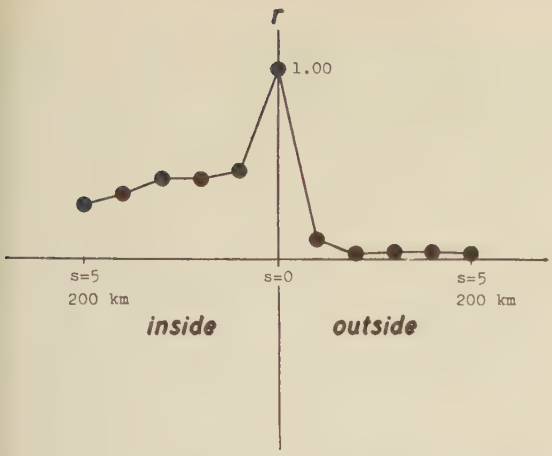

Fig. 9. Correlation coefficient inside and outside earthquake province.

The earthquake province may be said to represent a stationary site over which one seismic field continues to exist, although its intensity may vary according to time. Earthquake numbers in the compartments which belong to the same one earthquake province are commonly affected by this field intensity and this will explain why they vary sympathetically. The earthquake province is sharply bounded on its both sides and the boundaries appear to act as barriers which are hard for a seismic field to trepass.

The earthquake numbers in each of the six earthquake provinces are given in Table IX. The correlation coefficients among earthquake numbers in the six provinces are given in Table X. From the low values of coefficients given in the table, it is obvious that the seismic activities in the six earthquake provinces are almost independent events.

Table IX. Earthquake numbers in various earthquake provinces

	A	B	C	D	E	F
	125–127	2–6	11–16	19–21	25–27	31–34
1912	10	7	36	2	3	6
3	9	5	30	2	0	13
4	5	9	30	0	0	2
5	3	22	40	2	1	2
6	5	16	27	0	0	6
7	7	13	24	2	0	0
8	5	4	21	2	0	6
9	0	7	18	3	2	3
20	14	3	19	1	0	3
1	12	2	10	0	0	3
2	9	4	26	0	1	2
3	8	4	62	6	0	9
4	10	3	54	4	2	3
5	6	1	24	0	0	2
6	11	2	15	3	0	3
7	9	3	14	2	1	1
8	3	12	12	1	1	2
9	6	4	9	2	0	4
30	14	2	8	0	0	4
1	14	10	15	0	0	5
2	10	7	3	0	0	4
3	7	82	2	4	0	1
4	2	7	2	0	0	3
5	9	13	4	1	0	1
6	2	0	3	0	0	0
7	2	6	7	1	0	6
8	1	4	19	0	3	0
9	6	6	8	0	0	2
40	1	5	7	0	1	0
1	3	7	9	4	1	3
2	6	0	9	5	1	4
3	3	1	14	3	12	1
4	5	2	2	1	0	1
5	6	2	7	21	0	0
6	6	3	7	2	7	1
7	7	2	5	3	13	4
8	2	1	9	13	2	4
9	10	3	12	1	2	2
50	7	2	5	2	2	2
1	5	2	8	4	0	1
2	39	27	13	3	1	0
3	17	7	41	3	1	1
4	18	8	17	0	1	1
1955	6	13	10	0	3	0

Table X. Correlation coefficients between earthquake numbers in various earthquake provinces.

	A	B	C	D	E	F
A	1.00	0.16	0.13	−0.11	−0.11	−0.04
B	0.16	1.00	−0.07	−0.02	−0.14	−0.14
C	0.13	−0.07	1.00	−0.05	−0.08	0.38
D	−0.11	−0.02	−0.05	1.00	0.05	−0.03
E	−0.11	−0.14	−0.08	0.05	1.00	−0.11
F	−0.04	−0.14	0.38	−0.03	−0.11	1.00

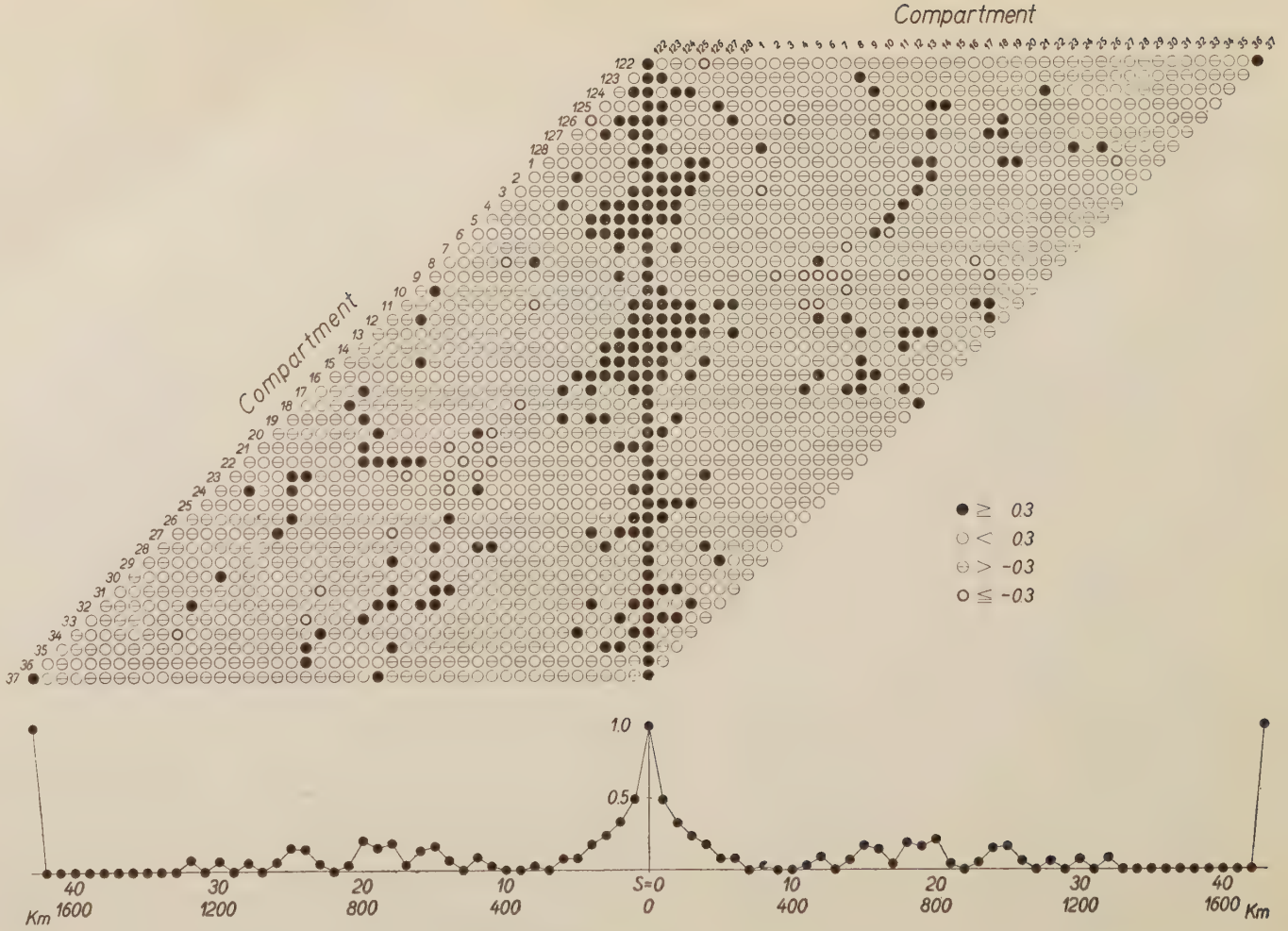

Fig. 10. Symbolic representation of correlation coefficients. Lower curve: percentage of black circles.

§ 7. Referring back to Fig. 5 again, it will be noted that the correlation coefficient becomes a little higher at the distance of $s=20$ or 800 km. Fig. 10 is simply a diagrammatic rearrangement of Fig. 5 and the correlation coefficients larger than 0.3 in absolute value are specifically indicated. The diagram shows at what distances the relatively high positive correlation coefficients appear in relation to each of the compartments. The lower curve in the same figure shows the number of such coefficients divided by the total number of coefficients corresponding to that distance. The percentage is very low between 6th to 14th compartment, and beyond that a blunt but well recognisable maximum is seen at about 18th–20th compartment. The question what this blunt maximum really means is as yet hard to answer.

References

Tsuboi, C.:
1955 On seismic activities, Geophys. Notes, **3**, No. 40.

A New Formula connecting Magnitude and Number of Earthquakes.

By

Chuji TSUBOI

Geophysical Institute, Tokyo University

Abstract

A new formula

$$\log n=(1-M/M_x)\log n_0$$

connecting the magnitude M and the number n of earthquakes is proposed, where

n_0.....number of earthquakes having a magnitude 0,
M_x .....magnitude of the largest conceivable earthquake.

This formula represents observational facts very nicely. It involves only one constant $\log n_0$, in a contrast with the formula by GUTENBERG and RICHTER

$$\log N=a+b\,(8-M)$$

which involves two. a and b in the above formula have beee found not to be quite independent.

The new formula implies that $n(M)$ is equal to $n_0{}^{f(M)}$, instead of being equal to $n_0\cdot\phi(M)$, as is usually taken for granted.

§ 1. B. GUTENBERG and C. F. RICHTER introduced a formula

$$\log N=a+b\,(8-M)$$

for expressing the relation between N and M, where N is the number of earthquakes which took place in a certain region during a certain length of time and which were $M\pm\Delta M/2$ in magnitude. ΔM is the interval of steps by which M is classified. An important feature of this formula lies in the fact that $\log N$ is a linear function of M and many subsequent studies have shown that this is true for most earthquake regions of the world.

In this formula, the constant a obviously represents $\log N_8$, which is the logarithm of the number of earthquakes having a magnitude $8\pm\Delta M/2$. The constant b is equal to $\log (N_M/N_{M+1})$ and represents the slope of $\log N$ with respect to M. The constant b is generally considered to be independent of both a and time and also to be a parameter which is characteristic to each seismic region concerned. If this is really so, this amounts to mean that the number of earthquakes of every magnitude increases with time in the same proportion, so that the results will be a parallel translation of the line in the $(\log N)$ $-M$ diagram as shown in Fig. 1.

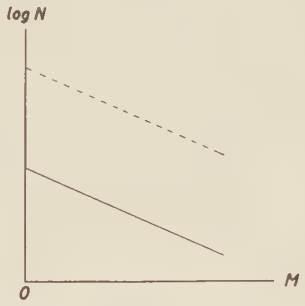

Fig. 1.

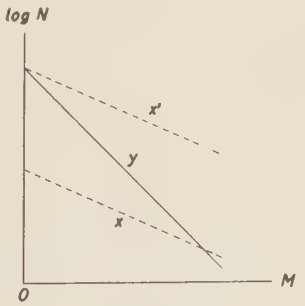

Fig. 2.

Now suppose the seismicities in two regions, say X and Y, are represented by the two lines x and y in Fig. 2, of which the slope is gentler for x than for y. Suppose also that in a long run of time, the earthquake number in X increases, and the line x is shifted to x′ until N_0 which is the number of earthquakes having zero magnitude in X, will coincide with N_0 in Y. If the parallel translation of the line is true, the natural consequence will be that the line x′ will be lying above the line y everywhere, indicating that earthquakes having greater magnitudes have been more numerous in region X than in Y. Although the time involved is of different length, can this statement be easily acceptable?

§2. In their book "Seismicity of the Earth", GUTENBERG and RICHTER (1949) described the results of their investigation of the number of shallow earthquakes in various regions of the world in relation to their magnitudes. The values of a and b in the formula

$$\log N = a + b(8 - M)$$

as given by them are listed here in Table I.

Table I. Values of a and b (GUTENBERG and RICHER) and α.

Religion	a	$b=\beta$	t	$\alpha=a+8b+\log t$
Alaska	−1.5	1.1	41	8.9
Mexico, Central America	−1.1	0.9	39	7.7
South America	−1.1	0.45	36	4.1
Kermadec Islands	−2.3	1.3	34	9.6
Solomon Islands	−1.23	1.01	36	8.4
Japan	−0.90	0.80	42	7.1
Sunda Islands	−1.5	0.9	39	7.3
Pamir to Eastern Asia	−1.7	0.6	41	4.7
Turkey	−2.1	0.9	41	6.7
Atlantic	−2.4	1.4	25	10.2
Indian Ocean	−2.4	1.3	41	9.6

On investigating the values listed in Table I, one will find that a and b are not quite independent. The larger the absolute value of a, the larger is the value of b generally. The values of a and b corresponding to the 11 regions are plotted in Fig. 3, in which the suspected dependency may be seen. It will be understood at least that there is a reason to suspect if a and b are dependent rather than are not.

It is to be noted here that the values given in Table I apply to the mean annual number of earthquakes in each of the 11 regions and also than ΔM was taken to be 1/4.

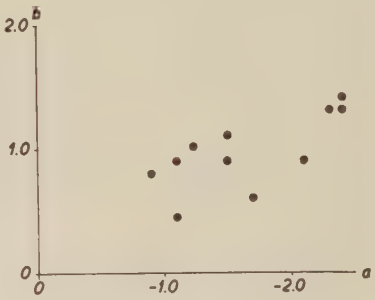

Fig. 3.

In deducing the mean annual number of earthquakes, the two authors must have divided the total number of earthquakes in each of the regions by the number of years for which the statistics was available for that region. The column under a heading t in Table I gives the number of years which was presumably taken in the statistics of GUTENBERG and RICHTER.

If n represents the total number of earthquakes in t years, it must be related to N as follows:

$$n = Nt$$

or

$$\log n = \log N + \log t.$$

If

$$\log N = a + b(8 - M)$$

as GUTENBERG and RICHTER suggested, then

$$\log n = a + 8b + \log t - bM,$$
$$= \alpha - \beta M,$$

where

$$\alpha = a + 8b + \log t$$

and

$$\beta = b.$$

The values of $\alpha = a + 8b + \log t$ are also

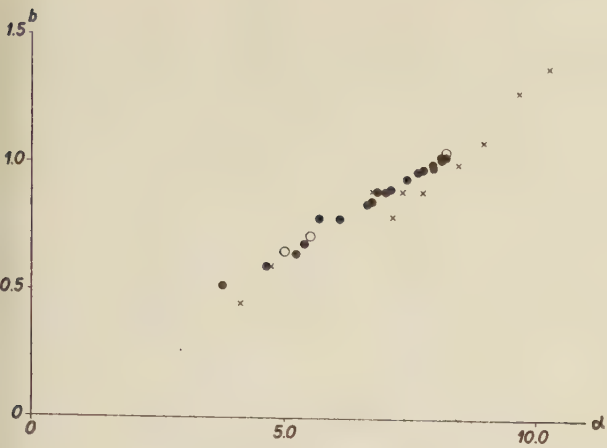

× 11 Regions in the statistics of GUTENBERG and RICHTER (Table I)
● Japan (Table II)
○ 3 Parts in Japan.

Fig. 4.

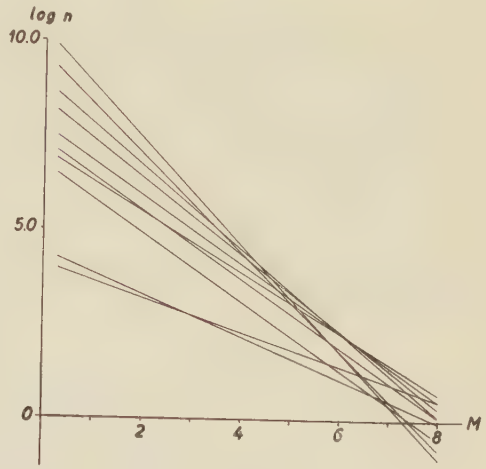

Fig. 5.

given in Table I. It will at once be noticed that the larger the value of α, the larger is the value of β also. The values of α and β are plotted in Fig. 4 which shows a beautifully linear relation between them. The relation may approximately be expressed by an equation :

$$\alpha=8\beta.$$

§ 3. Such a dependency as this can happen when

$$a+\log t=0.$$

Since a is the mean annual number of earthquakes having a magnitude $8\pm\Delta M/2$, we may write

$$\log N_8+\log t=0$$

or

$$n_8=N_8\, t=1$$

This implies that the number of earthquakes having this magnitude is only one, irrespective of region and time. This cannot of course be exactly true, but this would seem to mean that the number of earthquakes having this magnitude does not differ much from a region to another. As a matter of fact, the $(\log n)-M$ lines for the 11 regions which are drawn in Fig. 5 do appear to converge to a point at about $M=8$ on the M-axis. Although the number of earthquakes having zero magnitude differs considerably from a region to another, that having a magnitude about 8 does not.

If the relation

$$\alpha=8\beta$$

is put into the formula

$$\log n=\alpha-\beta M,$$

we get

$$\log n=\alpha-\frac{\alpha}{M}M$$
$$=\left(1-\frac{M}{8}\right)\alpha$$
$$=\left(1-\frac{M}{8}\right)\log n_0.$$

This formula, which works very nicely for all the regions, involves only one constant $\log n_0$, in a striking contrast with the classical formula

$$\log N=a+b\,(8-M)$$

which involves two constants a and b.

In the new formula, 8 is approximately the magnitude of the largest conceivable earthquake so that it will be written as M_x. Thus we get finally

$$\log n=(1-M/M_x)\log n_0,$$

where both n and n_0 are functions of time, of course, and the ratio of n and n_0 will also be a function of time such as

$$\log (n/n_0)=-M/M_x \log n_0.$$

According to this new formula, the parallel

translation of the $(\log n)-M$ line will not take place. Instead, the $(\log n)-M$ line will be shifted with its one end being hinged at one point on the M-axis. This means that smaller earthquakes will increase more and more in percentage with time.

§ 4. In 1952, the present writer (TSUBOI: 1952), referring to earthquakes in and near Japan, investigated how the constants a and b in the formula

$$\log N=a+b\,(8-M)$$

tend to change when more and more years are added into the statistics. The results of the study are listed in Table II. They can at once be used for deducing the values of the constants α and β in the new formula:

$$\log n=(a+8b+\log t)-bM$$
$$=\alpha-\beta M.$$

The values obtained are given in Table II.

The values of α and β are plotted in Fig. 4 also. Again, the points lie on a straight line

$$\alpha=8\beta.$$

Table II

year	a	$b=\beta$	$\alpha=a+8b+\log t$
1931	− 0.40	0.52	3.76
1931–32	− 0.97	79	5.65
31–33	− 0.67	60	4.61
31–34	− 0.80	65	5.20
31–35	− 0.86	69	5.36
31–36	− 1.05	79	6.05
31–37	− 1.25	90	6.80
31–38	− 1.10	85	6.60
31–39	− 1.15	86	6.68
31–40	− 1.23	90	6.97
31–41	− 1.25	91	7.07
31–42	− 1.30	95	7.38
31–43	− 1.35	98	7.60
31–44	− 1.36	99	7.71
31–45	− 1.44	1.04	8.06
31–46	− 1.39	1.00	7.89
31–47	− 1.41	1.01	7.90
31–48	− 1.43	1.03	8.07
31–49	− 1.46	1.04	8.14
31–50	− 1.46	1.04	8.16

Also in the same previous paper, the whole area of Japan was divided in three parts A, B, and C and the constants a and b were determined for each of the three parts separately, using a 20 year statistics of earthquakes. The results obtained were:

A: $\log N=-1.60+1.06\,(8-M)$,
B: $\log N=-1.57+0.72\,(8-M)$,
C: $\log N=-1.61+0.66\,(8-M)$,

The values of α which are deduced similarly are as follows:

A: 8.18
B: 5.49
C: 4.97

They agree very well with the corresponding values of 8β which are 8.48, 5.76 and 5.28 respectively. The three points plotted in Fig. 4 show this relation clearly. If we take a value of 7.6 instead of 8, the agreement is still better.

In the same previous paper, it was stated that "....if the total number of earthquakes in a certain area is twice as much as those in another, for instance, it does not mean that earthquakes of various magnitudes are equally double in number. Earthquakes with smaller magnitudes increase more rapidly than those with greater magnitudes do. ...."

All the above considerations equally point out that the distribution of earthquake numbers among various magnitudes is a feature which is neither stationary with time nor characteristic to a seismic region.

§ 5. If the formula

$$\log n=(1-M/M_x)\log n_0$$

is once accepted, the next problem will naturally be to understand what it really means. The classical formula

$$\log N=\log N_8+b\,(8-M)$$

can be written as

$$\log N=\log N_8+8b-bM$$
$$=\log N_0-bM$$

so that

$$N=N_0\phi(M).$$

N and N_0 will be proportional and the proportional factor $\phi(M)$ depends of M. On the other hand, the new formula can be transformed into

$$n=n_0^{1-M/M_x}$$

or

$$n=n_0^{f(M)}$$

In this case, $\log n$ and $\log n_0$ will be proportional and the proportional factor $f(M)$ depends on M.

Although the conclusion reached appears to be a rather strange one and is hard to apprehend from our usual understandings, it is a logical and perhaps an inevitable consequence of facts.

Here we will recall that a linear formula between $\log E$ and M was suggested by Gutenberg and Richter, such as

$$\log E=p+qM$$

where E is the energy of an earthquake having a magnitude M. p represents obviously $\log E_0$ and if we write E_x for the energy of the greatest conceivable earthquake, we get

$$\log E_x=\log E_0+qM_x,$$

and

$$M=(\log E-\log E_0)/q$$
$$M_x=(\log E_x-\log E_0)/q$$

and therefore

$$1-\frac{M}{M_x}=1-\frac{\log E-\log E_0}{\log E_x-\log E_0}$$
$$=\frac{\log (E/E_x)}{\log (E_0/E_x)}$$

Combining this with the new formula gives finally

$$\log n=\frac{\log (E/E_x)}{\log (E_0/E_x)}\log n_0$$

and we see that

$$f(M)=\frac{\log (E/E_x)}{\log (E_0/E_x)}.$$

References

Gutenberg, B., and Richter, C.F.:
1949 "Seismicity of the Earth". Princeton, U.S.A.

Tsuboi, C.:
1952 Magnitude-Frequency Relation for Earthquakes in and near Japan. Journ. Phys, Earth, **1**, 47-54.

On the Sensitivity Ratio of Clay

By

Shin'ichi YAMAGUCHI

Physical Department, Defence Academy, Yokosuka

Summary

By taking as sample Osaka alluvial clay which is called Kaolinite and the clay gathered from Okuramura land creep region, Yamagata prefecture, the author studied the sensitivity of clay. As the result, we could comprehend that it is due to the special water in case of the former clay, while in case of the latter clay it is due to the difference in the arrangement of the scale-like particles.

§ 1. Introduction

The clay generally lessens its strength only by remolding, without changing its water content. The ratio Sv/Sr, in which Sv is the strength of the undisturbed clay and Sr is the strength of the same clay fully remolded, with its water content unchanged, is called the sensitivity ratio. Since by remolding the clay changes its nature and the critical point of shear failure becomes obscure, the strength of the remolded clay Sr is determined from the stress for that strain which causes shear failure of the undisturbed clay. The sensitivity ratio varies considerably with the kind of clay, ranging from 2 to 500. So, the clarification of this property is important not only for soil mechanics, but also for geophysics, because several natural phenomena are associated with the disturbed soil. Two theories have been advanced to explain the differences in the property: the theory of A. Casagrande and that of K. Terzaghi.

Casagrande's theory is as follows: in a clay/silt mixture those clay particles which enter the lesser spaces between the silt particles are consolidated by higher stresses than those which lie in the larger spaces. This 'bond clay' possesses considerable strength. When such soils are remolded, the total strength decreases, because the strength due to bonding is destroyed.

K. Terzaghi's theory states that: if the soil is consolidated for a sufficient time, the stresses squeeze out the absorbed water, so that the particles come into contact with one another and at such point the true cohesion force functions. If any pressure applied from the outside is removed, the absorbed water returns gradually to the contact points of the particles, but it takes a fairly long time to do so completely. When the soil is remolded, the total strength becomes less, because the distance between the particles becomes greater.

Recently, O. Morretto[1] demonstrated that the remolded clay put in a state of rest gradually recovered its strength, and the strength ratio of the remolded clay after resting for the remolded clay became larger as the liquidity index of the clay sample became larger. Newland et al[2] showed that the sensitivity ratio becomes smaller as preconsolidation pressure is larger. Recent experiment by the author indicates that a paste which is consisted of the microparticles of clay below 1μ when in a state of rest increases its strength just in the same way as does the remolded clay containing all clay and silt particles.

According to Terzaghi's theory, the strength of the remolded clay declines as the time of resting increases. And according to Casagrande's theory, the strength of a paste which consists of the microparticles of clay below 1μ does not change when in a state of resting. Therefore both theories cannot always explain those experimental results.

Thus, the author attempted to clarify the problem of sensitivity. The samples he

used were taken from Osaka alluvial clay which is chiefly consisted of kaollinite and from Okuramura clay of Yamagata prefecture which is chiefly consisted of montmorillonite.

§ 2. Osaka Alluvial Clay

( ) *Sensitivity*

Many completely remolded specimens, 3.4cm in diameter and 8cm in height, were made and each was placed in a rubber sleeve closed with latex. Then, varying the period of resting for each specimen, their strengths were tested. Unconfined compression test

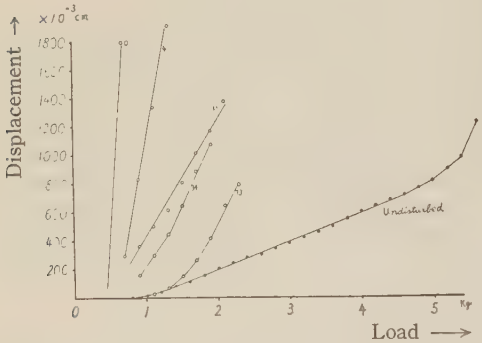

Fig. 2.1 Stress-strain relation in stress control test (6A6–6, 916–S) Figures in the diagram indicate resting days.

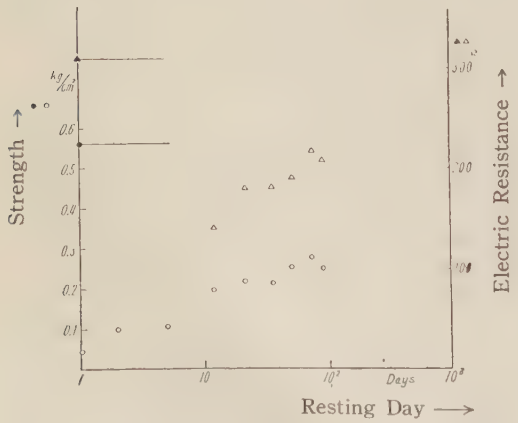

Fig. 2.2 Recovery of strength and of electric resistance.

	Strength	Resistance
Undisturbed Clay	●	▲
Remold Clay	○	△

was carried out in the controlled stress manner. The rate of increase of stress was 200gr/cm² min. The sensitivity ratio determined in this way was about 10. As the recovery of strength proceeds gradually, merely about one half of the strength was recovered within two months. Part of the results of the controlled stress unconfined compression test is shown in Fig. 2.1; and the recovery of strength, in Fig. 2.2.

(2) *Void Ratio and Electric Double Potential of Particle Surface*

Of the clay just before being remolded, of the clay immediately after being remolded with its water content unchanged and of the same clay after various period restings, the strength, void ratio and electric double sheet potential of particle surface were measured.

Void ratio should be calculated indirectly from the measured values of water content, specific gravity of soil particle and wet density of the clay. However, in the mensuration of wet density some errors may easily be accompanied due to the measurement of volume. Therefore, to obtain the more accurate value in the measurement of volume, the author adopted the following method ; a loaf of clay wrapped with paraffine was steeped into water and then its bouyancy was measured.

Electric double sheet potential of particle surface was calculated from the electro-osmotic equation,

$$V=\zeta r^2 HD/4\eta$$

in which V is the volume of water, passing through a cross section of the cylindrical tube with the uniform diameter, per unit time and ζ is electric potential difference between the fixed plane and the movable plane of the double sheet, η is the viscosity of water, r is the inner radius of the tube, D the dielectric constant of water and H is voltage gradient between the electric poles.

As both D and η being already known and r^2 possible to be estimated from the porosity by considering the void in the soil as a vacant, cylindrical tube, ζ can be calculated if H and V are measured. Of the values of ζ thus obtained, there was hardly recognized

any difference between the undisturbed clay and the remolded clay.

The void ratio of the remolded specimen proves a little larger than that of the undisturbed specimen.

On the other hand, from the linear relationship of logarithums both of the strength and of water content of the saturated undisturbed specimen,[3] the relation between the void and the strength can be determined. As the result, it was comprehended that the decrease of strength by remolding couldn't be explained according to such a small difference of the void ratio.

(3) *Electric Resistance*

Preparing the specimen in the same way as in the unconfined compression test and placing the electric poles, which are made of stainless steel and are insulated from the compression test apparatus, at the both ends, its resistance was measured by means of a Kohlraush bridge. As resistance does not change with frequency of the alternating electric current in the range from 50 to 10,000 cycles, 10,000 cycle alternating current was used. When the loads were put on the specimens during the experiment, some change appeared in the electric resistance. This may be interpreted due to a change of the contact area between the electric pole and specimen, so in carrying out the experiment, a load placed on the specimens was increased until the apparent electric conductivity reached saturation.

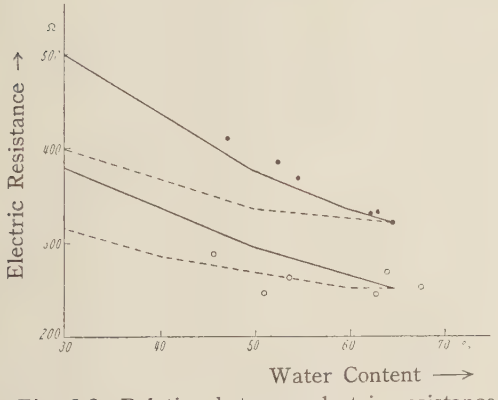

Fig. 2.3 Relation between electric resistance and water content (6A6-6, 920-S)
Undisturbed clay ●
Remold clay ○
Theoretical curve { Volume is constant ——
Air is not included .....

Many measurements were taken thus, and one example is shown in Fig. 2.3. Since the specimen measured in the loaded state differs from the original one both in diameter and in height, the adopted value is corrected to the original dimensions. If the size of the measured specimen is d^{cm} in diameter, 1^{cm} in height and its electric resistance is R, the converted electric resistance R' in terms of the standard size of the specimen must be shown as follows;

$$R' = \frac{8d^2}{3.4^2 1} R$$

In considering the result, we assume at first that the electric conductivity is concerned only with the contained water and that the clay particle is nonconductive body. By doing so, we determine the electric resistance for the volume-ratio of water in the clay alone.

Thence, the following equation can be obtained;

$$1/R_{sc} = 1/R_{sw}(r_w)^{2/3} \qquad (2.1)$$

where R_{sw} and R_{sc} are respectively the electric resistances, per unit area of the vertical section and per unit length, of the contained water and of the clay, and r_w is the volume ratio of contained water in the clay. When the water content is 65%, the clay consists merely of the particle and water, but if the water content becomes less, two extreme cases ought to be considered: one in which the volume shrinks as much as the water content decreases and air does not enter into the specimen, and the other in which as much air enters as water is lost and the volume does not shrink. The relation between the water content and the electric resistance for these two extreme cases calculated from the equation (2.1) is entered in Fig. 2.3.

The actual measured values when desiccated naturally in the atmosphere, indicate that the result accords, in case of the remolded clay, with the former instance where air does not enter into the specimen and the volume shrinks and, in case of the undisturbed

clay, with the latter instance where the volume does not shrink and air enters. Measuring the relation between the water content and the void ratio for the case in which the specimen is desiccated naturally in the atmosphere, we find it to be as stated. (Fig. 4.1).

Here, we discover a fairly distinct difference between the remolded and the undisturbed clays. That there is some difference in the electric resistance between the disturbed specimen and the remolded specimen, even if the water content or the void ratio of both specimens may be equal, is probably resulted from the fact that there is difference in the specific electric resistance of contained water between the two. But, scrutinizing Fig. 2.3 more closely, we may perceive that, if the water content is transferred about 20%, the volume—constant curves of the remolded specimen and of the undisturbed specimen overlap. This suggests that in the undisturbed sample there is about 20% water which evaporates in the desiccator, yet acts as a non-conductive body to electricity and that between the undisturbed clay and the remolded clay there is no difference in the electric conductivity of water excluding 20% portion afore-mentioned.

Of these two conclusions thus far delivered, the author advanced to investigate which is more appropriate, from another angle in the following chapter.

(4) *Specific Heat Capacity*

The specific heat of clay is measured in the following ways: the samples, which are all made 7cm in diameter, 7 or 8cm high and 500gr in weight, are covered with latex and placed in 1,000gr of water and heated. For heating, the electric heater (100v, 60w) was used. And the supplied electric voltage, being increased to 100v through the stabilizer beforehand, then dropped to 50v by the transformer. By doing so, the rate of the increase of temperature becomes 2–3°C per 20 min., and both clay and water are heated almost equally.

Then, the following equation, where Cv, Cw and Cc are each respectively the specific heats of the vessel, water and the clay, and the given thermal energy is En, the rise of temperature produced is T_1, is obtained;

$$En_1/T_1 = Cv + Cw + Cc \qquad (2.2)$$

And in the experiment performed exactly in the same way without the clay specimen, the equation

$$En_2/T_2 = Cv + Cw \qquad (2.3)$$

is derived, in which T_2 is the rise of temperature. Here, from (2.2) and (2.3) Cc can be obtained.

Next, by determining the water content of the clay and subtracting the heat capacity of the contained water, provided that water contained in the clay is invariably common, we can obtain the specific heat capacity of the clay particles alone. As is shown in Fig. 2.4, the specific heat of the undisturbed sample is twice or thrice as much as that of the remolded sample in spite of the fact that there is no difference in the specific heat of the clay particles.

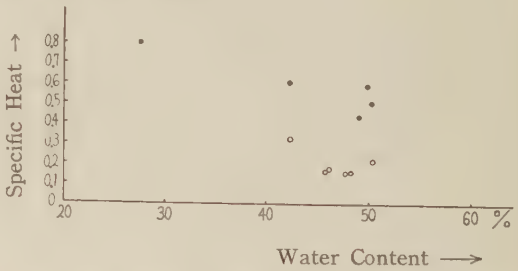

Fig. 2.4. Specific heat of clay particle (Taishobashi, No. 111, 20.87–21.76, 4–16A No. 106 B, 16.15–17.12

● Undisturbes clay ○ Remolded clay

These values seem to be too high in the case of the undisturbed sample and also, when compared with the specific heat of rock or of sand, 0.17–0.23.

These results come forth from estimating the specific heat capacity of all contained water in the undisturbed clay as 1.0, and yet, in reality, the special water as was already mentioned in (2.3) and the common water of which specific heat capacity is 1.0 are both comprized in the contained water of the undisturbed clay. Therefore, by presuming

that the special water turns into the common water as temperature rises and that in this process much latent heat is needed, we can elucidate the difference of heat capacity between the undisturbed clay and the remolded one.

If it be the case, the part of the special water must revert to common water when temperature rises, and, accordingly, the electric resistance must decrease inversely with the rise of temperature. In Fig. 2.5 the experimentally obtained relation between temperature and the electric resistance is shown.

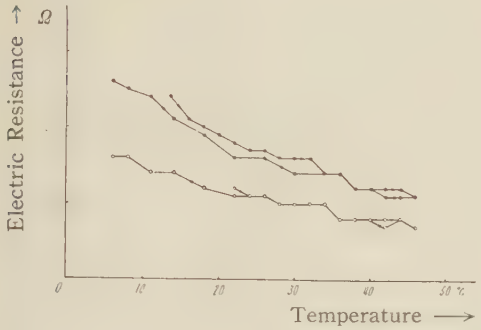

Fig. 2.5 Relation between electric resistance and temperature
Undisturbed clay ● (water content 38.9%)
Remold clay ○ (water content 39.1%)

It is found, as we expected, that the electric resistance decreases as temperature rises. Yet this process is reversible, so the electric resistance increases again if temperature falls. Of course, it is well known that the electric resistance of solution itself decreases as temperature rises. So, the specimens of the undisturbed clay, of the remolded clay and of the paste which is made from the dried and powdered clay particles and pure water, were investigated as for the relation between temperature and the electric resistance. The relation between the ratio of electric resistance at various temperature and that at 18°C, is shown in Fig. 2.6. Except in case of the undisturbed sample, every line lies almost on the same curve.

Examining this relation by taking the

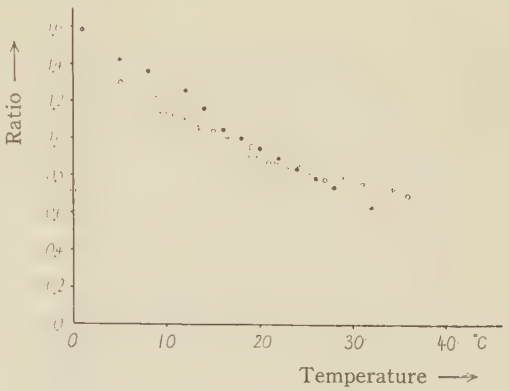

Fig. 2.6 Relation between electric resistance ratio R/R_0 and temperature. Where R_0 is the resistance at 18°C.

Undisturbed	●	Water Content 40%
Remolded	○	Water Content 40%
Paste	□	Water Content 67%
Paste	△	Water Content 100%
Dispersed system	×	Water Content 500%

logarithm of electric resistance as the axis of ordinate and the reciprocal of absolute temperature as the axis of abscissa, we obtain a straight line relation and the value of its gradient.

Since, except in case of the undistrubed clay, the straight line relation and the value of its gradient are in accord with the well-known relation between the viscosity of water (η) and temperature, $\eta \propto \exp(-Ew/kT)$ in which k is Boltzmann constant and Ew is is activation energy of water, we can assume that the change of electric resistance by temperature is caused by the change of viscosity coefficient of the soil moisture by temperature.

Next, we obtained the ratio of electric resistance at 8°C to that at 18°C for each water content, as shown in Fig. 2.7. As clearly shown in this figure, the case of undisturbed clay is distinguishable from the other cases.

The change of electric resistance by temperature in the paste or in the remolded clay, which is observed from the figure to occupy about 80% of the change of electric resistance by temperature in the undisturbed clay, was ascertained as caused by the change

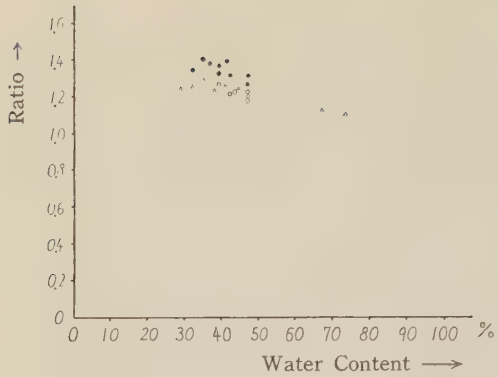

Fig. 2.7 Relation between electric resistance ratio (at 18°C to at 8°C) and water content.
● Undisturbed ○ Remolded △ Paste

of electric resistance by temperature in the soil moisture. Accordingly it is evident that some one fifth of the change of electric resistance by temperature in the undisturbed clay is owing to the change of special water into common water.

Then, the latent heat of special water can be calculated as follows : if the fresh saturated undisturbed clay, which keeps a water content of 40%, is heated from 8°C to 18°C, the electric resistance of the specimen falls from 250Ω to 190Ω. (cf. Fig. 2.5)

However, this change is not only due to the decrease of special water, but to the increase of electric conductivity of common water also.

Nevertheless, it may be considered that the change of resistance due to the decrease of special water alone is approximately (250–190)Ω/5=12Ω. This change, 12Ω, is equivalent to the change of 2% of special water into common water. (cf. Fig. 2.3) From the above consideration it is estimated that a rise of 1°C in temperature produces a 0.2% change of special water into common water. Since the difference of the specific heats between the undisturbed and clay the remolded clay (water content both 40%) is about 0.3–0.1, not merely from Fig. 2.4 but also in consideration of the experimental result in (2.9) we can estimate that the latent heat of special water is about 150–50 cal/gr, [(0.3∼0.1)–0.002].

(5) *Iufluence of Temperature on the Strength of Clay*

In the previous chapter, that there was found difference in the quantity of special water between the undisturbed clay and the remolded clay was delivered.

So, the author experimented if the difference between the undisturbed clay and the remolded one could be interpreted according to the quantity of special water.

As the temperature of the undisturbed clay increases, the contained special water turns into common water and displays the same effect as the increase of water content, so that the strength has to diminish. While in case of the remolded clay, however, it can be expected that the strength should rarely have any relation to temperature.

By leading water in the pressure chamber of the triaxial shear equipment into the capacious thermostat, the clay specimen equipped in the triaxial shear equipment was made surrounded by water at some constant temperature and was keeping the same temperature as that of water. About the clay specimen thus settled, stress controlled unconfined compression test was performed without giving any pressure to water in the pressure chamber. The size of the specimen and the rate of stress increase is quite the same as were refered to in 2.1. The thus obtained relation between temperature and the strength is, in case of the remolded clay, shown in Fig. 2.8 and in case of the un-

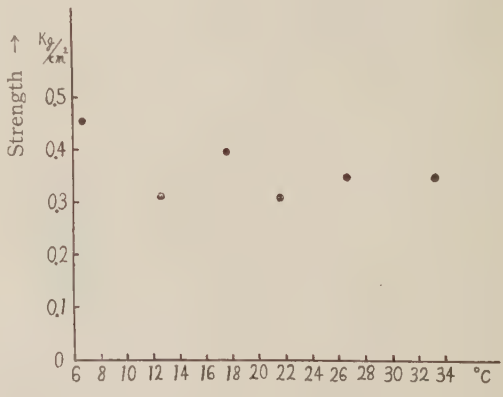

Fig. 2.8 Relation between strength and temperature of remolded clay (Taishobashi 208, 16.m16-17.m06A, Water content 49.5%)

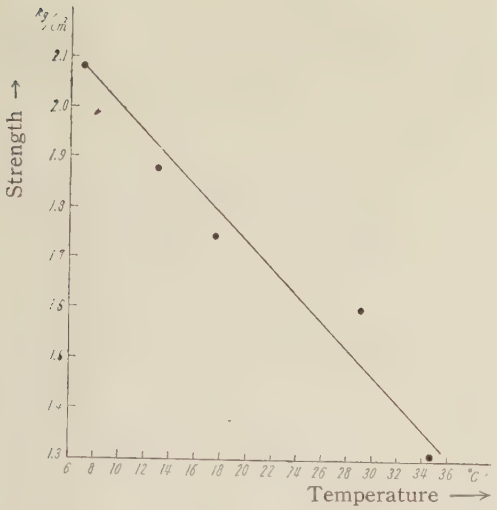

Fig. 2.9 Relation between strength and temperature of undisturbed clay (Taishobashi 208, 16.16–17.06, Water content 49.5%)

disturbed clay is shown in Fig. 2.9. From Fig. 2.9, we can observe that the strength of undisturbed clay lessens from 2.1kg/cm² to 1.3kg/cm² when temperature increases from 6°C to 36°C. On the other hand, it is also estimated from Fig. 2.5 that the electric resistance of clay specimen diminishes from 260Ω to 140Ω by the same amount of the increase of temperature. As was elucidated in 2.4, we may suspect that, out of the whole decrease of electric resistance of the undisturbed clay due to the rise of temperature, one fifth of its decrease is caused by special water tranforming into common water. Therefore, it can be considered that, in this case, the increase of common water is worth one fifth of (260–140)=120Ω, i.e. 24Ω. However, that the increase of water content worth 24Ω of the decrease of electric resistance is 4% is attained according to the relation between the water content and electric resistance of Fig. 2.3. The estimation thus indirectly taken that, by 4% of the increase of water content, the strength changes from 2.1kg/cm² to 1.3kg/cm² is well coincident with the strength and was content relation taken from the direct measurement of the effect of water content upon the strength.[3]

And from the relation between the water content and strength we may perceive that, if at 25°C, in order to fall 1.6kg/cm² of strength of the undisturbed clay of 0.4kg/cm² of strength of the remolded clay at the same water content, it is necessary to increase 18% of water content. This fact is equivalent to that, as was related upon the electric resistance of Fig. 2.3, if the electric resistance and watercontent relation curve of the undisturbed clay is shifted towards an origin by 20% of water content, it lies upon the same relation curve of the remolded clay. Assuming that the special water is non-conductive body and comparing as for the quantity of common water alone, we can estimate from the hitherto calculation that as to both the strength and the electric resistance any difference does not appear between the undisturbed clay and the remolded clay. The specimen of same shape was made of the fully remolded sample of undisturbed clay, the electric resistance of which is Ru, with its water content unchanged. If its electric resistance is Rr, the quantity Ws of common water in the undisturbed clay is expressed followingly;

$$Ws = Wc\,(Rr/Ru)^{3/2} \qquad (2.4)$$

where Wc is the water content measured by the ordinary method. As to the clay which was sampled from the extensive area, the author noticed that the strength was determined uniquely with the common water content taken by subtracting the special water content from the water content. It is shown in Fig. 2.10.

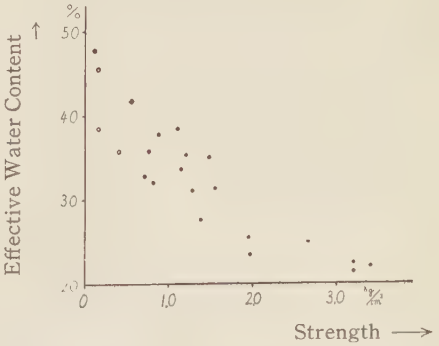

Fig. 2.10 Relation between strength and common water content.
● Undisturbed ○ Remold

(6) *Relation between Strength Recovery and Variation of Electric Resistance*

By the experiment so far, we apprehended that the strength of this clay was decided uniquely with the common water content obtained by subtracting the special water content from the water content measured by the ordinary method, and that according to the equation (2.4) the common water content was estimated from the values of electric resistance both in the undisturbed state and in the remolded state. Then, provided that the causes of the phenomenon of strength recovery of the remolded clay in resting are due to the increase of special water and to the decrease of common water during resting, the electric resistance of remolded clay must increase during the resting period. And that, in reality, the electric resistance, similar to the strength, increases in accordance with the proceeding of resting day is shown in Fig. 2.2. Therefore, it may be supposed that the strength recovery due to resting should be caused by the increase of special water content and by the decrease of common water content during the resting period.

(7) *Relation between Suction Force and Special Water Content*

It was corroborated that, as was aforementioned, the change of nature of clay either by remolding or not was owing to the change of quantity of special water, and consequently to the change of common water content. In this chapter, the relation between such special water content and suction force was studied.

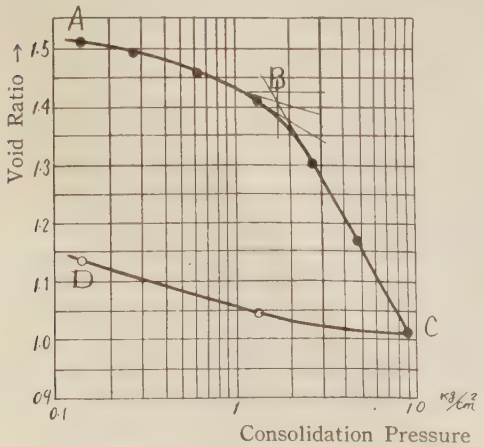

Fig. 2.11 Consolidation curve.
● Undisturbed clay
○ Remolded clay

Since consolidation pressure is considered theoretically as suction pressure, the relation between the consolidation pressure and water content can be regarded to be the same as the relation between the suction force and water contained. As shown in Fig. 2.11, the typical example of the relation between the void ratio and the consolidation pressure is expressed DEC in case of the remolded clay and ABC in case of the undisturbed clay. As the consolidation pressure becomes greater, or as the water content becomes diminished, the difference of void ratio between the undisturbed clay and the remolded clay becomes smaller. This suggests the fact that the quantity of special water in the remolded clay increases, as consolidation proceeds. Decreasing of the sensitivity ratio in accordance with proceeding of the consolidation is ascertained by the experiment.[2][4] And it is shown as well that the strength ratio between the remolded clay and the clay immediately after remolded goes larger as the degree of liquidity index is higher,* which may be interpreted as follows.

Between the strength S and the water content Wc, there is a relation,

$$\log S=\alpha-\beta\, Wc$$

in which α and β are constants.[3] Accordingly, if S changes to $(S+\Delta S)$ when Wc is diminished by Wc, we can get the following equation,

$$\log (S+\Delta S)/S=\beta\Delta W$$

The quantity of the decrease of common water in order that the special water may increase during resting is considered generally to be in proportion to the water content or to the liquidity index. So, we can be sure that the rate of increase of strength becomes larger as the liquidity index of the specimen is greater. In the experiment of microcalorimeter which will be mentioned after-

* Liquidity index=(Water Content−Plastic Limit)/(Liquid Limit−Plastic Limit)

wards, we see the fact that the difference of special water content between the undisturbed clay and the remolded one becomes small as the consolidation proceeds is no other than the fact that the special water content of the remolded clay increases whereas that of the undisturbed clay remains constant.

The author corroborates in the following experiment that the remolded clay, when its water content decreases so that its special water content increases, approaches to the undisturbed clay. Though, in case of this remolded specimen, its water content is comparatively small, air does not enter into it because the evaporation speed of its soil moisture is slow. The fact that the spacimen contains no air can be corroborated by the measurement of its void ratio. Of the specimens at various water contents air-dried naturally in the atmosphere, the author measured the electric resistance and the obtained result is shown in Fig. 2.12. The

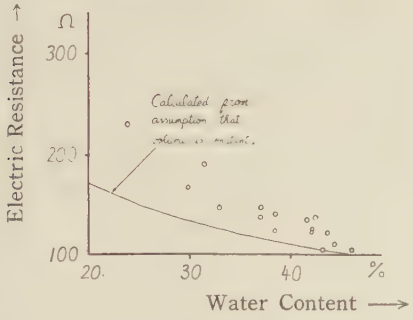

Fig. 2.12 Relation between water content and electric resistance of remolded clay which has low water content.

measured electric resistance shows greater value than that obtained according to the equation (2.1) by assuming that the spacimen should absorb as much air as the volume of water decreased from the initial water content, 46%. Since such a phenomenon means that the decrease of common water which holds electric conductivity is greater than that of water content ordinarily obtained, we ought to consider it as is owing to increasing of the special water content in accordance with decreasing of the water content. Howeve, if the electric conductivity of contained water suffers any change due to the variation of water content, the above-mentioned discussion can not be consisted.

Hence, taking the relation the electric conductivity of contained water and the water content obtained by the experiment, the author confirmed the following fact.

In suspension state where the water content of clay is great and the fraction of clay is small, as has been well-known in the field of electric chemistry of liquid, the electric conductivity of liquid part is in proportion to root of the volume concentration of clay particle. But the author took the result of experiment that, if water content is below 100%, the electric conductivity of liquid part might be considered as constant without having any relation to the water content.

(8) *Study on Specific Heat Capacity of Clay by Micro-calorimeter*

In the previous calorimeter-experiments much clay was used, but the quantity obtained by a thin wall sampler from a single location was small. Thus, the measurements of the specific heat capacity of clay at various water contents and the periods of rest were difficult because of the lack of much clay of one kind. To overcome this difficulty, a miniature calorimeter was adopted as shown in Fig. 2.13.

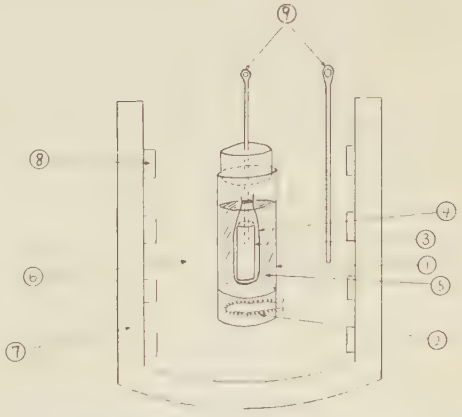

Fig. 2.13 Miniature Calorimeter
(1) Vessel (2) Heater of manganine line (3) Sample (4) Rubber Sleeve (5) Water of 120cc (6) Stilole resign (7) Vacuum bottle (8) Heater (9) Thermometer

The apparatus is the same as before used, but is of very small dimensions : the diameter of sample (3) is 3.4cm and the length is 8cm, the diameter of vessel (1) is 5cm and the height 25cm. The heater (2) attached to the bottom is made of manganine line in order to avoid the variation of electric resistance which is apt to arise due to the change of temperature. The electric voltage given in the heater, once having been made constant by the stabilizer, passed through the transformer to 6V.

The specimen, covered with a rubber sleeve, was submerged in 120cc of water[5] to ensure equal heating throughout. This miniature vessel was covered with a stirole resin,[6] the outside of which was attached to a thermos.[7]

With such an adiabatic method, the flow of heat in the outside cannot be neglected if the temperature of sample rises 5°C higher than the room temperature because of the small heat capacity of the vessel and its contents. Consequently, another electric heater[8] was inserted just in the inside of thermos and temperature inside the thermos was kept 2°C lower than the temperature of clay specimen, by controlling the voltage.

In such a way, the specific heat capacity of the remolded clay for various resting periods could be taken. The specific heat capacity of water contained in the clay could be determined by deducting the specific heat capacity of clay particles, which had been estimated from the specific heat experiment of clay particles dessicated at 110°C by using this micro-calorimeter. One example of the results of this experiment is shown in Fig. 2.14. The plotted values in Fig. 2.14 express the mean of three measured values. Clearly the specific heat capacity of contained water increases with the period of rest. This indicates that the special water in the clay mentioned above increases and the remolded clay itself, as the time of resting proceeds, approaches to the undisturbed clay.

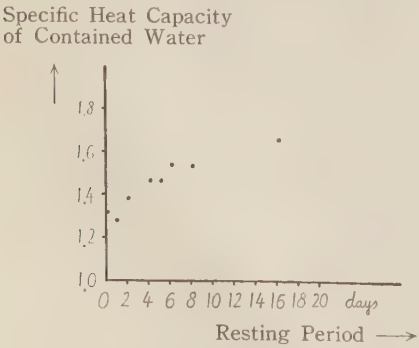

Fig. 2.14 Relation between specific heat capacity of contained water of remolded clay and resting period.

Next, we measured the specific heat capacity of contained water of the remolded clay and the undisturbed one of various water contents. The result is shown in Fig. 2.15. The relation between the specific heat of the contained water and the water content in the clay state was calculated followingly.

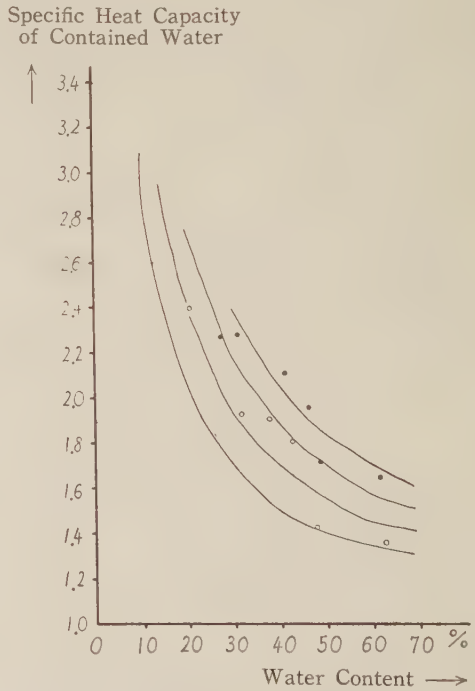

Fig. 2.15 Specific heat capacity of contained water in various water content of remolded and undisturbed clay.

● Undisturbed ○ Remolded

Assuming that the specific heat capacity of contained water, at 70% of water content in the clay state, is 1.3, 1.4, 1.5 or 1.6, and that the water lost when the water content

decreases from 70% is common water, of which specific heat is 1.0, in case at any water content Wc the mean specific capacity of contained water is accordingly expressed as

$$\{0.7\delta-(0.7-Wc)\}/Wc$$

where δ is 1.3, 1.4, 1.5 or 1.6. The measured values were compared with the calculated curves, and the water lost in the undisturbed clay was estimated to be common water. In the remolded clay, however, the increase of specific heat capacity of contained water corresponding to a decrease of water content cannot be explained away only as a result of the loss of common water. This means that in the remolded clay the special water is increasing corresponding to decreasing of water content.

This is also confirmed by the experiment that the strength variation of remolded clay the special water is increasing corresponding to decreasing of water content.

This is also confirmed by the experiment that the strength variation of remolded clay by temperature increases with the proceeding of resting period and approaches to the behaviour of undisturbed clay, as is shown in Fig. 2.16.

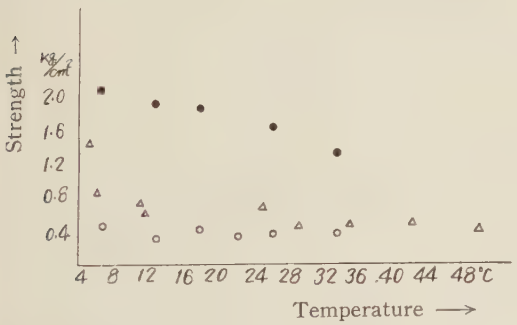

Fig. 2.16 Relation between strength and temperature

● Undisturbed ○ Remolded

△ 30 days rested after remolding

§3. Okuramura Clay of Yamagata Prefecture

(1) *Sensitivity*

Taken from the the part of creep type slide region, a sample of this clay might suffer considerable disturbance even in sistu state. Therefore, in the process of sampling, it was cut off by sawing so as not to break its skelton and was conveyed wrapped with vinyl cloth. The author considered the sample which had been rested in the laboratory for two years as the undisturbed clay. In reality, the experimental results of its strength recovery corroborate the appropriateness of his assumption.

Many specimens were made from the fully remolded clay with its water content unchanged and were conserved in polyethilene sack. The shape of sample is cylinder, 2cm in diameter and 5cm in height. By the strain controlled unconfined compression test, the temporal variation of stress and strain was self-recorded. The rate of compression displacement is about 6.7×10^{-3}cm/sec. From this record, the stress-strain relation curve can be obtained. One example is shown in Fig. 3.1. Since there is found some fluctuation in the water content of sample, the relation between the strength and resting day was taken according to the respective classes of its water content. And the result

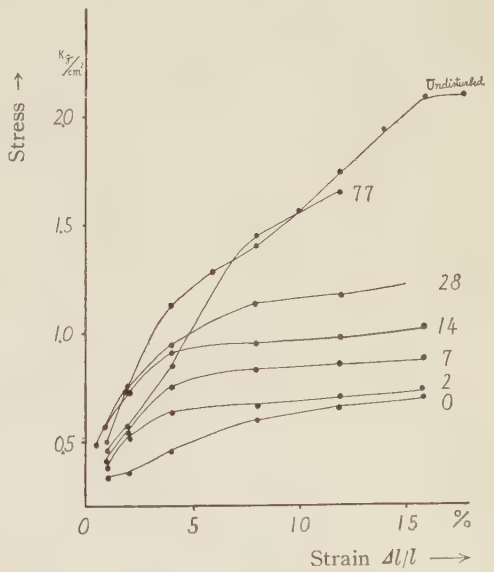

Fig. 3.1 Stress—Strain curves

Numbers in the diagram indicate the resting days.

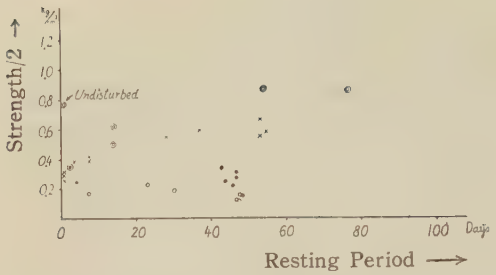

Fig. 3.2 Recovery of strength
Water content 36–40% ◎
41–46% ×
46–50% ●
51–55% ○

is shown in fig. 3.2. From it, we can perceive that the strength diminished by remolding completely recovers in about two months and Tshebotarioff's sensitivity ratio of the clay after resting is very small. (about 3).

(2) *Result of Creep Measurement*

In order to study the reason of sensitivity of this clay as delivered in 3.1, the measurements of void ratio, of the electric potential of particle surface double sheet were taken. The method of measurement is the same way as was performed in 2.2. As its consequence, it was observed that the void ratio and the electrical potential of particle surface double sheet are both alike almostly unchanged by remolding.

Moreover, the electric resistance and the specific heat capacity were measured by the same method as the one mentioned in chapter 2, and as well any change by remolding was not observed.

Lastly, the author could explain considerably clearly the difference between the undisturbed clay and the remolded clay by the creep measurement. This clay, if given shear stress, occurs stationary flow after some period. (see fig. 3.3)

Whereas the strain of common clay or metal is in proportion to the logarithm of time under the constant shear stress,[5] the strain of this clay is, as is noticed in case of the frozen clay, ice or the remolded clay, in proportion to time.

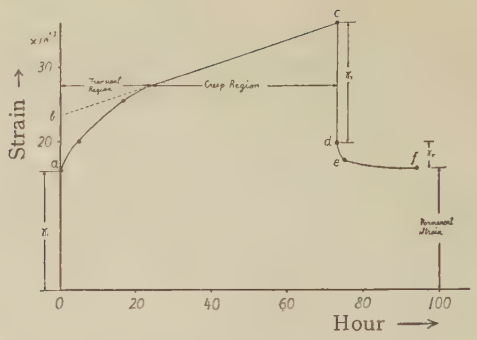

Fig. 3.3 Creep diagram (Normal stress 1.59kg/cm², Shear stress 0.318kg/cm²)
oa: transient strain after shear stress is given
ab: consolidation region
bc: steady flow region
cd: transient strain after shear is removed
def: retardation region

As the applied stress is varied, the strain rate changes. So, arranging the results of experiment, the author obtained the following equation as the relation between the strain rate γ and the stress τ :

$$\gamma = A \exp(B\tau)$$

As this creep occurs caused by the molecular rate and the flow process, by assuming that we may neglect the probability of the molecule removing from the lower position of potential to its higher position, A and B, both of which are constant with physical meanings, are expressed as follows :

$$A = 2\lambda n\textcircled{H}/h \exp(-E/\textcircled{H}) \qquad (3.1)$$
$$B = \lambda s/2\textcircled{H}$$

where $\textcircled{H}$ equals, KT, K is Boltzmann constant, T absolute temperature, λ is average distance projected in the direction of stress between equilibrium positions, n is the number of such process per length, h Plank's constant, E the free energy of activation for the process, and s is the section area of such process vertical to the direction of stress.

Of the remolded clay and the undisturbed, clay, the experimentally obtained A and B are shown in table 3.1.

As is recognized in table 3.1, B differs whether in the remolded or in the undisturbed clay. Within $B = \lambda s/2\textcircled{H}$, $\textcircled{H}$ does not change by remolding. Accordingly, that which

changed is λs. That the surface area of clay particle will not be changed is presumable, and that the void ratio of clay will be almostly unchanged too is ascertained by the experiment. Therefore, the values of λ and s until multiplied by direction cosine, i.e. the length of a latus of the three-dimentional net work made of the scale-like clay particles and the surface area of the scale-like particle are both unchanged by remolding. So, the fact that the value of λs changes means that the cross-angle of scale-like clay particles suffers some change.

If the scale-like particles of the undisturbed clay really form rectangular cross-angle, while those of the remolded clay crosses at random, the calculated ratio of B of both is well consistent with the values obtained by the experiment.

Table 3.1 Values of A and B

Kind	Remolded			Undisturbed			
Normal Stress	0.54kg/cm²	1.08 −2.00	2.13 −2.66	0.54	1.08	1.62	2.13
A	3.2×10^{-8}	5.0×10^{-9}	1.1×10^{-9}	6.3×10^{-9}	3.2×10^{-9}	1.6×10^{-9}	6.3×10^{-10}
B	7.2×10^{-6}	7.5×10^{-6}	8.3×10^{-6}	1.5×10^{-5}	1.1×10^{-5}	1.3×10^{-5}	1.2×10^{-5}

(3) *Re son of Sensitivity*

According to Table 3.1, it can be observed that the value of A is different whether for the remolded clay or for the undisturbed one, being small in the latter case, and that, as the normal stress increases, it becomes smaller togather in both cases. What is possible to be the cause of the change of A is estimated as is no other than the change of E or λ from the equation (3.1). As to what degree n or λ can change, the author speculated followingly.

By the measurement of electric resistance, we could ascertain that this clay is isotropic, so that we may consider $s=1/n^2$. Accordingly, $B=\lambda/2n^2$Ⓗ.

Then, as to the fact that B differs either in the remolded sample or the undisturbed one, two cases can be considered; one in which only λ changes by remolding and the other in which n alone changes by remolding. The variations of both cases were obtained from Table 3.1, and the results are shown in Table 3.2 and Table 3.3, where n_u, n_r and λ_u, λ_r represent respectively n and λ of the undisturbed specimen and the remolded specimen.

Table 3.2 Values of λ_u/λ_r, assuming λ is variable and n is constant.

Normal Stress	0.54kg/cm²	1.08−2.00	2.13−2.66
λ_u/λ_r	2.1	1.6	1.4(4)

Table 3.3 Values of n_r/n_u, assuming n is variable and λ is constant.

Normal Stress	0.54kg/cm²	1.08−3.00	2.13−2.16
n_r/n_u	1.4(5)	1.2(5)	1.2

Provided that the case of the undisturbed clay is standard and $\lambda_u n_u=1$, the equation (3.1) is expressed as follows:

$$\log A=13.08-1.08\times10^{13}E \qquad (3.2)$$

where Ⓗ$=4.0\times10^{-14}$, and $h=6.6\times10^{-27}$ are used.

In calculating log A of the remolded clay for the two cases, one in which λ changes in consequence of remolding and the other in which n changes in consequence of remolding, by utilizing table 3.2 and Table 3.3 respectively, some correction shown in Table 3.4 is

Table 3.4 Correction value of 13.08

Normal Stress	0.54kg/cm²	1.08–200	2.13–2.66
λ: variable n: constant	−0.32	−0.20	−0.16
n: variable λ: constant	0.16	0.10	0.08

needed to the value 13.08 in the equation (3.2).

By utilizing both table 3.4 and the equation (3.2), we can obtain the value of E from the value of A in Table 3.1. The result taken is shown in Table 3.5.

Table 3.5 Values of E

Kind		Remolded			Undisturbed			
Normal Stress		0.45kg/cm²	1.08–2.00	2.13–2.66	0.54	1.06	1.62	2.13
E	λ: variable n: constant	1.88×10^{-12}	1.96×10^{-12}	$2.02_5\times10^{-12}$	1.97×10^{-12}	2.00×10^{-12}	2.02×10^{-12}	2.06×10^{-12}
	n: variable λ: constant	$1.92_5\times10^{-12}$	1.99×10^{-12}	$2.04_5\times10^{-12}$				

The value of E obtained as for the creep would represent the quality of micro-particle, and the author will corroborate later in 3.4 that the microparticle plays a main role in the strength of this clay. Therefore, considering that the strength is defined with E and that it is in proportion to exp $(E/$Ⓗ$)$, we can express sensitivity ratio S_T followingly:

$$S_T=\exp\left[(Eu-Er)/\text{Ⓗ}\right]$$

in which Eu and Er are the values of E of both the undisturbed specimen and the remolded specimen respectively. The calculated values of S_T by using the values of Table 3.5 are shown in Table 3.6.

Table 3.6 Values of S_T

Normal Stress		0.54kg/cm²	1.08–2.00	2.13	Measured Values
S_T	λ: variable n: constant	9.3	3.5	2.4	3
	n: variable λ: constant	3.1	1.6	1.4(5)	

The result that the volues of S_T becomes smaller in accordance with the increase of normal stress is well consistent with the other reports.[2][4]

From the calculation hitherto, the author speculates as to the cause of sensitivity as follows.

The fact that the strength of this clay becomes different either by remolding or not, even at the same water content, or with the same void ratio, may be interpreted due to the reason that in the undisturbed state the arrangements of the scale-like clay particles are in good order and the removal of clay particles are performed under the condition of much activation energy, whereas in the remolded state the arrangements of the scale-like particles are at random, so that they can turn freely and their removals are possible even in the condition of less activation energy. (see Fig. 3.4)

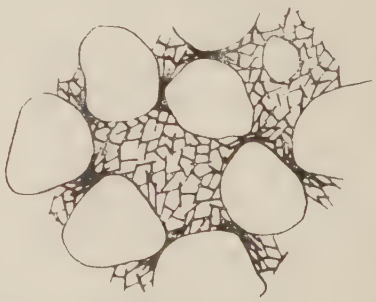

Fig. 3.4 Three dimensional network of clay (after Tan-tyong-kye's paper).

(4) *Strength Increase in Resting of the Paste made of Microparticles of Clay alone*

As was discussed so far, the sensitivity was explained according to the activation

energy obtained from the creep phenomenon. However, it might be possible that the larger particle of clay should play the main role in the strength, while the microparticle performs the main role in the creep phenomenon. And, according to Casagrande's theory it is also probable that the clay without silt should not give rise to bond clay so that it should hold no sensitivity.

Then, the author, utilizing the wet mechanical analysis, produced the paste consisted of the microparticles, the particle size of which is below 1μ, which were made by precipitating the larger clay particles and then by evaporating the remnant fluid. And he examined the aspect of the strength increasing of this paste during resting. The examined aspect that the strength of this clay reaches saturation in some two months of resting is similar to that of strength recovery of the original clay. (see Fig. 3.5) This proves nothing but the fact that the microparticle performs an important roles as well in the strength recovery of the original clay.

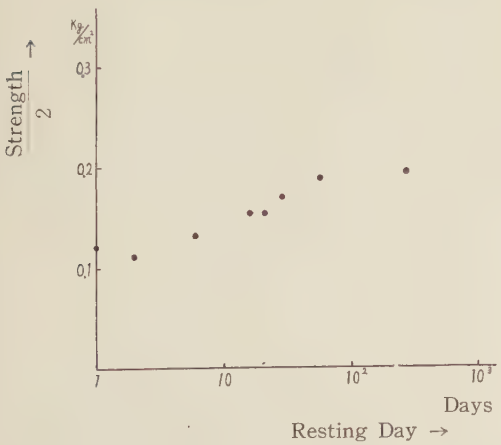

Fig. 3.5 Strength recovery of samples which are constituted with microparticle

Therefore, it may be appropriate that we should explain the sensitivity by the activation energy obtained from the creep phenomenon.

And the author studied experimentally, too, that the strength recovery of the clay paste consisted merely of the microparticles above-mentioned is not caused by the change of void ratio, and showed the result in Fig. 3.6. According to this figure, the void ratio is regarded as constant without any relation to

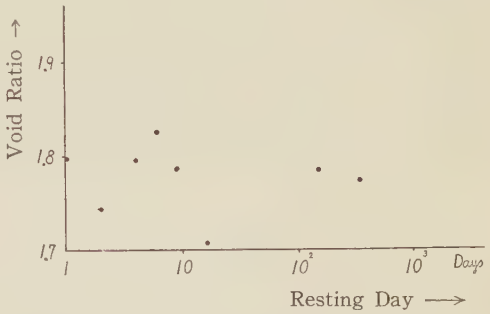

Fig. 3.6 Void ratio-resting day relation (Water content 66–71%) of the paste which consists of microparticles smaller than 1μ.

resting day. Then, in Fig. 3.7 and in Fig. 3.8 are shown the water content and the void ratio of each clay paste respectively classified by the particle size by the wet mechanical analysis, when put in the atmosphere and the weight of which keeps equilibrium. Since the condition in which the weight of clay is in state of equilibrium in the atmosphere is below the shrinkage limit, its void ratio ought to increase generally as the particle size becomes small.

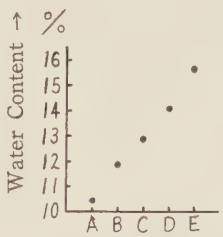

Fig. 3.7 Relation between water content, which is balanced with atmospheric vapour pressure, and particle size A–1.1μ, B–0.78μ, C–0.65μ, D–0.55μ, E–0.42μ.

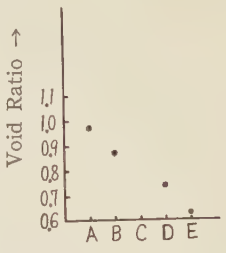

Fig. 3.8 Relation between critical void ratio and particle size A–1.1μ, B–0.7μ, C–0.65μ, D–0.55μ, E–0.42μ.

But Fig. 3.7 represents that the void ratio decreafes as the particle size becomes smaller. Such a fact is just consistent with the result estimated due to the assumption that this

clay paste forms three dimentional network of the scale-like clay particles of which thickness is uniform.[6] And the fact that, as shown in Fig. 3.8, the water content increases as the particle size becomes small proves that the surface area of clay particle per unit volume of clay increases as the particle size becomes smaller, since the thickness of absorbed water of clay particle which keeps equilibrium with the air can be regarded as uniform.

§ 4. Study on Shrinkage Process

In the previous chapter 3, we presumed that the strength of consolidation test was decided by the activation energy with which a clay particle passes by the neighbouring clay particle. This fact can be ascertained by the shrinkage process of clay when the soil moisture of which evaporates. Namely it means that, as the strength of clay is larger, its activation energy becomes greater and the shrinkage rate accordingly diminishes. Therefore, even when the evaporation rate of soil moisture remains constant, the clay may differ in the shrinkage rate, in the way of entering of air and in the process of variation of void ratio due to the difference of strength.

Then, the following experiment was performed. Preparing a lot of undisturbed specimens and remolded specimens, we desiccated them naturally in the atmosphere. By varying the desiccation period, we can obtain the specimens in various stages of the process of desiccation. The water content and the void ratio of these specimens in every stages were measured and shown in Fig. 4.1 and Fig. 4.2. As was expected, of Osaka alluvial clay, the void ratio of undisturbed specimen is greater than that of remolded specimen at the same water content. Of Okuramura clay of Yamagata prefecture, however, the void ratio of remolded specimen proves a little greater than that of undisturbed specimen at the same water content. Whereas the strength of Osaka alluvial clay, for instance when its water content is 40%, is about 6.0kg/cm², that of Okuramura clay, when its water

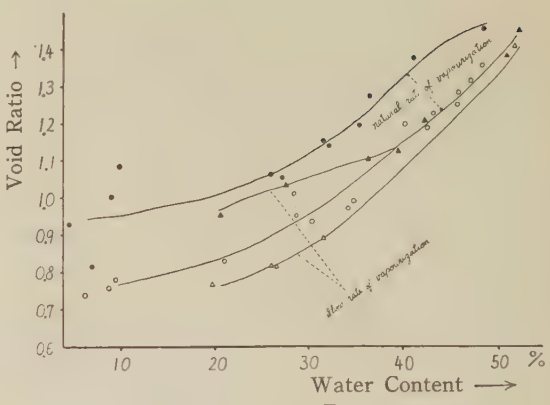

Fig. 4.1 Drying process of Ōsaka alluvial clay

	Undisturbed	Remold
Natural dry	●	○
Slow dry	▲	△

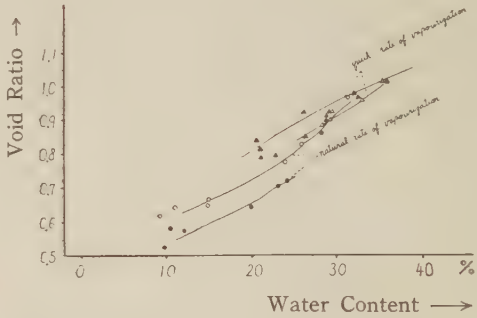

Fig. 4.2 Drying process of Ōkuramura clay

	Undisturbed	Remold
Natural clay	●	○
Quick dry	▲	△

content is the same as the former, is only about 0.8kg/cm² and its activation energy is small too. So, in case of Okuramura clay, since the shrinkage rate can follow the evaporation rate of the soil moisture even in the undisturbed state, the rate of air entering into the clay in the process of desiccation does not differ whether for the remolded specimen or for the undisturbed specimen. Consequently, it may be considered that the void ratio of remolded specimen becomes greater by the air content entered by remold-

ing than that of undisturbed specimen. To corroborate this idea furthermore, the author put the Osaka clay in the saturated-vapour chamber in the desiccator which contained water in stead of the drying medicine in the bottom, and desiccated it slowly, while Okuramura clay was desiccated rapidly in the drying owen. In consequence, as shown in Fig. 4.1, in the former case there scarcely appears any difference between the remolded specimen and the undisturbed specimen in their void ratio, but the void ratio of undisturbed specimen becomes greater again than that of the remolded one, if below a certain water content. It can be interpreted that, as the water content diminishes, both the strength and the activation energy become greater together and the shrinkage rate of the undisturbed specimen correspondingly decreases too much to follow the evaporation rate of such a degree.

On the other hand, in case of Okuramura clay, the void ratio of undisturbed specimen becomes surely greater. This fact proves that the shrinkage rate is exceeded by the evaporation ratio of soil moisture. Though the shrinkage rate can accompany the evaporation rate in the exterior part of remolded specimen, that rate is so large that the shrinkage in the interior part of the specimen cannot follow. As its consequence, many cracks are produced.

Then the author made the dimension of the specimen smaller or flatened, or keeping the door of the drying oven open to check the evaporation rate and yet such cracks couldn't be prevented. So, by taking the inner, more-or-less uniform shrinking part of specimen, the void ratio and the water content were measured. Though every aspects of the change of water content could not be grappled, it can yet be observable that the void ratio of remolded specimen becomes smaller, compared with that of the undisturbed specimen at the same water content. (see Fig. 4.2)

§ 5. Conclusion

By taking as sample both Osaka alluvial clay which is called Kaolinite and the clay gathered from Yamagata prefecture, Okuramura land creep region, the author studied as to the sensitivity. As the result, we could comprehend that it was explained due to the special water in case of the former clay while in case of the latter clay it was explained according to the difference of the arrangement of the scale-like particles.

Acknowledgement

This author sincerely wishes to express his cordial thanks to Dr. K. Sassa, Prof. of Geophysical Institute of Kyoto Univ., and to Dr. S. Murayama, Prof. of Civil Engineering Institute of Kyoto Univ., for their guidances and instructions all the time throughout this study.

References

(1) O. Morretto:
"Effect of Natural Hardening oh the Unconfined Compression Strength of Remolded Clay.", Proc. 2nd Int. Conf. Soil Mech. and Found. Engr. vol. **1**, pp. 137

(2) P. L. Newland et al:
"A Study of the Sensitivity Resulting from Consolidation of a Remoulded Clay.", Proc. 4th Int. Conf. Soil Mech. and Found. Engr. vol. **1**, pp. 83

(3) S. Murayama et al:
The Effect of the Moisture Content on the Strength of an Alluvial Clay., Disaster Prevention Research Inst. Bul. No. **12** pp. 5

(4) Y. Ishii et al:
Researches on the Engineering Properties of Alluvial Clays., Trans. of the Japan Soc. of Civil Engr. No. **30**. (1955).

(5) S. S. Vialov et al:
"Rheological Processes in Frozen Soils and Dense Clay.", Proc. 4th Int. Conf. Soil Mech. and Found. Engr. vol. **1** pp. 120

(6) T. V. Lambe:
"The Structure of Inorganic Soil.", Proc. A.S.C.E. vol. **79** Separate No. 315

Gravity Survey on Kuttyaro Caldera Lake.

By

Izumi YOKOYAMA

Geophysical Institute, Hokkaido University.

Abstract

A gravimeter survey was made on the frozen surface of the gigantic caldera lake, Kuttyaro. A Gravity low, reaching −46 milligals, was found, with iso-anomaly contour lines conforming the caldera shape. A layer of coarse pumice thickening toward the centre is required to account for the observed anomalies. This is compatible with volcanological inferences. Gravity anomaly distributions at several other calderas are discussed also.

§ 1. Introduction

Lake Kuttyaro, located in the eastern part of Hokkaido, (Fig. 1), Japan, represents the western half of a circular caldera which was formed in Quaternary age. Measuring about 20km in diameter, this is one of the most gigantic calderas on the earth. A small island at the centre of the lake and parasitic volcanoes in the eastern half of the caldera erupted after its formation. Pumice which was ejected at the time of the catastrophe of the caldera-formation is found widely spread around the lake, and in fact, even at the shore of the Okhotsk Sea as distant as 50km from the volcano. As for geophysical phenomena in this district, it is known that a moderate earthquake (M=6.0) occurred in May 1938 being accompanied by small crustal deformations. The hypocentre of this earthquake was located at the south-east corner of the lake and 20km in depth, although no more detailed studies were prosecuted. Being interested in the underground structure of this typical caldera, the present writer wished to get gravity anomaly values on the lake.

Fig. 1. Topographic sketch-map of Kuttyaro and Akan calderas. Contour-interval is 200m.
K: Lake Kuttyaro, A: Lake Akan,
M: Lake Masyu.

At present, gravity measurement on water is of course very difficult. But fortunately the lake water freezes hard in winter, so that a Worden gravimeter could be used on the surface of the frozen lake. A gravity survey on the ice surface was carried out in March 1958. The Bouguer anomalies on and near the lake are shown in Fig. 2, which also contains the anomalies obtained by the Geographical Survey Institute by another series of gravimeter survey along the route of precise levels along the eastern margin of the caldera. Since our gravity points are situated on the level surface of the lake, the free air reduction and the Bouguer reduction are

uniform throughout the lake. This fact simplifies the calculation very much. Topography corrections are very small and can safely be ignored in the following discussion. A conspicuous fact to be noted in the figure is that a relatively low anomaly which reaches about −46 milligals, is found, the lines of equal anomaly being concentric with the centre of the caldera. Comparing the distribution of Bouguer anomalies with that of depth of the lake, shown in Fig. 3, no

Fig. 2. Distribution of Bouguer anomalies on the Kuttyaro caldera (in milligal).

relation is found between them, and therefore the Bouguer anomalies observed may be regarded as due to the subterranean structure of a larger scale.

Here, the writer intends to interpret the Bouguer anomalies found on this Kuttyaro caldera and to discuss its subterranean structure, together with those of other calderas from the standpoint of volcanology.

Fig. 3. Distribution of the depth of Lake Kuttyaro (in meter) after H. TANAKADATE.

§ 2. Subterranean structure of the Kuttyaro caldera from the gravity anomalies

The gravity potential due to a certain anomalous subterranean mass distribution can be expressed in the following Bessel Fourier series form :

$$\Delta U(r,\theta,z)=\sum_n\left\{\int_0^\infty \frac{B_{nk}}{k} J_n(kr)\exp(-kz)\,dk\right\}\begin{matrix}\cos\\ \sin\end{matrix} n\theta \qquad (1)$$

using customary notations. From this expression for the potential, we get the gravity anomaly at the earth's surface $z=0$ as follows :

$$\Delta g(r,\theta)=\sum\left\{\int_0^\infty B_{nk}J_n(kr)\,dk\right\}\begin{matrix}\cos\\ \sin\end{matrix} n\theta\ . \qquad (2)$$

Assuming that the distribution of gravity anomaly on the Kuttyaro caldera shown in Fig. 2 is nearly concentric, (2) can be converted into a simpler form :

$$\frac{1}{2\pi}\int_0^{2\pi}\Delta g(r,\theta)\,d\theta=\int_0^\infty B_{ok}J_o(kr)\,dk\ .$$

The left-hand side is the average of $\Delta g(r,\theta)$ taken over the whole azimuth θ along a circle $r=r$, drawn around the centre. Denoting this average by $\Delta g(r)$, we get

$$\Delta g(0)=\int_0^\infty B_{ok}\,dk,$$

and

$$\overline{\Delta g(r)} = \int_0^\infty B_{0k} J_0(kr)\, dk.$$

By the method of least squares, the five coefficients B_{01}, B_{02}, - -, B_{05} in the above expression are determined over the range from $r=0$ to $r=10$km in Fig. 4 by averaging the gravity values in eight directions with 30°

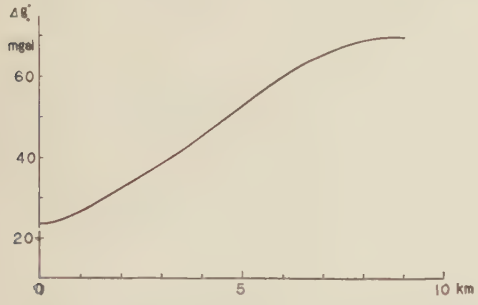

Fig. 4. Radial distribution of Bouguer anomalies on the Kuttyaro caldera.

intervals around the centre of the caldera. The outermost circle is so large in radius that the gravity anomaly on it becomes negligibly small. Here, the centre of the caldera is taken at the point where the contours of the Bouguer anomaly appear to converge in Fig. 2 and this point coincides well with the geometrical centre of the caldera-rim. The coefficients thus deduced are as follows;

$B_{01}=27.6$, $B_{02}=11.4$, $B_{03}=7.0$, $B_{04}=2.3$, $B_{05}=2.1$. (milligal)

In the present case, the gravity anomaly at the depth $z=z$ is given by

$$\Delta g_z(r, z) = \int_0^\infty B_{0k} J_0(kr) \exp(-kz)\, dk. \qquad (3)$$

Using the above coefficients B_{01}, B_{02}, - -, B_{05}, the approximate distribution of gravity anomalies at various depths are calculated as shown in Fig. 5 until the series ceases to be convergent. The higher harmonics increase in prominence as the anomaly producing mass is approached, since the value of k is larger for the higher harmonics than for the lower, but they are unlikely to exceed materially the lower harmonics in amplitude

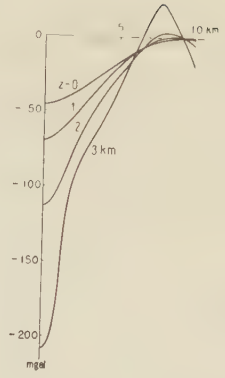

Fig. 5. Gravity anomalies at the various depths.

unless the mass is reached. The depth at which the above integral ceases to converge does not affirm that there are no sources down to that depth, but rather implies that it is more probable that the sources are to be found at that depth and greater. In Fig. 5, the curve of the field at a depth of 2km becomes much steeper than the original one, varying by about 110 mgals within a horizontal distance of 10km. This remarkable variation in anomaly may indicate that the anomaly producing mass is distributed at a comparatively shallow place from the horizon of the depth 2km with a probable density contrast. If a greater depth is assumed inconceivably high density contrasts are required to reproduce the field.

In the above discussion, we reached the conclusion that the gravity anomalies observed on the Kuttyaro caldera are due to masses that are shallow, relative to the least horizontal distance in which the anomaly changes in its whole amplitude. The absolute value of the depth is put out of the question because, anyhow, the problem is clearly indeterminate. In this case an excellent and simple approximation to the mass distribution is given by

$$m(r) = -\frac{\Delta g(r)}{2\pi G}. \qquad (4)$$

At the centre of the caldera $r=0$, $\Delta g(0)$ amounts to –46 mgals. Then $m(0)$ is obtained as -1.1×10^5 gr./cm. If we assume the density contrast to be 0.3 gr./cm^3, the thick-

ness of the subterranean mass at the centre becomes about 4 km. Similarly, the distribution of the coarse material which is responsible for the negative gravity anomalies is obtained as shown in Fig. 6. The selection

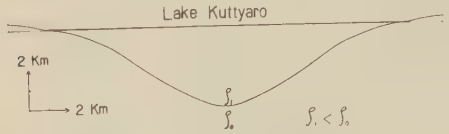

Fig. 6. Distribution of the coarse material at the Kuttyaro caldera.

of the value of density contrast 0.3gr./cm^3 admittedly holds some ambiguity, though the value around this may be a probable one corresponding to $\rho_0=2.0$ gr./cm^3 and $\rho_1=1.7$ gr./cm^3 in Fig. 6.

On the other hand, a cylindrical structure of which the axis extends vertically with a low density is also conceivable beneath the lake for approximately interpreting the observed gravity anomalies. In this model, the boundary surface of the cylinder needs to be situated far inward from the present caldera-rim: The writer believes that the subterranean structure as shown in Fig. 6 is the most probable, because the above-mentioned cylindrical structure is to be accompanied by a discontinuity in the profile of the gravity field but the actual results do not show any such discontinuities with in the accuracy of the survey. In other words, the caldera-rim itself does not represent the vertically deep-rooted fault from the view-point of density contrast.

§ 3. Mass-defect caused by the caldera-formation

The total anomalous mass or mass-defect is given by the theorem of GAUSS which relates the integrated anomally over a horizontal plane to the limit of the detectable gravity anomaly in the following form:

$$M=\frac{1}{2\pi G}\int_{-\infty}^{\infty}\int_{-\infty}^{\infty}\Delta g(x,y)\,dxdy \qquad (5)$$

where G is the gravitational constant. Thus the total anomalous mass M can uniquely be determined from the gravity values observed at the surface while its distribution is indeterminate. If the discussion is confined to the caldera-formation, the distribution of gravity anomaly on the Kuttyaro caldera may safely assumed to be symmetric around its centre including unobserved areas where the parasitic cones erupted after the caldera-formation. The total mass-defect for this caldera is calculated by (5) using the radial distribution of gravity anomaly shown in Fig. 4 and is found to be

$$M=7.8\times10^{10}\text{ tons.}$$

For reference, another estimation is possible on the basis of the subterranean structure shown in Fig. 6. The volume of low density material in Fig. 6 is roughly 3×10^{11}m^3 and if multiplied by the density-contrast 0.3gr./cm^3, the total mass-defect reaches 9×10^{10} tons. The change in the density-contrast does not affect this estimation very much.

The above values of the total mass-defect beneath the caldera should be almost equal to or less than that of the total material ejected from the caldera, because some parts of ejecta might have their origin at the deeper places than the region which was discussed above. In fact, Y KATSUI (1958) has studied the distribution of ejected pumice around the caldera and estimated their total volume at 10^{11}m^3 in the order of magnitude. Considering that the density of pumice is approximately 1.5~2.0gr./cm^3, the mass-defect found by the gravity survey is compatible with the total mass of ejected pumice and is therefore evidently due to the pumice-eruptions accompanied by the formation of the caldera.

This volume of ejecta from the Kuttyaro caldera, which is 10^{11}m^3, is a match for that in the greatest volcanic eruption in historical times, namely, the 1815 eruption of Tambora in Indonesia although the description of this eruption does not afford a precise estimation of its ejecta.

§ 4. Discussion

The mechanism by which enormous amount of pumice was ejected and by which the Kuttyaro caldera was formed, cannot definitely

be understood solely by the results of the gravity survey, but the eruption, accompanied by the accumulation of pumice, may clearly be said to have been so violent, that the region from the surface to a depth 3~4 km, was completely devastated. In order to gain a clear understanding of the caldera-formation and the subsequent volcanic activities, the following few references may be interesting.

H. Kuno (1953) classified Japanese calderas as of Krakatoa- and Glencoe-type of H. Williams (1941) according to their causes of formation. According to his discussion, in the calderas of Krakatoa-type, the post-caldera lavas comprise a rock series formed through contamination of the same magma by granitic material, whereas in those of Glencoe-type, the post-caldera lavas represent an advanced stage of crystallization of the pre-caldera lavas. An example of the former is Kuttyaro caldera, which was devastated to a depth 3~4 km during the eruption of a tremendous amount of pumice as mentioned before, and that of the latter is the Mihara caldera, Oosima Volcano, which was formed by the subsidence of a massive mass of rocks separated from the surroundings by a comparatively simple system of ring fissures, without a pumice eruption. From this geological standpoint, low Bouguer anomalies should be observed on the calderas of Krakatoa-type and the high Bouguer anomalies on the calderas of Glencoe-type. Actually, the result of a gravity survey carried out on Volcano Mihara by the present author and H. Tazima (1957) shows the high anomaly amounting to about 15 milligals. In addition to the above example, C. Tsuboi and his colleagues (1954) observed a low anomaly reaching about 20 milligals on the Aso caldera in Kyûsyû which is of Krakatoa-type. On Lake Akan which is a part of the Akan caldera, Krakatoa-type, a gravity anomaly showing the same tendency as the Kuttyaro caldera was also observed in March 1958. These results of observations, though rather few in number, seem to justify the said geological classification concerning the formation of the calderas, but the mechanism of subsidence or collapse is another problem. Although several theories have been put forward by geologists in regard to this problem, the present writer does not consider them to be well established, especially from the geophysical standpoint.

If the subterranean structures of many calderas in the world are studied by geophysical methods, the old and much-disputed questions as to the caldera-formation will be revived and a valuable contribution to physics of the earth-crust may be expected. At the same time, physical properties of rocks in the deep and the depth of the magma-reservoir need be studied in relation to the caldera-formation.

In conclusion, the writer wishes to express his sincere thanks to Prof. C. Tsuboi who encouraged the writer throughout the course of this study and to Messrs. H. Tajima, T. Murase and I. Onda for their kind cooperation in the field observations. His sincere thanks are also due to the Director of the Earthquake Research Institute who kindly lent the Worden gravimeter to him.

References

Katsui, Y.:
1958 Akan and Kuttyaro Volcanoes (in Japanese). Chikyu-Kagaku, **39**, 19–29.

Kuno, H.:
1953 Formation of calderas and magmatic evolution, Trans. Amer. Geophys. Union, **34**, 267–280.

Tsuboi, C. Jitsukawa, A. and Tajima, H.:
1954 Gravity survey along the lines of precise levels throughout Japan by means of a Worden gravimeter. Bull. Earthq. Res. Inst. Suppl. Vol. 4, 476–552.

Williams, H.:
1941 Calderas and their origin. Univ. Calif. Pub., Bull. Dept. Geol. Sci., v. **25**, 239–346

Yokoyama, I. and Tajima, H.:
1957 A gravity survey on Volcano Mihara, Ooshima Island by means of a Wordern gravimeter. Bull. Earthq. Res. Inst., **35**, 23–33.

Ray-theoretical Construction of Dispersive RAYLEIGH *Waves*

By

Kyozi TAZIME

Department of Geophysics, Faculty of Science, Hokkaido University, Sapporo.

Summary

Many studies have been published on dispersive RAYLEIGH waves. However they were mainly confined within either dispersion-curves or ratios of vertical displacement to horizontal one where POISSON's ratio of the layer was usually assumed to be 0.25. The present author has attempted to carry out more general studies than before on absolute amplitudes for various values of POISSON's ratio. In order to investigate the superficial waves near the surface of the earth, scholars must undertake these general studies, though theoretical treatments will be considerably troublesome.

For this purpose, displacement-potentials have been expressed with reflecting coefficients in this paper where a useful operator has been derived from the characteristic equation.

The characteristic equation in general has been expressed by a hyperbola.

§ 1. General expressions of multiply reflected rays.

"Solid layer over solid half space" (EWING *et al.*, 1957) will be studied here. Displacement-potentials (LAMB, 1903) of P and S-waves in each layer can be expressed respectively as follows:

$$\phi_1=A_1e^{i\alpha_1 z}+B_1e^{-i\alpha_1 z}\ ,\quad \psi_1=C_1e^{i\beta_1 z}+D_1e^{-i\beta_1 z}\ , \tag{1.1}$$

$$\phi_2=B_2e^{-i\alpha_2 z}\ ,\quad \psi_2=D_2e^{-i\beta_2 z}\ , \tag{1.2}$$

where the common factor of $\exp\{i(\omega t-\xi x)\}$ is omitted and the original ray is excluded.

In the above equations notations are employed as follows:

ρ_j; density,

λ_j, μ_j; LAMÉ's elastic constants,

ω; circular frequency,

ξ; circular wave-number in the direction of x which is taken as horizon,

$$\xi^2=h_j^2-\alpha_j^2=k_j^2-\beta_j^2\ ,\quad h_j=\omega/v_{pj}\ ,\quad k_j=\omega/v_{sj}\ ,$$

$$v_{pj}=\{(\lambda_j+2\mu_j)/\rho_j\}^{1/2}\ ,\quad v_{sj}=(\mu_j/\rho_j)^{1/2}\ ,$$

j; the number of the layer counted from the most superficial layer.

Recalling "SOMMERFELD's radiation condition" (SOMMERFELD, 1949) to mind, the writer chooses the signs of the wave-number as next:

$$\xi=\bar{\xi}-i\hat{\xi}\ ,\quad \alpha_j=\bar{\alpha}_j-i\hat{\alpha}_j\ ,\quad \beta_j=\bar{\beta}_j-i\hat{\beta}_j \tag{1.3}$$

where $\bar{\xi}, \hat{\xi}, \cdots \hat{\beta}_j$ are all positive and real.

$A_1, B_1, \cdots, D_2$ in (1.1) and (1.2) are arbitrary constants which are to be decided by the boundary conditions. It is very troublesome to decide these six unknown factors from six simultaneous equations. Therefore another method will be attempted here.

Reflecting coefficients as to displacement-potentials on the upper and the lower boundaries of the superficial layer will be indicated by

$$(A, B, C, D) \text{ and } (A', B', C', D')\ , \tag{1.4}$$

respectively in the order of PP, PS, SP and SS-reflections.

Considering the line source of P-wave at E in Fig. 1, the P-ray going downwards from

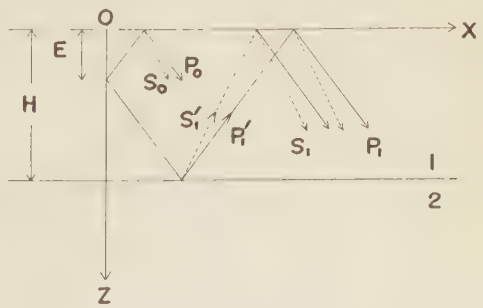

Fig. 1. Space-coordinates under consideration.

the origin will be reflected once on the lower boundary. Then the secondary P and S-rays, indicated by P_1' and S_1', will be generated.

The ray having the notation of $'$ is in agreement with the ray going upwards, corresponding to the first term of (1.1). By the reflections of P_1' and S_1' on the upper and the lower boundaries, number of rays will again be doubled at each reflection. In this case, the ray of P′-type must be proportional, as it was, to $\exp(i\alpha_1 z)$ and the ray of S′-type to $\exp(i\beta_1 z)$. Thus P′ and S′-rays twice reflected on the lower boundary can be totaled as P_2' and S_2'.

Taking account of phase-lags, (P_2', S_2') and (P_1', S_1') can be related by the next equations.

$$\left.\begin{aligned} P_2' &= P_1'\{AA'e^{-2i\alpha_1 H}+BC'e^{-i(\alpha_1+\beta_1)H}\}+S_1'e^{i(\alpha_1-\beta_1)z}\{DC'e^{-i(\alpha_1+\beta_1)H}+AC'e^{-2i\alpha_1 H}\}\,, \\ S_2' &= P_1'e^{-i(\alpha_1-\beta_1)z}\{AB'e^{-i(\alpha_1+\beta_1)H}+BD'e^{-2i\beta_1 H}\}+S_1'\{DD'e^{-2i\beta_1 H}+CB'e^{-i(\alpha_1+\beta_1)H}\}\,. \end{aligned}\right\} \quad (1.5)$$

Putting

$$\left.\begin{aligned} a &= AA'e^{-2i\alpha_1 H}+BC'e^{-i(\alpha_1+\beta_1)H}\,, & b &= DC'e^{-i(\alpha_1+\beta_1)H}+CA'e^{-2i\alpha_1 H}\,, \\ c &= AB'e^{-i(\alpha_1+\beta_1)H}+BD'e^{-2i\beta_1 H}\,, & d &= DD'e^{-2i\beta_1 H}+CB'e^{-i(\alpha_1+\beta_1)H}\,, \end{aligned}\right\} \quad (1.6)$$

(1.5) will be extended to more general forms:

$$\left.\begin{aligned} P_2'e^{-i\alpha_1 z} &= aP_1'e^{-i\alpha_1 z}+bS_1'e^{-i\beta_1 z}\,, \\ P_3'e^{-i\alpha_1 z} &= aP_2'e^{-i\alpha_1 z}+bS_2'e^{-i\beta_1 z}\,, \\ &\cdots\cdots\cdots\cdots\cdots\cdots\,, \\ P_{n+1}'e^{-i\alpha_1 z} &= aP_n'e^{-i\alpha_1 z}+bS_n'e^{-i\beta_1 z}\,. \end{aligned}\right\}$$

$$\therefore\quad (\sum_n P_n'+P_{n+1}'-P_1')e^{-i\alpha_1 z}=a\sum_n P_n'e^{-i\alpha_1 z}+b\sum_n S_n'e^{-i\beta_1 z}\,, \qquad (n=1, 2, 3, \cdots\infty)\,, \quad (1.7)$$

in which either $P_{n+1}' \ll P_1'$ or $P_{n+1}' \ll \sum_n P_n'$ when n becomes large. Thus one has

$$P_{n+1}' \ll \sum_n P_n' - P_1'\,.$$

Neglecting the left hand member in comparison with the right, (1.7) will be reduced to

$$(a-1)(\sum_n P_n')e^{-i\alpha_1 z}+b(\sum_n S_n')e^{-i\beta_1 z}=-P_1'e^{-i\alpha_1 z}\,. \quad (1.8)$$

In the same manner as the above, one gains, from the second relation of (1.5),

$$c(\sum_n P_n')e^{-i\alpha_1 z}+(d-1)(\sum_n S_n')e^{-i\beta_1 z}=-S_1'e^{-i\beta_1 z}\,. \quad (1.9)$$

Letting (1.8) and (1.9) be simultaneous equations, one obtains

$$(\sum_n P_n')e^{-i\alpha_1 z}=\frac{bS_1'e^{-i\beta_1 z}-(d-1)P_1'e^{-i\alpha_1 z}}{(a-1)(d-1)-bc} \quad \text{and} \quad (\sum_n S_n')e^{-i\beta_1 z}=\frac{cP_1'e^{-i\alpha_1 z}-(a-1)S_1'e^{-i\beta_1 z}}{(a-1)(d-1)-bc}\,. \quad (1.10)$$

Putting, then, the P-ray going downwards from the line source as

$$\exp\{-i\alpha_1(z-E)\}\,, \quad (1.11)$$

one sees

$$P_1'=e^{-i\alpha_1(H-E)}A'e^{-i\alpha_1(H-z)} \quad \text{and} \quad S_1'=e^{-i\alpha_1(H-E)}B'e^{-i\beta_1(H-z)}\,.$$
$$\therefore\quad P_1'e^{-i\alpha_1 z}=A'e^{i\alpha_1 E}e^{-2i\alpha_1 H} \quad \text{and} \quad S_1'e^{-i\beta_1 z}=B'e^{i\alpha_1 E}e^{-i(\alpha_1+\beta_1)H}\,. \quad (1.12)$$

On the contrary, putting the P-ray going upwards from the origin as

$$\exp\{i\alpha_1(z-E)\}\,, \tag{1.13}$$

one sees

$$P_1'e^{-i\alpha_1 z}=ae^{-i\alpha_1 E} \quad \text{and} \quad S_1'e^{-i\beta_1 z}=ce^{-i\alpha_1 E}\,. \tag{1.14}$$

Because (1.11) and (1.13) are generated from the origin at the same time, P_1' and S_1' must be expressed by the sum of (1.12) and (1.14):

$$P_1'e^{-i\alpha_1 z}=A'e^{-2i\alpha_1 H}e^{i\alpha_1 E}+ae^{-i\alpha_1 E}\,, \qquad S_1'e^{-i\beta_1 z}=B'e^{-i(\alpha_1+\beta_1)H}e^{i\alpha_1 E}+ce^{-i\alpha_1 E}\,. \tag{1.15}$$

Putting (1.15) into (1.10), one gets

$$\left.\begin{aligned}(\sum_n P_n')e^{-i\alpha_1 z}&=[\{bB'e^{-i(\alpha_1+\beta_1)H}-(d-1)A'e^{-2i\alpha_1 H}\}e^{i\alpha_1 E}+(bc-ad+a)e^{-i\alpha_1 E}]/M\\ \text{and}\quad (\sum_n S_n')e^{-i\beta_1 z}&=[\{cA'e^{-2i\alpha_1 H}-(a-1)B'e^{-i(\alpha_1+\beta_1)H}\}e^{i\alpha_1 E}+ce^{-i\alpha_1 E}]/M\end{aligned}\right\} \tag{1.16}$$

where

$$M=(a-1)(d-1)-bc \tag{1.17}$$

and the right hand members ought to coincide respectively with A_1 and C_1 in (1.1).

The ray going downwards in the superficial layer can be easily calculated from the rays going upwards which have already been obtained. Employing notations of (P_1, S_1), (P_2, S_2), $\cdots$ for rays going downwards, one has the following relations:

$$\left.\begin{aligned}P_0&=e^{-i\alpha_1 F}Ae^{-i\alpha_1 z}\\ P_1&=P_1'Ae^{-2i\alpha_1 z}+S_1'Ce^{-i(\alpha_1+\beta_1)z}\,,\\ P_2&=P_2'Ae^{-2i\alpha_1 z}+S_2'Ce^{-i(\alpha_1+\beta_1)z}\,,\\ &\cdots\cdots\cdots\cdots\cdots\cdots\,,\\ P_n&=P_n'Ae^{-2i\alpha_1 z}+S_n'Ce^{-i(\alpha_1+\beta_1)z}\,.\end{aligned}\right\}$$

$$\therefore\quad \{(\sum_n P_n)+P_0\}e^{i\alpha_1 z}=A\{e^{-i\alpha_1 E}+(\sum_n P_n')e^{-i\alpha_1 z}\}+C(\sum_n S_n')e^{-i\beta_1 z}\,. \tag{1.18}$$

In the same manner as the above, one obtains

$$\{(\sum_n S_n)+S_0\}e^{i\beta_1 z}=B\{e^{-i\alpha_1 E}+(\sum_n P_n')e^{-i\alpha_1 z}\}+D(\sum_n S_n')e^{-i\beta_1 z}\,. \tag{1.19}$$

Putting (1.16) into the right hand members of (1.18) and (1.19), one gets

$$\left.\begin{aligned}\{(\sum_n P_n)+P_0\}e^{i\alpha_1 z}&=[\{bAB'e^{-i(\alpha_1+\beta_1)H}-(d-1)AA'e^{-2i\alpha_1 H}+cCA'e^{-2i\alpha_1 H}\\ &\quad -(a-1)CB'e^{-i(\alpha_1+\beta_1)H}\}e^{i\alpha_1 E}+\{cC-(d-1)A\}e^{-i\alpha_1 E}]/M\\ \text{and}\quad \{(\sum_n S_n)+S_0\}e^{i\beta_1 z}&=[\{bBB'e^{-i(\alpha_1+\beta_1)H}-(d-1)BA'e^{-2i\alpha_1 H}+cDA'e^{-2i\alpha_1 H}\\ &\quad -(a-1)DB'e^{-i(\alpha_1+\beta_1)H}\}e^{i\alpha_1 E}+\{cD-(d-1)B\}e^{-i\alpha_1 F}]/M\end{aligned}\right\} \tag{1.20}$$

in which the right hand members ought to coincide respectively with B_1, and D_1 in (1.1).

ϕ_2 and ψ_2 in (1.2), if need be, can be calculated from $(e^{i\alpha_1 F}+B_1)e^{-i\alpha_1 H}$ and $D_1e^{-i\beta_1 H}$, multiplying the refracting coefficients on the lower boundary.

Reflecting coefficients A, B, C and D are easily expressed as follows:

$$\left.\begin{aligned}A&=-\left\{\left(\frac{\beta_1^2}{\xi^2}-1\right)^2-4\frac{\alpha_1}{\xi}\frac{\beta_1}{\xi}\right\}\Big/\left\{\left(\frac{\beta_1^2}{\xi^2}-1\right)^2+4\frac{\alpha_1}{\xi}\frac{\beta_1}{\xi}\right\}=D\,,\\ B&=4\frac{\alpha_1}{\xi}\left(\frac{\beta_1^2}{\xi^2}-1\right)\Big/\left\{\left(\frac{\beta_1^2}{\xi^2}-1\right)^2+4\frac{\alpha_1}{\xi}\frac{\beta_1}{\xi}\right\}=-\left(\frac{\alpha_1}{\beta_1}\right)C\,,\end{aligned}\right\} \tag{1.21}$$

and they have the relation:

$$AD-BC=1\ . \tag{1.22}$$

Using (1.6) and (1.22), one obtains the next expressions from (1.16), (1.17) and (1.20):

$$\left.\begin{aligned}
A_1=&[\{A'e^{-2i\alpha_1 H}+D(B'C'-A'D')e^{-2i(\alpha_1+\beta_1)H}\}e^{i\alpha_1 E}\\
&+\{AA'e^{-2i\alpha_1 H}+BC'e^{-i(\alpha_1+\beta_1)H}+(B'C'-A'D')e^{-2i(\alpha_1+\beta_1)H}\}e^{-i\alpha_1 E}]/M\ ,\\
B_1=&[\{AA'e^{-2i\alpha_1 H}+CB'e^{-i(\alpha_1+\beta_1)H}+(B'C'-A'D')e^{-2i(\alpha_1+\beta_1)H}\}e^{i\alpha_1 E}\\
&+(A-D'e^{-2i\beta_1 H})e^{-i\alpha_1 E}]/M\ ,\\
C_1=&[\{B'e^{-i(\alpha_1+\beta_1)H}-B(B'C'-A'D')e^{-2i(\alpha_1+\beta_1)H}\}e^{i\alpha_1 E}\\
&+\{AB'e^{-i(\alpha_1+\beta_1)H}+BD'e^{-2i\beta_1 H}\}e^{-i\alpha_1 E}]/M\ ,\\
D_1=&[\{BA'e^{-2i\alpha_1 H}+DB'e^{-i(\alpha_1+\beta_1)H}\}e^{i\alpha_1 E}+\{B+B'e^{-i(\alpha_1+\beta_1)H}\}e^{-i\alpha_1 E}]/M\ ,
\end{aligned}\right\} \tag{1.23}$$

in which

$$M=1-\{AA'e^{-2i\alpha_1 H}+DD'e^{-2i\beta_1 H}+(B'C'-A'D')e^{-2i(\alpha_1+\beta_1)H}+(BC'+B'C)e^{-i(\alpha_1+\beta_1)H}\}\ . \tag{1.24}$$

§ 2. A useful operator derived from the characteristic equation of superficial waves.

If the right hand side in (1.24) is zero, ξ and ω must be related in general by the equation,

$$M(\xi,\omega)=0 \tag{2.1}$$

which is called the characteristic equation of dispersive RAYLEIGH waves.

In this case, one sees that

$$U=\frac{d\omega}{d\xi}=-\left(\frac{\partial M}{\partial \xi}\right)\Big/\left(\frac{\partial M}{\partial \omega}\right)\ , \tag{2.2}$$

where U means group-velocity. Denoting phase-velocity by c, the next relation may be obtained from (2.2):

$$\omega\left(\frac{1}{U}-\frac{1}{c}\right)=-\frac{1}{M_\xi(\xi,\omega)}\left(\omega\frac{\partial}{\partial\omega}+\xi\frac{\partial}{\partial\xi}\right)M(\xi,\omega)\ , \tag{2.3}$$

in which one may find that the operator,

$$\vartheta=\left(\omega\frac{\partial}{\partial\omega}+\xi\frac{\partial}{\partial\xi}\right)\ , \tag{2.4}$$

has two remarkable properties:

$$\vartheta(\alpha_j,\beta_j)=\alpha_j,\beta_j \qquad \text{and} \qquad \vartheta(\alpha_j/\xi,\beta_j/\xi)=0\ . \tag{2.5}$$

On LOVE waves,

$$F(\xi,\omega)=1-Ke^{-2i\eta_1 H}=0 \tag{2.6}$$

must hold (TAZIME, 1957). Now, because

$$\vartheta\eta_j=\eta_j \qquad \text{and} \qquad \vartheta(\eta_j/\xi)=0\ , \tag{2.7}$$

and the reflecting coefficient, K, is composed of the ratio of $\eta_2/\eta_1=(\eta_2/\xi)/(\eta_1/\xi)$ alone, the next calculation will be very easily executed:

$$\vartheta F(\xi, \omega) = -\vartheta K e^{-2i\eta_1 H} = -K\vartheta e^{-2i\eta_1 H} = 2i\eta_1 H K e^{-2i\eta_1 H} . \tag{2.8}$$

Then (2.6) must hold in (2.8), so one has from (2.3)

$$\omega\left(\frac{1}{U}-\frac{1}{c}\right) = -\frac{2i}{F_\xi(\xi, \omega)}\eta_1 H$$

or

$$A = -\frac{2i}{\eta_1 F_\xi(\xi, \omega)} = \frac{\omega}{\eta_1^2 H}\left(\frac{1}{U}-\frac{1}{c}\right) , \tag{2.9}$$

which latter is the amplitude-function of LOVE waves, being the same as that already obtained by the other troublesome method (TAZIME, 1957).

§ 3. Short notes on the characteristic equation.

Exchanging reflecting coefficients as to displacement-potentials by those as to vertical displacements, one may find that (2.1) with (1.24) is similar to the expression that was found by TOLSTOY and EUGENE (1953).

Moreover, the form of (1.24) will not be changed by replacing air over the superficial layer with any medium when reflecting coefficients on the upper boundary take proper expressions other than (1.21).

As far as is discussed in this section, such a general case will be considered. Now (1.24) can be rewritten as

$$\begin{aligned} M = &\{1-(AD-BC)^{1/2}(A'D'-B'C')^{1/2}e^{-i(\alpha_1+\beta_1)H}\}^2 - \{(AA')^{1/2}e^{-i\alpha_1 H} - (DD')^{1/2}e^{-i\beta_1 H}\}^2 \\ &- e^{-i(\alpha_1+\beta_1)H}\{BC'+CB'+2(ADA'D')^{1/2}-2(AD-BC)^{1/2}(A'D'-B'C')^{1/2}\} . \end{aligned} \tag{3.1}$$

Putting

$$\left.\begin{aligned} &p=(\alpha_1+\beta_1)H/2 , \quad q=-(\alpha_1-\beta_1)H/2 , \\ &X=e^{ip}-(AD-BC)^{1/2}(A'D'-B'C')^{1/2}e^{-ip} , \quad Y=(AA')^{1/2}e^{iq}-(DD')^{1/2}e^{-iq} , \\ &l^2=BC'+CB'+2(ADA'D')^{1/2}-2(AD-BC)^{1/2}(A'D'-B'C')^{1/2} , \end{aligned}\right\} \tag{3.2}$$

(3.1) may be expressed as

$$M = e^{-i(\alpha_1+\beta_1)H}(X^2-Y^2-l^2) . \tag{3.3}$$

If in (3.3)

$$l = 0 , \tag{3.4}$$

the characteristic equation (2.1) must be reduced to

$$M(\xi, \omega) = (X-Y)(X+Y) = 0 \tag{3.5}$$

which is a very simple form.

Using the last expression in (3.2), (3.4) should be satisfied by the next two conditions:

$$BC' = B'C \quad \text{besides} \quad A'D'/AD = B'C'/BC . \tag{3.6}$$

If the medium above the superficial layer has the same elastic property as that of the medium below the layer, one may find

$$A = A' , \quad B = -B' , \quad C = -C' \quad \text{and} \quad D = D' . \tag{3.7}$$

In this case, therefore, (3.6) will be satisfied and l becomes zero. This means that dispersive RAYLEIGH waves in a plate being placed in any isotropic homogeneous medium must have a characteristic equation of a type similar to (3.5).

§ 4. Dispersive RAYLEIGH waves in a plate.

As has been seen in the previous section, of course l in (3.2) becomes zero if air exists above and below a plate. In this case, reflecting coefficients have relations (3.7) and expressions (1.21). Therefore M in (3.3) may be solved into

$$M(\xi, \omega)=e^{-i(\alpha+\beta)H}M^{(1)}(\xi, \omega)\cdot M^{(2)}(\xi, \omega) \tag{4.1}$$

in which

$$M^{(1)}=X-Y=(e^{ip}-e^{-ip})-A(e^{iq}-e^{-iq}) \quad \text{and} \quad M^{(2)}=X+Y=(e^{ip}-e^{-ip})+A(e^{iq}-e^{-iq})\,. \tag{4.2}$$

$$M^{(1)}(\xi, \omega)=0 \qquad \text{and} \qquad M^{(2)}(\xi, \omega)=0 \tag{4.3}$$

correspond respectively to the characteristic equations of symmetric modes and antisymmetric modes of dispersive RAYLEIGH waves.

In order to construct cylindrical waves generated from a line source of P-wave at $z=E$, the next operation must be done upon plane waves as (1.1):

$$\int_{-\infty}^{\infty}\left\{\begin{matrix}\phi\\ \psi\end{matrix}\right\}\frac{d\xi}{\alpha}\,. \tag{4.4}$$

Thus displacement-potentials of dispersive RAYLEIGH waves will be gotten by such a calculation as

$$[\phi \text{ or } \psi]_{M=0}=\pi i[\text{residues in (4.4)}]. \tag{4.5}$$

Putting (1.21), (1.22) and (3.7) into (1.23), and performing the operations (4.4) and (4.5), one will obtain the following expressions (TAZIME, 1958):

$$\left.\begin{aligned}[A_1]_{M^{(1)}=0}&=-\pi i\left[\frac{M^{(2)}}{4\alpha M_\xi^{(1)}}G(e^{i\alpha E}e^{-i\alpha H}+e^{-i\alpha E})\right]_{M^{(1)}=0}\,,\\ [B_1]_{M^{(1)}=0}&=-\pi i\left[\frac{M^{(2)}}{4\alpha M_\xi^{(1)}}G(e^{i\alpha E}+e^{-i\alpha E}e^{i\alpha H})\right]_{M^{(1)}=0}\,,\end{aligned}\right\} \tag{4.6}$$

in which

$$G=\frac{e^{i\beta H}-e^{-i\beta H}}{\{e^{i\cdot(\alpha+\beta)/2\cdot H}-e^{-i\cdot(\alpha+\beta)/2\cdot H}\}\{e^{i\cdot(\alpha-\beta)/2\cdot H}-e^{-i\cdot(\alpha-\beta)/2\cdot H}\}}\,,$$

and

$$\left.\begin{aligned}[C_1]_{M^{(1)}=0}&=-\pi i\left[\frac{Be^{-i\beta H}}{2\alpha M_\xi^{(1)}}(e^{i\alpha E}e^{-i\alpha H}+e^{-i\alpha E})\right]_{M^{(1)}=0}\,,\\ [D_1]_{M^{(1)}=0}&=\pi i\left[\frac{Be^{-i\alpha H}}{2\alpha M_\xi^{(1)}}(e^{i\alpha E}+e^{-i\alpha E}e^{i\alpha H})\right]_{M^{(1)}=0}\,.\end{aligned}\right\} \tag{4.7}$$

Then putting (4.6) and (4.7) into (1.1), one has

$$\left.\begin{aligned}[\phi]_{M^{(1)}=0}&=-\pi i\left[\frac{M^{(2)}}{4\alpha M_\xi^{(1)}}G\{e^{i\alpha\cdot(E-H/2)}+e^{-i\alpha\cdot(E-H/2)}\}\{e^{i\alpha\cdot(z-H/2)}+e^{-i\alpha\cdot(z-H/2)}\}\right]_{M^{(1)}=0}\,,\\ [\psi]_{M^{(1)}=0}&=-\pi i\left[\frac{B}{2\alpha M_\xi^{(1)}}e^{-i\cdot(\alpha+\beta)/2\cdot H}\{e^{i\alpha\cdot(E-H/2)}+e^{-i\alpha\cdot(E-H/2)}\}\{e^{i\beta\cdot(z-H/2)}-e^{-i\alpha\cdot(z-H/2)}\}\right]_{M^{(1)}=0},\end{aligned}\right\} \tag{4.8}$$

or applying (2.3) to the calculation of $M_\xi^{(1)}$,

$$\left.\begin{aligned}
[\phi]_{M^{(1)}=0} &= -\frac{2\pi\omega}{\alpha^2 H}\left(\frac{1}{U}-\frac{1}{c}\right)\left(1-\frac{\beta}{\alpha}\frac{\sin\alpha H}{\sin\beta H}\right)^{-1}\cos\alpha\left(E-\frac{H}{2}\right)\cos\alpha\left(z-\frac{H}{2}\right), \\
[\psi]_{M^{(1)}=0} &= i\frac{2\pi\omega}{\alpha^2 H}\left(\frac{1}{U}-\frac{1}{c}\right)\left(1-\frac{\beta}{\alpha}\frac{\sin\alpha H}{\sin\beta H}\right)^{-1}\left(\frac{\beta^2/\xi^2-1}{2\beta/\xi}\right)\frac{\cos(\alpha H/2)}{\cos(\beta H/2)} \\
&\quad\times\cos\alpha\left(E-\frac{H}{2}\right)\sin\beta\left(z-\frac{H}{2}\right),
\end{aligned}\right\} \tag{4.9}$$

since

$$B=\frac{\sin\beta H}{\sin\{(\alpha-\beta)H/2\}}\left(\frac{\beta^2/\xi^2-1}{2\beta/\xi}\right)\frac{\cos(\alpha H/2)}{\cos(\beta H/2)}, \tag{4.10}$$

when $M^{(1)}=0$.

Following procedures similar to the above, one will also reach

$$\left.\begin{aligned}
[\phi]_{M^{(2)}=0} &= -\frac{2\pi\omega}{\alpha^2 H}\left(\frac{1}{U}-\frac{1}{c}\right)\left(1-\frac{\beta}{\alpha}\frac{\sin\alpha H}{\sin\beta H}\right)^{-1}\sin\alpha\left(E-\frac{H}{2}\right)\sin\alpha\left(z-\frac{H}{2}\right), \\
[\psi]_{M^{(2)}=0} &= i\frac{2\pi\omega}{\alpha^2 H}\left(\frac{1}{U}-\frac{1}{c}\right)\left(1-\frac{\beta}{\alpha}\frac{\sin\alpha H}{\sin\beta H}\right)^{-1}\left(\frac{\beta^2/\xi^2-1}{2\beta/\xi}\right)\frac{\sin(\alpha H/2)}{\sin(\beta H/2)} \\
&\quad\times\sin\alpha\left(E-\frac{H}{2}\right)\cos\beta\left(z-\frac{H}{2}\right),
\end{aligned}\right\} \tag{4.11}$$

since

$$B=\frac{\sin\beta H}{\sin\{(\alpha-\beta)H/2\}}\left(\frac{\beta^2/\xi^2-1}{2\beta/\xi}\right)\frac{\sin(\alpha H/2)}{\sin(\beta H/2)}, \tag{4.12}$$

when $M^{(2)}=0$.

These results (4.9) and (4.11) have been verified with those derived from the ordinary method by solving four simultaneous equations of boundary conditions for finding A_1, B_1, C_1 and D_1 in (1.1).

§ 5. Dispersive RAYLEIGH waves in a superficial layer resting on half space absolutely rigid.

Reflecting coefficients A', B', C' and D' on the lower boundary of the layer are calculated in this case as follows:

$$\left.\begin{aligned}
A' &= -\{1-(\alpha/\xi)(\beta/\xi)\}/\{1+(\alpha/\xi)(\beta/\xi)\}=D', \\
B' &= 2(\alpha/\xi)/\{1+(\alpha/\xi)(\beta/\xi)\}=-(\alpha/\beta)C',
\end{aligned}\right\} \tag{5.1}$$

having the next relation with each other,

$$A'D'-B'C'=1. \tag{5.2}$$

Between (1.21) and (5.1), further, another relation is to be found,

$$BC'=B'C. \tag{5.3}$$

Putting (1.21), (1.22), (5.1), (5.2) and (5.3) into (3.2), one has the characteristic equation

$$X^2-Y^2=l^2,$$

where

$$X=e^{ip}-e^{-ip}\,,\qquad Y=(AA')^{1/2}(e^{iq}-e^{-iq})\,,\qquad l^2=2(BC'+AA'-1)\,. \tag{5.4}$$

Because α as well as β, contained in p and q, may be either real or purely imaginary, (5.4) will be divided practically into the next three cases.

(i) $c<v_p<v_s$; $\alpha=\bar{\alpha}$, $\beta=\bar{\beta}$.

$$A=-\left\{1-4\frac{\bar{\alpha}}{\xi}\frac{\bar{\beta}}{\xi}\Big/\left(\frac{\bar{\beta}^2}{\xi^2}-1\right)^2\right\}\Big/\left\{1+4\frac{\bar{\alpha}}{\xi}\frac{\bar{\beta}}{\xi}\Big/\left(\frac{\bar{\beta}^2}{\xi^2}-1\right)^2\right\},\quad A'=-\left(1-\frac{\bar{\alpha}}{\xi}\frac{\bar{\beta}}{\xi}\right)\Big/\left(1+\frac{\bar{\alpha}}{\xi}\frac{\bar{\beta}}{\xi}\right).$$

Looking back at (1.21), (1.22) and (5.2), one sees

$$BC'=-\{(1-A^2)(1-A'^2)\}^{1/2}\,,$$

because c/v_s is larger than $\sqrt{2}$ in this case.

Therefore (5.4) may be rewritten as

$$\left.\begin{aligned}&X=\sin\left\{\left(\frac{\bar{\beta}}{\xi}+\frac{\bar{\alpha}}{\xi}\right)\frac{\xi H}{2}\right\},\qquad Y=(AA')^{1/2}\sin\left\{\left(\frac{\bar{\beta}}{\xi}-\frac{\bar{\alpha}}{\xi}\right)\frac{\xi H}{2}\right\},\\&l^2=\frac{1}{2}[1-AA'+\{(1-A^2)(1-A'^2)\}^{1/2}]\,.\end{aligned}\right\} \tag{5.5}$$

(ii) $v_p>c>v_s$; $\alpha=-i\hat{\alpha}$, $\beta=\bar{\beta}$.

Putting

$$\tan\delta=4\frac{\hat{\alpha}}{\xi}\frac{\bar{\beta}}{\xi}\Big/\left(\frac{\bar{\beta}^2}{\xi^2}-1\right)^2\quad\text{and}\quad\tan\delta'=\frac{\hat{\alpha}}{\xi}\frac{\bar{\beta}}{\xi}\,,$$

one has

$$A=-e^{2i\delta}\quad\text{and}\quad A'=-e^{2i\delta'}\,.$$

On the other hand, from (1.21) and (5.1), one has

$$BC'=8ie^{i(\delta+\delta')}\left\{\frac{\hat{\alpha}}{\xi}\frac{\bar{\beta}}{\xi}\Big/\left(\frac{\beta^2}{\xi^2}-1\right)\right\}\cos\delta\cos\delta'\,. \tag{5.6}$$

Therefore (5.4) may be rewritten as

$$\bar{X}\hat{X}=l_*^2$$

where

$$\left.\begin{aligned}&\bar{X}=e^{(\hat{\alpha}H)/2}\cos\frac{1}{2}(\bar{\beta}H-\delta-\delta')-e^{-(\hat{\alpha}H)/2}\cos\frac{1}{2}(\bar{\beta}H+\delta+\delta'),\\&\hat{X}=e^{(\hat{\alpha}H)/2}\sin\frac{1}{2}(\bar{\beta}H-\delta-\delta')+e^{-(\hat{\alpha}H)/2}\sin\frac{1}{2}(\bar{\beta}H+\delta+\delta'),\\&l_*^2=\sin(\delta+\delta')\pm\{\sin^2(\delta+\delta')-\sin^2(\delta-\delta')\}^{1/2}=\frac{1}{4}\sin\delta\cos\delta'(c/v_s)^4.\end{aligned}\right\} \tag{5.7}$$

(iii) $v_p>v_s>c$; $\alpha=-i\hat{\alpha}$, $\beta=-i\hat{\beta}$.

$$A=-\left\{1+4\frac{\hat{\alpha}}{\xi}\frac{\hat{\beta}}{\xi}\Big/\left(\frac{\hat{\beta}^2}{\xi^2}+1\right)^2\right\}\Big/\left\{1-4\frac{\hat{\alpha}}{\xi}\frac{\hat{\beta}}{\xi}\Big/\left(\frac{\hat{\beta}^2}{\xi^2}+1\right)^2\right\},\quad A'=-\left(1+\frac{\hat{\alpha}}{\xi}\frac{\hat{\beta}}{\xi}\right)\Big/\left(1-\frac{\hat{\alpha}}{\xi}\frac{\hat{\beta}}{\xi}\right),$$

$$BC'=-8\frac{\hat{\alpha}}{\xi}\frac{\hat{\beta}}{\xi}\left(\frac{\hat{\beta}^2}{\xi^2}+1\right)\Big/\left[\left(1-\frac{\hat{\alpha}}{\xi}\frac{\hat{\beta}}{\xi}\right)\left\{\left(\frac{\hat{\beta}^2}{\xi^2}+1\right)^2-4\frac{\hat{\alpha}}{\xi}\frac{\hat{\beta}}{\xi}\right\}\right].$$

Therefore (5.4) may be rewritten as

$$\left.\begin{aligned} X&=\sinh\left\{\left(\frac{\hat{\alpha}}{\xi}+\frac{\hat{\beta}}{\xi}\right)\frac{\xi H}{2}\right\}, \qquad Y=-(AA')^{1/2}\sinh\left\{\left(\frac{\hat{\alpha}}{\xi}-\frac{\hat{\beta}}{\xi}\right)\frac{\xi H}{2}\right\}, \\ l^2&=\frac{\hat{\alpha}}{\xi}\,\frac{\hat{\beta}}{\xi}\left\{\left(\frac{\hat{\beta}^2}{\xi^2}+1\right)^2-4\frac{\hat{\alpha}}{\xi}\,\frac{\hat{\beta}}{\xi}\right\}^{-1}\left(1-\frac{\hat{\alpha}}{\xi}\,\frac{\hat{\beta}}{\xi}\right)^{-1}\left(\frac{c}{v_s}\right)^4. \end{aligned}\right\} \tag{5.8}$$

Keeping (5.4) in mind, one may obtain displacement-potentials through process similar to that of the previous section. Results are shown by

$$\left.\begin{aligned} [\phi]_{H=0}=&-\frac{\pi\omega}{\alpha^2 H}\left(\frac{1}{U}-\frac{1}{c}\right)[\cos\alpha(z-E)\sin 2p+AA'\sin 2q)+A'\sin\{\alpha(z+E)+2q\} \\ &-A\sin\{\alpha(z+E)-2p\}]\Big/\{\sin 2p+AA'\sin 2q+(\beta/\alpha)(\sin 2p-AA'\sin 2q)\}, \end{aligned}\right\} \tag{5.9}$$

and

$$\left.\begin{aligned} [\psi]_{H=0}=&\,i\frac{\pi\omega}{\alpha^2 H}\left(\frac{1}{U}-\frac{1}{c}\right)[B\{\cos(\alpha E+\beta z-2p)+A'\cos(\alpha E-\beta z+2q)\}+B'\{\cos(\alpha E+\beta z) \\ &+A\cos(\alpha E-\beta z)\}]\Big/\{\sin 2p+AA'\sin 2q+(\beta/\alpha)(\sin 2p-AA'\sin 2q)\}. \end{aligned}\right\}$$

References

EWING, JARDETZKY and PRESS:
1957 Elastic Waves in Layered Media. McGRAW-HILL.

LAMB, H.:
1903 On the Propagation of Tremors Over the Surface of an Elastic Solid. Phil. Trans. Roy. Soc. (London) A, **203**, 1–42.

SOMMERFELD, A.:
1949 Partial Differential Equations in Physics. Acad. Press.

TAZIME, K.:
1957 Minimum Group Velocity, Maximum Amplitude and Quarter Wave-length Law. Journ. Phys. Earth, **5**, 43–50.
1958 An Application of the Ray Theory to Stratified Layers (6). Zisin II, **11**, 203–205.

TOLSTOY and EUGENE:
1953 Dispersive Properties of Stratified Elastic and Liquid Media. Geophysics, **18**, 844–870.

Transition from Solid to Liquid Superficial Waves in a Plate.

By

Kyozi TAZIME

Department of Geophysics, Faculty of Science, Hokkaido University, Sapporo.

Summary

Even if POISSON's ratio reaches 0.5, neither $M_1^{(1)}$ nor $M_1^{(2)}$ can coincide with the first order of superficial liquid waves. Each branch of dispersive RAYLEIGH waves should correspond respectively to $\sin\bar{\alpha}H=0$ or $\sin\bar{\beta}H=0$. The former is not other than the dispersion-curves of liquid waves. On the contrary, amplitudes must be zero on the latter. Not always does the first order of dispersive RAYLEIGH waves correspond to the first order of $\sin\bar{\alpha}H=0$.

It must be noted that notations and expressions in this paper will follow those employed and obtained in the previous paper by the present author (TAZIME, 1959).

§ 1. Superficial waves in a liquid plate.

It may be difficult for a liquid plate to exist in actual fact, but one can consider it. Taking space-coordinates as shown in Fig. 1 and assuming a line source at $z=E$, displacement-potential of superficial waves can be written as

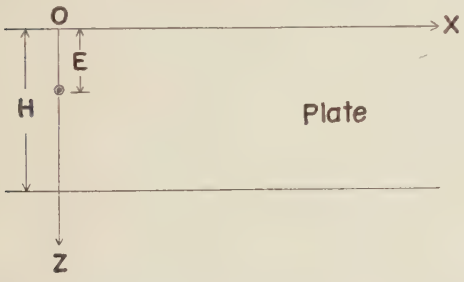

Fig. 1. Space-coordinates under consideration.

$$[\phi]_{M^{(1)}}=-\frac{2\pi\omega}{\bar{\alpha}^2H}\left(\frac{1}{U}-\frac{1}{c}\right)\sin\bar{\alpha}E\sin\bar{\alpha}z \qquad (1.1)$$

in which the characteristic equation is given by

$$M^{(1)}=0 \quad \text{that is} \quad \sin\bar{\alpha}H=0\,. \qquad (1.2)$$

§ 2. Dispersive RAYLEIGH waves in a solid plate.

In a solid plate, as well known, $M^{(1)}$ and $M^{(2)}$-waves must exist. Displacement-potentials of them can be expressed as follows.

(i) $c\geqq v_p>v_s$; $\alpha=\bar{\alpha}$, $\beta=\bar{\beta}$.

$$\left.\begin{aligned}[\phi]_{M^{(1)}_{n=0}}&=-\frac{2\pi\omega}{\bar{\alpha}^2H}\left(\frac{1}{U}-\frac{1}{c}\right)\left(1-\frac{\bar{\beta}}{\bar{\alpha}}\frac{\sin\bar{\alpha}H}{\sin\bar{\beta}H}\right)^{-1}\cos\bar{\alpha}\left(E-\frac{H}{2}\right)\cos\bar{\alpha}\left(z-\frac{H}{2}\right),\\ [\psi]_{M^{(1)}_{n=0}}&=i\frac{2\pi\omega}{\bar{\alpha}^2H}\left(\frac{1}{U}-\frac{1}{c}\right)\left(1-\frac{\bar{\beta}}{\bar{\alpha}}\frac{\sin\bar{\alpha}H}{\sin\bar{\beta}H}\right)^{-1}\left(\frac{\bar{\beta}^2/\xi^2-1}{2\bar{\beta}/\xi}\right)\frac{\cos(\bar{\alpha}H/2)}{\cos(\bar{\beta}H/2)}\cos\bar{\alpha}\left(E-\frac{H}{2}\right)\sin\bar{\beta}\left(z-\frac{H}{2}\right)\end{aligned}\right\} \qquad (2.1)$$

in which the characteristic equation is given by

$$M^{(1)}=0 \quad \text{that is} \quad \sin\tfrac{1}{2}(\bar{\alpha}+\bar{\beta})H+A\sin\tfrac{1}{2}(\bar{\alpha}-\bar{\beta})H=0\,. \qquad (2.2)$$

And

$$\left.\begin{aligned}[\phi]_{M^{(2)}=0}&=-\frac{2\pi\omega}{\bar{\alpha}^2H}\left(\frac{1}{U}-\frac{1}{c}\right)\left(1-\frac{\bar{\beta}}{\bar{\alpha}}\frac{\sin\bar{\alpha}H}{\sin\bar{\beta}H}\right)^{-1}\sin\bar{\alpha}\left(E-\frac{H}{2}\right)\sin\bar{\alpha}\left(z-\frac{H}{2}\right),\\ [\psi]_{M^{(2)}=0}&=i\frac{2\pi\omega}{\bar{\alpha}^2H}\left(\frac{1}{U}-\frac{1}{c}\right)\left(1-\frac{\bar{\beta}}{\bar{\alpha}}\frac{\sin\bar{\alpha}H}{\sin\bar{\beta}H}\right)^{-1}\left(\frac{\bar{\beta}^2/\xi^2-1}{2\beta/\xi}\right)\frac{\sin(\bar{\alpha}H/2)}{\sin(\bar{\beta}H/2)}\sin\bar{\alpha}\left(E-\frac{H}{2}\right)\cos\bar{\beta}\left(z-\frac{H}{2}\right)\end{aligned}\right\} \tag{2.3}$$

in which

$$M^{(2)}=0 \qquad \text{that is} \qquad \sin\tfrac{1}{2}(\bar{\alpha}+\bar{\beta})H-A\sin\tfrac{1}{2}(\bar{\alpha}-\bar{\beta})H=0\,. \tag{2.4}$$

A in (2.2) and (2.4) means PP-reflecting coefficient as to displacement-potential on the boundaries of the plate.

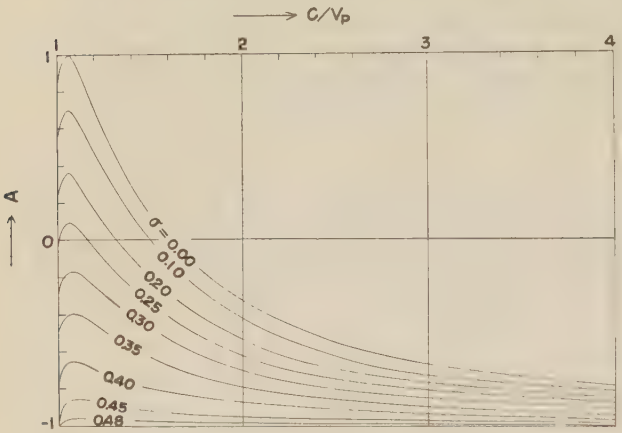

Fig. 2. PP-reflecting coefficient on the boundaries.

Letting rigidity of the plate tend to zero, A above mentioned will, as illustrated in Fig. 2, approach to -1, whichever value phase-velocity may have. In this case, (2.2) and (2.4) will be reduced to

$$\left.\begin{aligned}&\cos(\bar{\alpha}H/2)\sin(\bar{\beta}H/2)=0\\ &\qquad\text{for } M^{(1)}\text{-waves},\\ &\sin(\bar{\alpha}H/2)\cos(\bar{\beta}H/2)=0\\ &\qquad\text{for } M^{(2)}\text{-waves}.\end{aligned}\right\} \tag{2.5}$$

Therefore the dispersion-curves for $M^{(1)}$-waves will be given by

$$\cos(\bar{\alpha}H/2)=0 \qquad \text{or} \qquad \sin(\bar{\beta}H/2)=0\,.$$

The former of them was contained in (1.2), that is $M^{(1)}=0$, and one sees that

$$[\phi]_{M^{(1)}=0}=[\phi]_{M^{(1)}=0} \qquad \text{and} \qquad [\psi]_{M^{(1)}=0}=0\,.$$

On the other hand when the latter is satisfied, one sees that

$$[\phi]_{M^{(1)}=0}=[\psi]_{M^{(1)}=0}=0\,,$$

because $\{1-(\bar{\beta}/\bar{\alpha})(\sin\bar{\alpha}H/\sin\bar{\beta}H)\}^{-1}$ in (2.1) becomes zero.

Next, the dispersion-curves for $M^{(2)}$-waves will be given by

$$\sin(\bar{\alpha}H/2)=0 \qquad \text{or} \qquad \cos(\bar{\beta}H/2)=0\,.$$

The former of them, again, was contained in (1.2) and one sees that

$$[\phi]_{M^{(2)}=0}=[\phi]_{M^{(1)}=0} \qquad \text{and} \qquad [\psi]_{M^{(2)}=0}=0\,,$$

whichever value z may have.

On the other hand when the latter is satisfied, one sees that

$$[\phi]_{M^{(2)}=0}=[\psi]_{M^{(2)}=0}=0\,,$$

because $\sin\bar{\beta}H$ in (2.1) again becomes zero.

Thus letting rigidity of the plate tend to zero, branches corresponding to $\cos(\bar{\alpha}H/2)=0$ and $\sin(\bar{\alpha}H/2)=0$ alone can survive, otherwise amplitudes of displacement-potentials become zero. The surviving two branches coincide respectively with the branches of the liquid waves of the odd order and the even one, as seen in (1.2).

(ii) $v_p \geqq c \geqq v_s$; $\alpha=-i\hat{\alpha}$, $\beta=-\bar{\beta}$.

$$\left.\begin{aligned}
[\phi]_{M^{(1)}=0} &= \frac{2\pi\omega}{\hat{\alpha}^2 H}\left(\frac{1}{U}-\frac{1}{c}\right)\left(1-\frac{\bar{\beta}}{\hat{\alpha}}\frac{\sinh\hat{\alpha}H}{\sin\bar{\beta}H}\right)^{-1}\cosh\hat{\alpha}\left(E-\frac{H}{2}\right)\cosh\hat{\alpha}\left(z-\frac{H}{2}\right),\\
[\psi]_{M^{(1)}=0} &= -i\frac{2\pi\omega}{\hat{\alpha}^2 H}\left(\frac{1}{U}-\frac{1}{c}\right)\left(1-\frac{\bar{\beta}}{\hat{\alpha}}\frac{\sinh\hat{\alpha}H}{\sin\bar{\beta}H}\right)^{-1}\left(\frac{\bar{\beta}^2/\xi^2-1}{2\bar{\beta}/\xi}\right)\frac{\cosh(\hat{\alpha}H/2)}{\cos(\bar{\beta}H/2)}\\
&\quad\times\cosh\hat{\alpha}\left(E-\frac{H}{2}\right)\sin\bar{\beta}\left(z-\frac{H}{2}\right)
\end{aligned}\right\} \tag{2.6}$$

in which the characteristic equation is given by

$$M^{(1)}=0 \quad \text{that is} \quad e^{\hat{\alpha}H/2}\sin\left(\frac{\bar{\beta}H}{2}-\delta\right)+e^{-\hat{\alpha}H/2}\sin\left(\frac{\bar{\beta}H}{2}+\delta\right)=0. \tag{2.7}$$

And

$$\left.\begin{aligned}
[\phi]_{M^{(2)}=0} &= -\frac{2\pi\omega}{\hat{\alpha}^2 H}\left(\frac{1}{U}-\frac{1}{c}\right)\left(1-\frac{\bar{\beta}}{\hat{\alpha}}\frac{\sinh\hat{\alpha}H}{\sin\bar{\beta}H}\right)^{-1}\sinh\hat{\alpha}\left(E-\frac{H}{2}\right)\sinh\hat{\alpha}\left(z-\frac{H}{2}\right),\\
[\psi]_{M^{(2)}=0} &= i\frac{2\pi\omega}{\hat{\alpha}^2 H}\left(\frac{1}{U}-\frac{1}{c}\right)\left(1-\frac{\bar{\beta}}{\hat{\alpha}}\frac{\sinh\hat{\alpha}H}{\sin\bar{\beta}H}\right)^{-1}\left(\frac{\bar{\beta}^2/\xi^2-1}{2\bar{\beta}/\xi}\right)\frac{\sinh(\hat{\alpha}H/2)}{\sin(\bar{\beta}H/2)}\\
&\quad\times\sinh\hat{\alpha}\left(E-\frac{H}{2}\right)\cos\bar{\beta}\left(z-\frac{H}{2}\right)
\end{aligned}\right\} \tag{2.8}$$

in which

$$M^{(2)}=0 \quad \text{that is} \quad e^{\hat{\alpha}H/2}\cos\left(\frac{\bar{\beta}H}{2}-\delta\right)-e^{-\hat{\alpha}H/2}\cos\left(\frac{\bar{\beta}H}{2}+\delta\right)=0. \tag{2.9}$$

δ in (2.7) and (2.9) means phase-lag of displacement-potential at *PP*-reflection on the boundaries of the plate.

Letting the rigidity of the plate tend to zero, the above mentioned δ will, as illustrated in Fig. 3, approach to zero within the very wide region near $c=v_p$. In this case, (2.7) and (2.9) will be reduced to

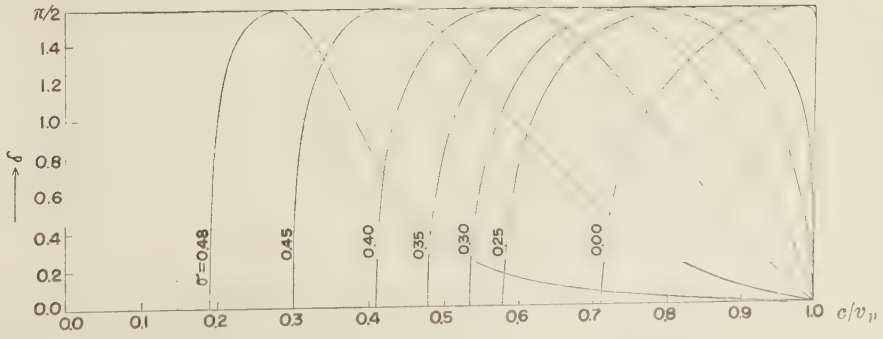

Fig. 3. Phase-lag at *PP*-reflection on the boundaries.

$$\left.\begin{aligned} &\cosh(\hat{\alpha}H/2)\sin(\bar{\beta}H/2)=0 \qquad \text{for} \quad M^{(1)}\text{-waves}\,, \\ &\sinh(\hat{\alpha}H/2)\cos(\bar{\beta}H/2)=0 \qquad \text{for} \quad M^{(2)}\text{-waves}\,. \end{aligned}\right\} \tag{2.10}$$

Because $\cosh(\hat{\alpha}H/2)$ cannot be zero, the dispersion-curves for $M^{(1)}$-waves must be $\sin(\bar{\beta}H/2)=0$. Putting this into (2.6), one sees that

$$[\phi]_{M^{(1)}=0}=[\psi]_{M^{(1)}=0}=0\,.$$

On the other hand, the dispersion-curves for $M^{(2)}$-waves will be given by

$$\sinh(\hat{\alpha}H/2)=0 \qquad \text{or} \qquad \cos(\bar{\beta}H/2)=0\,.$$

The former of them makes c equal to v_p for any value of ξH and one sees that the right hand sides of (2.8) become zero at the same time, because U must be equal to c in this case.

When the latter is satisfied, one sees that

$$[\phi]_{M^{(2)}=0}=[\psi]_{M^{(2)}=0}=0\,,$$

because $\sin\bar{\beta}H$ becomes zero.

(iii) $v_p>v_s\geqq c$; $\alpha=-i\hat{\alpha}$, $\beta=-i\hat{\beta}$.

$$\left.\begin{aligned} [\phi]_{M^{(1)}=0} &= \frac{2\pi\omega}{\hat{\alpha}^2H}\left(\frac{1}{U}-\frac{1}{c}\right)\left(1-\frac{\hat{\beta}}{\hat{\alpha}}\frac{\sinh\hat{\alpha}H}{\sinh\hat{\beta}H}\right)^{-1}\cosh\hat{\alpha}\left(E-\frac{H}{2}\right)\cosh\hat{\alpha}\left(z-\frac{H}{2}\right)\,, \\ [\psi]_{M^{(1)}=0} &= i\frac{2\pi\omega}{\hat{\alpha}^2H}\left(\frac{1}{U}-\frac{1}{c}\right)\left(1-\frac{\hat{\beta}}{\hat{\alpha}}\frac{\sinh\hat{\alpha}H}{\sinh\hat{\beta}H}\right)^{-1}\left(\frac{\hat{\beta}^2/\xi^2+1}{2\hat{\beta}/\xi}\right)\frac{\cosh(\hat{\alpha}H/2)}{\cosh(\hat{\beta}H/2)} \\ &\quad\times\cosh\hat{\alpha}\left(E-\frac{H}{2}\right)\sinh\hat{\beta}\left(z-\frac{H}{2}\right) \end{aligned}\right\} \tag{2.11}$$

in which the characteristic equation is given by

$$M^{(1)}=0 \qquad \text{that is} \qquad \sinh\tfrac{1}{2}(\hat{\alpha}+\hat{\beta})H+A\sinh\tfrac{1}{2}(\hat{\alpha}-\hat{\beta})H=0\,. \tag{2.12}$$

And

$$\left.\begin{aligned} [\phi]_{M^{(2)}=0} &= -\frac{2\pi\omega}{\hat{\alpha}^2H}\left(\frac{1}{U}-\frac{1}{c}\right)\left(1-\frac{\hat{\beta}}{\hat{\alpha}}\frac{\sinh\hat{\alpha}H}{\sinh\hat{\beta}H}\right)^{-1}\sinh\hat{\alpha}\left(E-\frac{H}{2}\right)\sinh\hat{\alpha}\left(z-\frac{H}{2}\right)\,, \\ [\psi]_{M^{(2)}=0} &= i\frac{2\pi\omega}{\hat{\alpha}^2H}\left(\frac{1}{U}-\frac{1}{c}\right)\left(1-\frac{\hat{\beta}}{\hat{\alpha}}\frac{\sinh\hat{\alpha}H}{\sinh\hat{\beta}H}\right)^{-1}\left(\frac{\hat{\beta}^2/\xi^2+1}{2\hat{\beta}/\xi}\right)\frac{\sinh(\hat{\alpha}H/2)}{\sinh(\hat{\beta}H/2)} \\ &\quad\times\sinh\hat{\alpha}\left(E-\frac{H}{2}\right)\cosh\hat{\beta}\left(z-\frac{H}{2}\right) \end{aligned}\right\} \tag{2.13}$$

in which the characteristic equation is given by

$$M^{(2)}=0 \qquad \text{that is} \qquad \sinh\tfrac{1}{2}(\hat{\alpha}+\hat{\beta})H-A\sinh\tfrac{1}{2}(\hat{\alpha}-\hat{\beta})H=0\,. \tag{2.14}$$

A in (2.12) and (2.14) means again PP-reflecting coefficient.

Letting rigidity of the plate tend to zero, A must be confined to -1, as illustrated in Fig. 4.

In this case, (2.12) and (2.14) will be reduced to

$$\left.\begin{aligned} &\cosh(\hat{\alpha}H/2)\sinh(\hat{\beta}H/2)=0 \qquad \text{for} \quad M^{(1)}\text{-waves}\,, \\ &\sinh(\hat{\alpha}H/2)\cosh(\hat{\beta}H/2)=0 \qquad \text{for} \quad M^{(2)}\text{-waves}\,. \end{aligned}\right\} \tag{2.15}$$

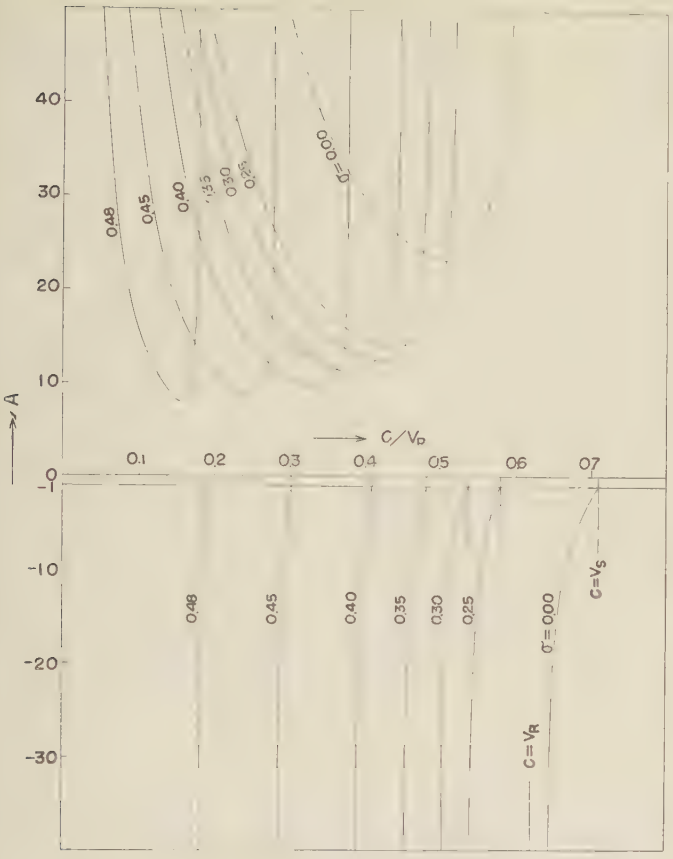

Fig. 4. *PP*-reflecting coefficient on the boundaries.

As one sees that

$$\sinh(\hat{\alpha}H/2)\cosh(\hat{\alpha}H/2)\cosh(\hat{\beta}H/2)$$

cannot be zero ,

the branches corresponding to $\sinh(\hat{\beta}H/2)=0$ can alone exist, with the result that the right hand sides of (2.11) become zero at the same time. Thus one has also

$$[\phi]_{M^{(1)}{}_0}=[\psi]_{M^{(1)}{}_0}=[\phi]_{M^{(2)}{}_0}=[\psi]_{M^{(2)}{}_0}=0 .$$

It has been recognized in this section that dispersive RAYLEIGH waves in a solid medium should be reduced to superficial waves in a liquid at the limit when rigidity is taken as zero. In the following section, processes of transition will be investigated.

§ 3. Numerical calculations of the dispersion-curves for various POISSON'S ratios.

At the limit when POISSON's ratio arrives at 0.5, A in Fig. 2, being c/v_p larger than unity, must be -1 for any value of c/v_p.

Turning attention to A for general POISSON's ratios, one sees that A will always approach again to -1 if $c/v_p \gg 1$. Therefore (2.5) must be satisfied as before, for any σ if $c/v_p \gg 1$.

Considering the above two circumstances with Fig. 2, it may be expected that the nearer σ approaches to 0.5, the wider becomes the range satisfying (2.5).

If $c/v_p=1$, (2.5) must be satisfied again, because $A=-1$ for any value of σ. As $\bar{\alpha}=0$ in this case, $\sin(\bar{\beta}H/2)$ must always be zero. Thus one has

$$\xi H/2=(m\pi/2)\{(v_p/v_s)^2-1\}^{-1/2},$$
m being even for $M^{(1)}$-waves. (3.1)

For $M^{(2)}$-waves, on the other hand, such a relation as (3.1) cannot always be obtained, because $\sin(\bar{\alpha}H/2)$ may be zero in (2.5).

If $c/v_s=1$, (2.10) must be satisfied, because δ in Fig. 3 is zero for any value of σ. As $\cosh(\hat{\alpha}H/2)\sinh(\hat{\alpha}H/2)$ cannot be zero in this case, it may be expected that the dispersion-curves of $M^{(1)}$ and $M^{(2)}$-waves will coincide, for $\xi H \gg 1$, respectively with $\sin(\bar{\beta}H/2)=0$ and $\cos(\bar{\beta}H/2)=0$. At $c/v_s=\sqrt{2}$, δ becomes always $\pi/2$, therefore the dispersion-curves of $M^{(1)}$ and $M^{(2)}$-waves must coincide respectively with $\cos(\bar{\beta}H/2)=0$ and $\sin(\bar{\beta}H/2)=0$ at a point where $v_p > c > v_s$.

As one has seen by now, for any value of σ

$$\sin\bar{\alpha}H=0 \quad \text{and} \quad \sin\bar{\beta}H=0 \qquad (3.2)$$

might be the bases with respect to dispersion-curves of dispersive RAYLEIGH waves.

In Fig. 5 are shown the curves given by (3.2), that is

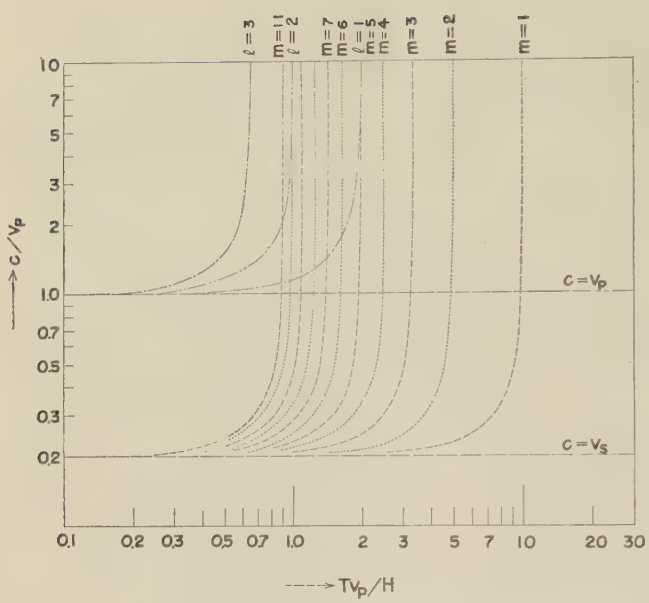

Fig. 5. Chain-lines correspond to $\bar{\alpha}H=l\pi$, while broken and dotted lines to $\bar{\beta}H=m\pi$. $T=2\pi/\omega$.

$$\bar{\alpha}H=l\pi \quad \text{and} \quad \bar{\beta}H=m\pi \tag{3.3}$$

where l and m represent positive integers, indicating orders of these curves. The curves given by $\sin\bar{\beta}H=0$ must be shifted to rightward with increase in σ, though the curves given by $\sin\hat{\alpha}H=0$ need not. In Fig. 5, for an example, the curves for $\sigma=0.48$ are exhibited. Deducing from (2.5), odd orders of l and even orders of m will belong to $M^{(1)}$. On the contrary, even orders of l and odd orders of m will belong to $M^{(2)}$-waves.

Then the dispersion-curves for $\sigma=0.48$ were calculated, as shown by full lines in Fig. 6 where the other lines correspond respectively to those in Fig. 5.

All matters expected at the beginning of this section have appeared satisfactorily in Fig. 6.

At $c/v_p=10$, $M_3^{(1)}$ coincides with $l=1$ while $M_1^{(1)}$, $M_2^{(1)}$ and $M_4^{(1)}$ coincide respectively with $m=2$, 4 and 6.

At $c/v_p=1$, all $M_n^{(1)}$-branches coincide with $m=2$, 4, 6, 8 and so on.

At $c/v_s\to 1$, all $M_n^{(1)}$ coincide again with the above m's.

$M_0^{(1)}$ alone, however, must be excluded from the systematic curves above described. Excluding $M_0^{(2)}$, all expected matters have in practice been also justified as to $M_n^{(2)}$-branches in Fig. 6.

In Figs. 7 to 10, the dispersion-curves for several values of POISSON's ratio are illustrated in the same manner as that in Fig. 6.

§ 4. Some noteworthy points.

As $M_n^{(2)}$-waves could be discussed similarly to $M_n^{(1)}$, the latter alone will be discussed here.

(1) If $c/v_p \gg 1$, the dispersion-curves always coincide with any one of the curves given by (2.5), whatever value σ may have.

(2) If $c/v_p \gg 1$, periods of the former and of the latter equation in (3.3) should coincide with each other under the next condition,

$$m=(v_p/v_s)l\,. \tag{4.1}$$

Because even orders of m must correspond to odd orders of l, the lowest order of m satisfying (4.1) is 2 for $l=1$, resulting in $v_p/v_s=2$ or $\sigma=0.33$.

If $\sigma<0.33$, no curve indicated by m exists to the right of the curve indicated by $l=1$ with which $M_1^{(1)}$ always coincides in this case.

If $\sigma>0.33$, on the other hand, some curves indicated by m appear to the right of $l=1$. The nearer σ approaches to 0.5, the larger becomes the number of m-curves to the right of $l=1$ where the order of n is equal to $m/2$.

(3) On dotted and broken lines in Figs. 6 to 10, as investigated in the second section, amplitudes of displacement-potentials are zero. Though the dispersion-curves may be calculated, no wave can exist there in practice.

(4) It may be expected, on the other hand, that on chain lines, amplitudes will be large. Indeed amplitudes on full lines differ from zero, but the maximum amplitude, being infinitely large, must be attained on chain lines at

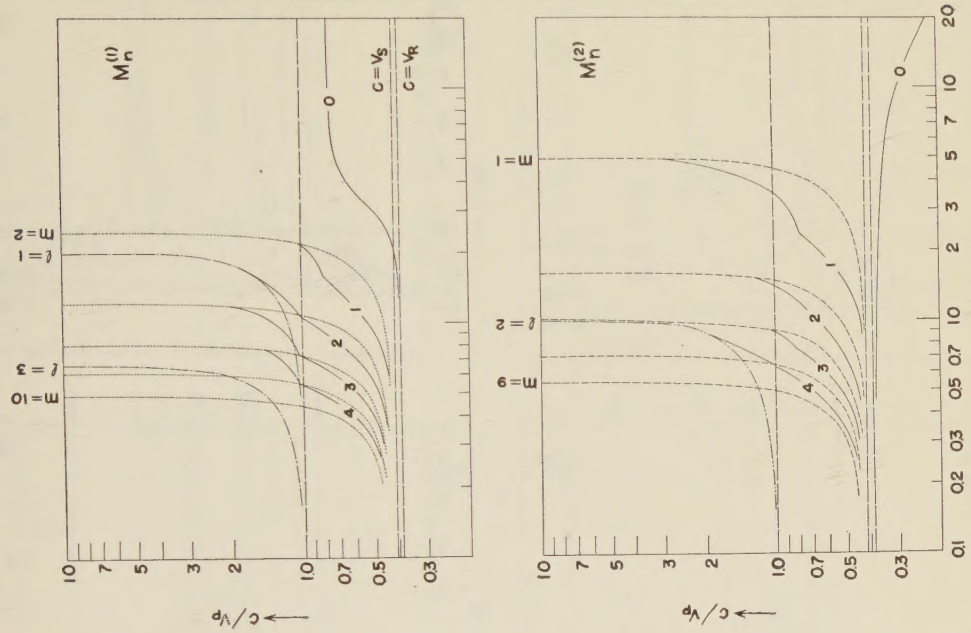

Fig. 7. Dispersion-curves for $\sigma=0.40$.

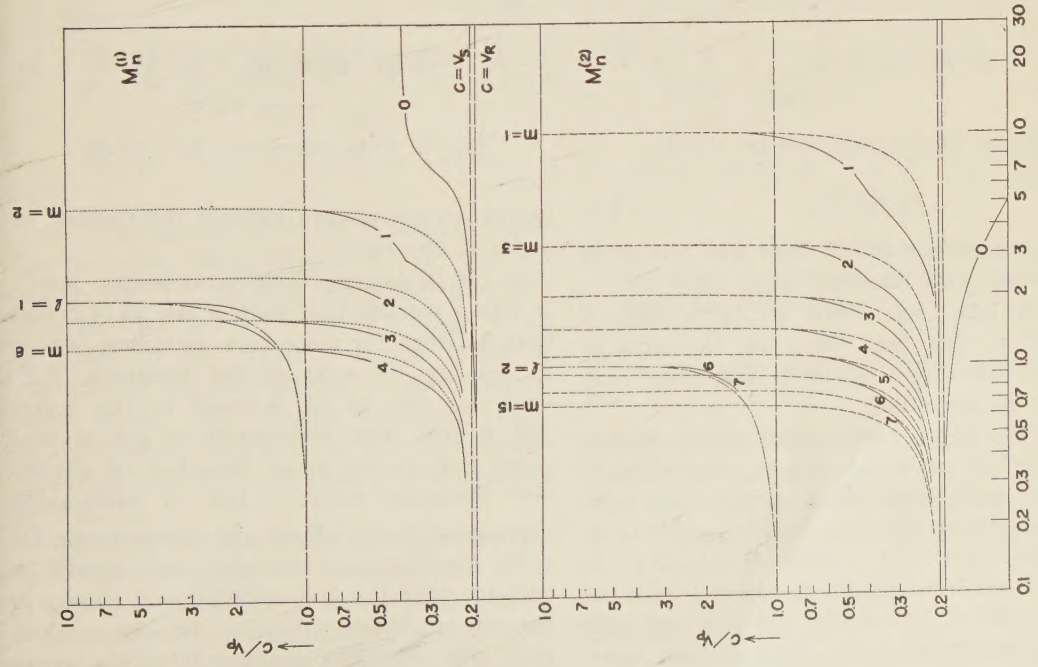

Fig. 6. Dispersion-curves for $\sigma=0.48$. v_R means the velocity of ordinary RAYLEIGH wave.

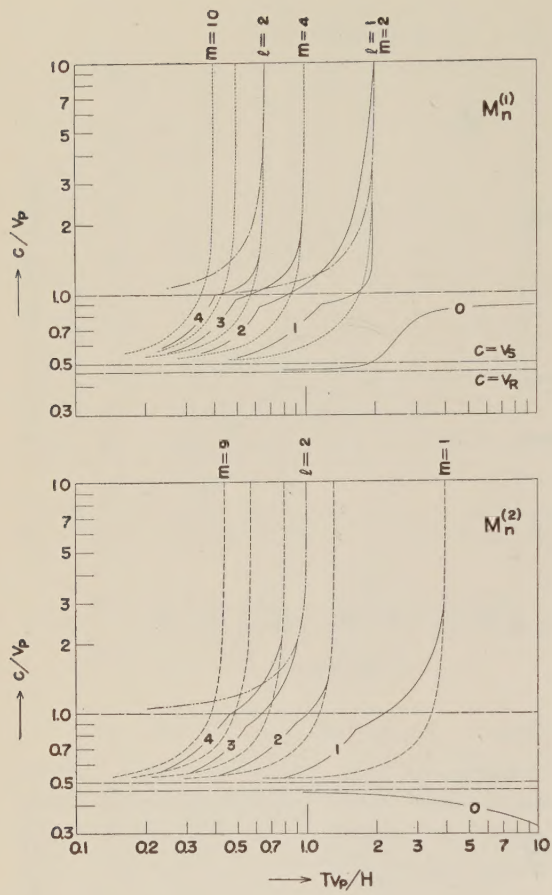

Fig. 8. Dispersion-curves for $\sigma=0.33$.

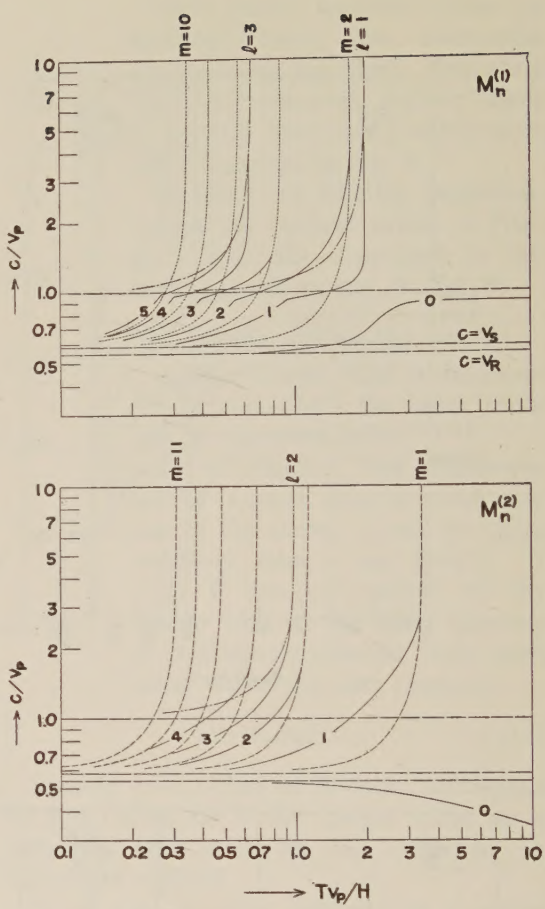

Fig. 9. Dispersion-curves for $\sigma=0.25$.

$$Tv_p/H=2/l\,. \tag{4.2}$$

Finite amplitudes on full lines are trivial in comparison with infinitely large one.

(5) It has been found to be wrong, if $\sigma>0.33$, to say that the lower the order of dispersive RAYLEIGH waves is, the larger may become its amplitude.

(6) The order of superficial waves, such as LOVE waves or liquid waves, consisting of either S or P-waves alone indicates the number of nodes in the layer at the same time. However $M_3^{(1)}$ for $\sigma=0.48$ at $c/v_p\gg 1$, as above described, should correspond with the liquid wave of $l=1$ which has only one node in the superficial layer. One will see moreover that $M_4^{(1)}$ for $\sigma=0.48$ has not four nodes. Thus the order of $M_n^{(1)}$ and $M_n^{(2)}$ waves cannot always indicate the number of nodes in the layer.

(7) (4.2) means "half wave-length law". It was a wonder that such a law as (4.2) had been satisfied for dispersive RAYLEIGH waves in practice, in spite of the existence of P-waves as well as of S-waves in the layer. But it has been understood in the present paper that among many branches of dispersive RAYLEIGH waves a few of them must correspond to $\sin\bar{\alpha}H=0$ and others to $\sin\bar{\beta}H=0$. Amplitudes of the latter ones cannot be so large that the law containing v_p alone will become important. It must be also noticed that the order of dispersive RAYLEIGH waves cannot be determined from the "wave-length law" observed.

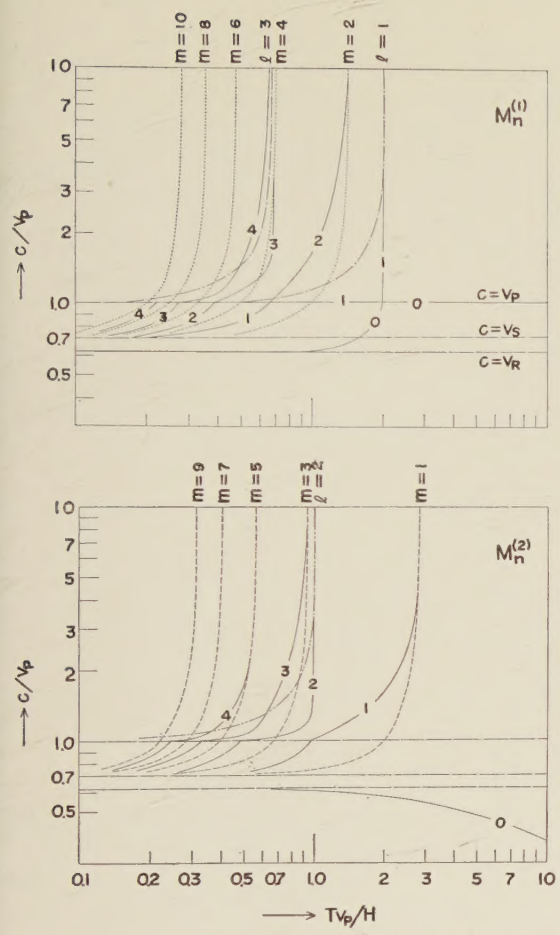

Fig. 10. Dispersion-curves for $\sigma=0.00$.

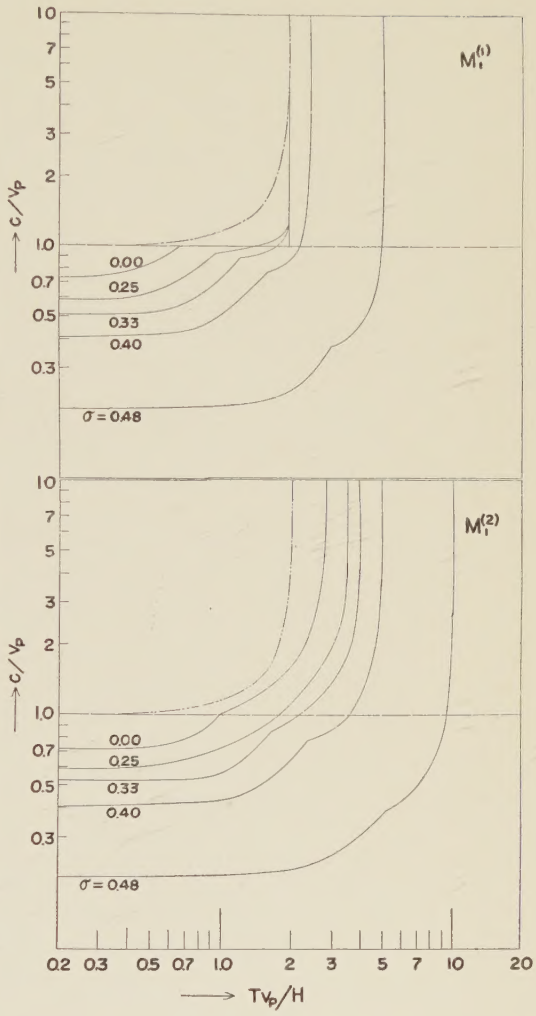

Fig. 11. Comparison of dispersion-curves for the first order of M-waves to the curve for the first order of liquid waves.

(8) Picking out $M_1^{(1)}$, $M_1^{(2)}$ and the curve for $l=1$ alone from Figs. 6 to 10, one will obtain Fig. 11. In this figure $M_1^{(1)}$ and $M_1^{(2)}$ diverge from the curve for $l=1$ when σ approaches to 0.5. Thus it should not be expected that the two curves, for solid and for liquid waves, will coincide with each other at the limit of $\sigma=0{,}5$. The process of transition from solid to liquid cannot be understood by Fig, 11.

According to the present investigation, one sees, the process is very complicated. When σ is near 0.5, the first order of liquid waves is constructed approximately of many higher orders of $M_n^{(1)}$-waves and the second order of liquid waves is constructed approximately of many higher orders of $M_n^{(2)}$-waves and so on.

The present author thinks that conclusions reached in this section as to waves in a plate may be somewhat common to general dispersive RAYLEIGH waves in superficial layers.

References

TAZIME, K.:
1958 Ray-theoretical Construction of Dispersive RAYLEIGH Waves. Journ. Phys. Earth, **6**.